MULTI-HAZARD RELIABILITY OF ELECTRIC POWER TRANSMISSION NETWORKS WITH SPATIALLY CORRELATED COMPONENTS

A THESIS SUBMITTED TO
THE GRADUATE SCHOOL OF NATURAL AND APPLIED SCIENCES
OF
MIDDLE EAST TECHNICAL UNIVERSITY

BY

UMUT ALTAY

IN PARTIAL FULFILLMENT OF THE REQUIREMENTS
FOR
THE DEGREE OF MASTER OF SCIENCE
IN
STATISTICS

SEPTEMBER 2019

Approval of the thesis:

MULTI-HAZARD RELIABILITY OF ELECTRIC POWER TRANSMISSION NETWORKS WITH SPATIALLY CORRELATED COMPONENTS

submitted by **UMUT ALTAY** in partial fulfillment of the requirements for the degree of **Master of Science in Statistics Department, Middle East Technical University** by,

Prof. Dr. Halil Kalıpçılar
Dean, Graduate School of **Natural and Applied Sciences** _____

Prof. Dr. Ayşen Dener Akkaya
Head of Department, **Statistics** _____

Prof. Dr. Ayşen Dener Akkaya
Supervisor, **Statistics, METU** _____

Prof. Dr. Mehmet Semih Yücemen
Co-Supervisor, **Civil Engineering, METU** _____

Examining Committee Members:

Assoc. Prof. Dr. Özlem Türker Bayrak
Inter Curricular Courses-Statistics, Çankaya University _____

Prof. Dr. Ayşen Dener Akkaya
Statistics, METU _____

Prof. Dr. Mohammad Qamarul Islam
Statistics, METU _____

Date: 13.09.2019

I hereby declare that all information in this document has been obtained and presented in accordance with academic rules and ethical conduct. I also declare that, as required by these rules and conduct, I have fully cited and referenced all material and results that are not original to this work.

Name, Surname: Umut Altay

Signature:

ABSTRACT

MULTI-HAZARD RELIABILITY OF ELECTRIC POWER TRANSMISSION NETWORKS WITH SPATIALLY CORRELATED COMPONENTS

Altay, Umut
Master of Science, Statistics
Supervisor: Prof. Dr. Ayşen Dener Akkaya
Co-Supervisor: Prof. Dr. Mehmet Semih Yücemen

September 2019, 157 pages

Many network systems such as, gas and water pipelines, power transmission and distribution systems, highways and communication systems extend spatially over large geographical regions. Such network systems are composed of interconnected components which form paths. Correlation, resulting from similar topography, soil conditions as well as external loading due to the same environmental factors, between the behaviour of those elements should be taken into consideration and be quantified. In this respect the spatial correlation proportional to the distance amongst the components should be taken into consideration. The main objective of this thesis is to investigate the system reliability of electric power transmission networks under multi-hazard (seismic load, wind pressure, ice accretion and wear out) conditions by concentrating especially on the modelling and quantification of spatial correlation in a format suitable for the implementation in the evaluation of network reliability. In this respect the main concepts of the random field theory is applied and the scale of fluctuation is also be utilized as a measure of spatial correlation. A case study based on real life data is presented in order to illustrate the implementation of the methods developed in the thesis.

Keywords: Random Field, Scale of Fluctuation, Electric Power Network Reliability, Multi-Hazard, Spatial Correlation.

ÖZ

ELEMANLARI ARASINDA MEKANSAL KORELASYON OLAN ELEKTRİK İLETİM AĞLARININ ÇOK BOYUTLU TEHLİKE ALTINDAKİ GÜVENİRLİĞİ

Altay, Umut
Yüksek Lisans, İstatistik
Tez Danışmanı: Prof. Dr. Ayşen Dener Akkaya
Ortak Tez Danışmanı: Prof. Dr. Mehmet Semih Yücemen

Eylül 2019, 157 sayfa

İletişim, gaz, su, enerji iletim ve dağıtım ve ulaşım şebekeleri geniş coğrafi alanlara yayılmış bağlaşımlı sistemlerdir. Bu şebekeler güzergahları oluşturan elemanlardan müteşekkildir. Benzer topoğrafya, zemin koşulları ve aynı iklim özelliklerinden kaynaklanan çevresel yüklere maruz kalma nedenleri ile bu elemanların davranışları arasında oluşacak korelasyonun dikkate alınması ve sayısallaştırılması gerekir. Bu nedenle de sistem elemanları arasındaki mesafe ile orantılı mekânsal korelasyon önemli olacaktır. Bu tezin ana amacı, çoklu tehlikeye (sismik yük, buzlanma, rüzgar basıncı, eskime-yıpranma) maruz elektrik iletim sistemlerinin güvenirliğinin, özellikle mekânsal korelasyonun modellenmesi ve sayısallaştırılması üzerinde durularak incelenmesi ve geliştirilecek mekânsal korelasyon modelinin kolayca kullanılabilecek bir formatta olmasıdır. Bu bağlamda, rassal alan kuramının başlıca prensipleri uygulanmıştır ve dalgalanma ölçeği de mekânsal korelasyonun sayısallaştırılmasında kullanılmıştır. Önerilen yöntemin uygulaması gerçek verilere dayanan bir örnek çalışma ile gösterilmiştir.

Anahtar Kelimeler: Rassal Alan, Dalgalanma Ölçeği, Elektrik İletim Ağı Güvenirliği, Çok Boyutlu Tehlike, Mekansal Korelasyon.

To my family.

ACKNOWLEDGEMENTS

I would like to express my sincere gratitude to my supervisor Prof. Dr. Ayşen D. Akkaya who has supported me since the beginning of my study. I want to thank her for her encouraging and patient approach. This thesis would not have been possible without her guidance.

I also would like to thank my co-supervisor Prof. Dr. M. Semih Yücemen for his valuable suggestions and encouraging comments during the progress of this thesis. I am grateful to him for his supportive and patient guidance.

I am also grateful to Prof. Dr. Ayşen D. Akkaya and Prof. Dr. M. Semih Yücemen for encouraging me to apply for both IASSAR (The International Association for Structural Safety and Reliability) and TUBITAK scholarships and their guidance during these processes.

I would like to thank Prof. Dr. Oğuzhan Hasançebi from Civil Engineering Department for devoting his time for modelling the mechanical resistances of power transmission towers. I am also grateful to him for sharing his knowledge and documents with me.

I am grateful to Prof. Dr. Sinan Akkar from Boğaziçi University Kandilli Observatory and Earthquake Research Institute for sharing the fault maps with me.

I want to thank Prof. Dr. Nezih Güven from Electrical and Electronics Engineering Department for explaining me the main design of the power transmission networks and sharing his knowledge and documents with me.

During this thesis I consulted staff of TEİAŞ many times and they were always available, friendly and helpful. I especially would like to thank to Kemal Hür, Hüseyin

Sağlam, Murat Çiçek and TEİAŞ Bursa Regional Office for sharing their knowledge, line diagrams, transmission tower drawings and ice maps with me.

I also would like to thank Ali Koçak from Kaan Havacılık A.Ş. for sharing his expert opinion with me about wear out effects on the power transmission lines.

The scholarship provided by TUBITAK (The Scientific and Technological Research Council of Turkey) within the context of TUBITAK-118M718 project is gratefully acknowledged.

TABLE OF CONTENTS

LIST OF TABLES

TABLES

LIST OF FIGURES

FIGURES

CHAPTER 1

INTRODUCTION

Lifeline networks (communication, gas and water distribution, energy transmission and distribution, transportation) are interconnected systems that span over large geographical areas consisting of the main elements and their subcomponents that take upon various tasks for the functionality of the system. They connect human population to the natural (fresh water, natural gas, etc.) and human made (electricity) sources, provide mobility to the people and materials (transportation networks), transmit data and information (communication networks), dispose the waste water out (sewerage system).

Since the aim of constructing infrastructural networks is to make sure that the whole population has access to the vital sources, they unavoidably geographically extend parallel to the population's propagation. The main consequence of the widespread spatial coverage is the necessity to be ready to face with broad range of natural loads due to different climate conditions and seismic activities. It is possible for an infrastructure system to fulfill the task of conveying the energy and resources to the consumption points, only by the functionality of its elements. Successful achievement of this task requires some precautions and changes in engineering designs if necessary. The very first step of the whole effort is to predict the hazardous potential of the location-specific natural forces which are formed within spatial coverage and nearby the concerned network.

Due to the inherent uncertainties of the environmental conditions; it is not possible to detect the exact load values that will be caused by the environmental and natural factors, prior to the occurrence of the relevant event. The existing uncertainties necessitate the assessment of probabilities rather than the exact values. Statistics,

probability and reliability theory, allows one to make inferences by the past observations and can estimate the probabilities of the expected exposure levels of the network components to the environmental loads. These metrics provide an insight into the future functionality of the system in question and enable the elimination of interruptions that may arise from environmental hazards by taking the necessary precautions.

This research will be carried out by concentrating especially on the modelling and quantification of multi-hazard conditions by taking into consideration the main failure modes. The quantitative assessment of the network reliability to the level of distance based similarities amongst the environmental loads will be investigated by spatial correlation and scale of fluctuation in a format suitable for the implementation in the evaluation of network reliability.

1.1 Aim and Scope of the Study

The main objective of this study is to investigate the probabilistic reliability assessment of electric power transmission networks, the components of which, are subjected to seismic loads, wind pressure, atmospheric ice accretion and wear out. More specifically, the aim is to focus on consolidation of the failure and survival probabilities under various environmental loads of both the network itself and its components into the overall representative probabilistic reliability bounds.

It is possible to classify the main elements forming an overhead electric power transmission network as stations (electricity generation stations and transformer centers), support structures (transmission towers) and line sections (conductors between the towers). Line sections are usually modeled as long straight segments.

In this study, different types of components of an electric power transmission network are assumed to be vulnerable against different types of natural hazards. These assumptions provide an opportunity for demonstration of reliability assessment of the network elements under various types of hazards besides the computational simplicity. In addition to that; since the system is spread over a large region, there will be many

cases where the same type of elements are evaluated under various levels of loads with respect to their geographic locations.

Probabilistic structural reliability assessment of the whole lifeline system consists of a composition of the individual fragility evaluations of the network elements and the interactions between their behaviours due to the connection types amongst them. In this context; while the structural reliability of a lifeline system is examined, the correlation amongst the behavior of the system components should be taken into consideration and be quantified. For this quantification, spatial correlation proportional to the distance between the system elements will be important. In this respect, the main concepts of the random field theory will be applied and the scale of fluctuation will also be utilized as a measure of spatial correlation.

1.2. Background and Review of Previous Work

Structural reliability is a field of study where the theory of probability and civil engineering overlap. This interdisciplinary nature, lets one to extend and enrich the deterministic results by the probabilistic methods. Probabilistic reliability assessment of lifeline systems; as one of the branches of the mentioned interdisciplinary field, has been gaining more and more importance in the last decades.

Until recently, various studies were conducted on the reliability assessment of lifeline systems. The majority of these researches focused on the loads like landslides, liquefaction and the ground acceleration. Those loads are significantly effective especially on the transportation networks besides the water and the natural gas distribution systems; the components of which, are mostly buried pipelines and in a direct interaction with large soil masses that surround them.

In terms of the structural reliability; probabilistic analysis of the seismic activities, more specifically the expected peak ground accelerations within various return periods are of critical importance. The enormous power and the destructiveness of the earthquakes and the events that are caused by them such as liquefaction and landslides, give this importance to the seismic activities.

In order to evaluate the seismicity successfully, a researcher needs to have detailed information on various sub topics such as properties and classification of the seismic sources, earthquake occurrence models, ground motion prediction equations and the resulting ground accelerations. Some of the studies on network reliability and on the seismic hazard, provide very detailed comprehensive information on these topics.

Selçuk (1996), investigated the network reliability based on an algorithm developed by Yoo and Deo (1988). The main reasons to construct the study on this algorithm are given as its effectiveness on the needed computation time for large networks and, besides that, the inclusion of the lengths of the subcomponents in spatial domain. A Fortran package called ”LIFEPACK” was coded and used for the applications. Three reliability evaluation studies were carried out namely; highway network of Boston city, natural gas and water distribution networks located in Turkey using the ”LIFEPACK” package.

Liu, et al. (2004), proposed a method to generate many scenario earthquakes that are consistent in time and space with the seismic properties of the considered region. As a case study, the power network in Taiwan was evaluated by assuming that it is subjected to seismic hazard due to the proposed scenario earthquakes.

Adachi (2007), investigated and introduced a new approach for network reliability evaluation in a region of moderate seismicity. The network reliability was investigated by considering the functional interactions among the network facilities and the shortest path algorithm was employed to evaluate the cascading failures. Bounds of failure probabilities were constructed in the context of spatial correlation of seismic intensities. In a case study, the implementation of the proposed method was demonstrated.

Adachi and Ellingwood (2009), investigated the consideration of spatial correlations of seismic intensities while evaluating the network reliability. The lower and upper bounds of sub-component failure probabilities were constructed to evaluate network functionality under the seismic intensities which were computed using the ground

motion prediction equations proposed by Atkinson and Boore (1995). A case study was carried out to illustrate the evaluation of the network performance in the context of network serviceability under an earthquake, the epicenter of which, is close to the southwest end of the New Madrid Seismic Zone.

Öztürk (2008), emphasized on the comparison of different probabilistic earthquake models and investigated the sensitivity of the hazard analysis results to the selection amongst them. For this purpose, uncertainties involved in the different steps of modelling were investigated. The five ground motion prediction equations, which were developed for Turkey by the previous researchers, were explained besides the ones that are commonly in use. A comprehensive theoretical explanation of the elements of statistical seismicity is available as well. There also exist two case studies based on real data; to illustrate the effects of different sources of uncertainties to the results.

Yavuz (2013), examined the seismic reliability of buried continuous pipelines. The loads due to the internal pressure and temperature changes were also explained as the operating loads. An explanation of the effects of longitudinal and transverse permanent ground deformation and buoyancy due to liquefaction besides the fault crossing effects on the line segments are given as well. Implementation of the theoretical background on the real life data was demonstrated by two case studies.

Özcan (2016), explained the theoretical background and the elements of probabilistic seismic hazard analysis in detail. These elements; namely, specifications of different types of seismic sources, magnitude recurrence relationships, occurence models and four different ground motion prediction equations are explained comprehensively. The main concepts of structural reliability were mentioned by the focus on highway system components. These theoretical concepts were illustrated and explained by a case study focused on Bursa province.

Wind, is another phenomenon which is very important in the reliability assessment of lifeline systems. When wind interacts with an obstacle on its way, a wind pressure is formed on the obstacle surface and this pressure can easily create a force which can destroy, bend or uproot that object. Due to this potential; the expected severity of the wind force is also paid attention in the reliability studies; especially in the ones that the elements of the network are partially or completely installed above the ground surface.

Ice and snow are two other sources of the environmental loads. Snowflakes, in most cases, can easily stick to various surfaces and each other. Since they can hold on each other, a snowfall has a potential to end up as huge snow piles. In contrast to their soft and fluffy look, these masses create great vertical loads on the structures and the surfaces like roofs depending on the amount of the accumulation. Ice layer on the other hand, may form on the structures and the components due to the various reasons such as freezing rain and atmospheric humidity. Since it is not as common as the atmospheric ice accretion in Turkey, in this thesis, freezing rain will not be investigated. The main source of the ice layer formation will be the accretion due to the humidity in the air. The ice, on the network components causes vertical force due to its weight. In addition to that; since the surfaces of the icy components become larger and thicker than their initial area and diameter, they are exposed to significantly higher wind pressure which yields to greater wind loads.

Ellingwood and Tekie (1999), carried out a probabilistic reinvestigation of the wind load parameters and the wind load combinations in ASCE Standard 7 (1996) and suggested that the wind load factor to be increased from 1.3 to around 1.5, to make the reliability more consistent with the gravity load combination based design. They also suggested an error reducing revision in the exposure classification approach of ASCE Standard 7 (1996).

ASCE 7.05 Minimum Design Loads for Buildings and Other Structures (2006), is a comprehensive and informative document which defines different types of environmental loads besides the dead and live loads. The design factors involved in the evaluation of these loads are also explained.

Fırat (2007), carried out a study on the reliability of the components of reinforced concrete structures under seismic, snow and wind loads besides the dead and live loads. A probability based load and resistance factor design criterion was developed with respect to the local environmental conditions of Turkey and the various sources of uncertainties due to the construction techniques and the material properties. The Advanced First Order Second Moment Method (AFOSM) is used as the probabilistic method.

ASCE Manuals and Reports on Engineering Practice No. 74, the third edition of the Guidelines for Electrical Transmission Line Structural Loading (2010), gives a detailed insight on the wind and ice loads on the power grids. All the parameters involved in the wind force and ice accretion computations related to the power transmission networks are explained in detail.

The research on the reliability assessment of the lifeline systems under combined loads and multi-hazard conditions, as another point of view, provide useful information as well as the studies focusing on a single hazard. Since the networks are spread geographically, it is highly possible for their components to be exposed to various types of environmental loads. Multi-hazard studies help to explore and understand the possible ideas and methods on combining various loads throughout the evaluation process. The spatial correlation dependent on the distances amongst the network components; is also taken into consideration by some of the studies to measure the level of the similarities in the responses of the components against the environmental loads.

Salman (2016), worked on the reliability evaluation of electric power networks subjected to hurricanes and earthquake hazards. The system reliability was explained based on the topology of the network. Effects of climate change on the network were also investigated by the wind loads due to hurricanes. Besides the probabilistic and scenario-based analysis, risk mitigation strategies were considered as well.

Salman and Li (2016), carried out a study which considered the reliability of an electric power system under seismic loads and the wind loads due to the hurricanes. Component reliability was also considered by the fragility functions and to demonstrate the application of the mentioned background, a case study was conducted using a power network installed in Shelby County, Tennessee.

1.2.1. Electric Power Transmission Networks

Electricity is the most vital energy source that not only feed countless different kinds of devices that we use, but also feed the sub-components of many other infrastructure systems like water and gas distribution networks.

The facilities in which the electricity is generated are called power plants. Power plants use various inputs like coal, natural gas and nuclear materials to generate energy. Lately; some generation facilities that use clean and safe sources like solar energy, wind force and wave energy emerged as well. The construction locations of each type of those stations are chosen according to the proximity to the locations of the main sources like coal mines, dams, windy hills, etc. While these regions are mostly far away from the residential and industrial areas, the power is needed to be transmitted between the locations of generation and consumption, which is the main reason for the widespread geographical coverage of the transmission networks.

The power generation and transmission process can be roughly explained as follows: As a first step, the generation facilities produce electricity and feed the step-up transformer stations. These stations, increase the voltage to a suitable level by a step-up transformers in them for the purpose of being transmitted to the distant regions. The power plants and the step-up transformer stations will be considered as the

generation stations as if they are the parts of the same facility. This is where both the transmission process and the duties of the electric power transmission network starts.

The electricity is transmitted by the conductor cables throughout the whole network. In overhead networks; for the purpose of preventing any unwanted interactions and discharges, conductors need to be lifted up to a safe height to provide the needed clearance from the ground itself and the structures and the plants on it. That necessity can be satisfied by planting support structures along the line both to carry the weight of the cables and to elevate them. Since the transmission network components are designed according to the required capability of handling the higher voltages compared to the distribution systems, their segments have more and thicker cables. Because of the need for carrying the heavy weight and for preventing any electrical shortcuts and discharges due to the high voltage levels, the support structures in the transmission systems are also not the same as the ones in distribution grids.

The support structures, which are called transmission towers, are designed as the steel lattice truss structures to be able to both handle the weight and provide the required height. There are various types of transmission towers in use. While some of them are guyed to the ground by steel cables, some others are fixed to the ground by their own pods. Their design heights may also vary according to the terrain on which they will be erected such as the water or valley passages and the areas between the hills.

The electricity is transmitted by the conductor cables that are specifically designed according to the required capabilities for mid and high voltage levels. The considered network parts in this study carry 154 kV and 380kV energy, both of which are classified as high voltage. The power, flows through the conductors as three phases. In transmission designs, bundles of two, three or four cables are employed since it is more beneficial to use cable bundles instead of one thick cable due to the “skin effect”. The segments of the power transmission network in and around Bursa, are mostly designed as three phases, every one of which is composed of a bundle of three cables and spacers that prevent cables from touching each other.

With respect to that structure, every segment will be assumed to be composed of three phases, in other words, nine cables. According to the information that is obtained based on a personal meeting with the engineers in Turkish Electricity Transmission Corporation (TEİAŞ), when one of the phases, in other words, one of the three-bundles fails, the system detects the failure and leaves that part of the network out of order immediately until the required repair is done. In this study, the failure of one of the phases, will be accepted as the failure criterion of the considered segment.

The three-phase transmission system and the "skin effect" will not be explained since they are beyond the scope of this thesis. This information is only used while defining the failure criterion of the segments. Those topics may be explored in detail based on the engineering literature.

The power passes through the overhead conductor lines which are supported by the transmission towers until the step-down transformer stations, which will be considered as the end-points of the transmission infrastructure. Since the devices that are used in the residential areas like cities and towns don't need and can not handle high voltage, another transformation is required before feeding the local infrastructure.

The power is transformed from high voltage to the mid and/or low voltage in step-down transformer stations. These facilities feed the local distribution systems with the suitable level of voltage demanded by them. Local distribution networks are not considered within the context of this study.

1.2.2. Reliability of Electric Power Transmission Networks

The fact that the electric power transmission networks are spread over a wide geographical area, causes the elements forming these systems to be subjected to various environmental loads such as ground movements, wind pressure, atmospheric ice accretion and wear out effect.

Lifeline networks behave as large bodies, and because of that, their performance directly depends on the performance of their components. Since the functionality of

the lifeline networks are mainly evaluated over the capability of maintaining the uninterrupted flow; while conducting a probabilistic reliability analysis, it can be useful and practical to consider the whole network as a system of various paths. When it comes to the electric power transmission networks; the transmission lines composed of the conductors and support structures between the consecutive stations (power plants and /or transformer stations), are considered as the paths.

The relations between the paths and their components are very similar to the ones between the whole network and its paths. The elements of an electric power transmission network, may face two types of disconnection, in other words failure. The components may fail due to being damaged too much to keep working. Besides this, if the consecutive component fails, the element may become out of order due to the interruption in the flow even itself is not damaged. Such failures are called cascading failures. Similarly; a path may fail due to its own damaged parts besides being disconnected due to a consecutive path.

In evaluating the system reliability, the connection types between the elements are also important. There are two types of connections, namely series and parallel. Two elements in a network may be connected to each other in a serial way. In this case, failure of one of them leaves the system disconnected as well. Unlike that; in a parallel connection case, two elements are connected as the alternatives to each other. If one of them is damaged, then the power still keeps flowing over the other one and the system remains functional.

All of the situations mentioned above, will be considered in the following chapters and in the case study.

The widespread installation of the electric power transmission networks; makes their components open to the various types of environmental forces since the system components are installed at the locations; the geographic properties of which, vary largely. Within the geographical conditions of Turkey; since the examined network will be an overhead one and is installed on a seismically active region, the most

hazardous conditions are expected to be originated from the wind force, ice accretion, seismic loads and wear out effect.

This diversity of the load conditions, requires a comprehensive approach which allows the reliability of the network to be evaluated over different return periods and under all expected load conditions, in other words, a multi-hazard approach is necessary.

1.3. Organization of the Study

This study is organized in six chapters.

Chapter 1 provides a brief information on the research subject and reviews the existing literature on it.

Chapter 2 characterizes and introduces the environmental loads and their effects that the electrical power transmission networks are vulnerable against.

Chapter 3 defines and introduces the fragility side of the study. The behaviour of the network components under the mentioned loads are characterized based on their fragility functions.

Chapter 4 provides methods for probabilistic reliability assessment of both the individual network components and the whole network. The involvement of spatial correlation among the network elements is considered, explained and evaluated as well.

Chapter 5 demonstrates the application of the probabilistic network reliability assessment methods presented in previous chapters. To achieve this, a case study is conducted using real life data of the electric power transmission network installed in and around Bursa province. Spatial correlation among the network components is also considered as another aspect of the case study.

Chapter 6 summarizes the whole study and explains the results, besides presenting and commenting on them.

CHAPTER 2

ASSESSMENT OF MULTI-HAZARD DEMANDS ON THE ELECTRIC POWER TRANSMISSION NETWORKS

The natural hazards may occur due to various environmental loads. In this chapter; the seismic loads, wind pressure, atmospheric ice accretion and wear out effects will be investigated and the methods to characterize them will be considered and explained.

2.1 Return Period

The results of the probabilistic hazard and reliability assessments are always explained by stating the corresponding time periods to provide a tangible analysis output. Before starting to investigate the hazard demands and their combined effect on the network, the role of these periods on the reliability evaluation needs to be clarified. Therefore, a crucial concept, namely the return period has to be defined. The concept "return period" represents the probability that the load is exceeded at least once in a specific time period (in years). The exceedance probabilities based on the economic life time for the network components (for example for 50 years) corresponding to the return periods that will be used in this study, namely 50, 100, 500, 1000 and 2500 years are given in Table 2.1 below.

Table 2.1. *Return periods and the exceedance probabilities*

Return Period (years)	Probability that the load will be exceeded in 50 Years $= 1-(1-1/RP)^{50}$
50	0.6358 ≅ 64%
100	0.3949 ≅ 39%
500	0.0952≅ 10%
1000	0.0487 ≅ 5%
2500	0.0198≅ 2%

2.2 Characterization of Seismic Demand

Tectonic plates are very large ground masses that move and push each other slowly but continuously. While this ongoing movement, mechanical stress may accumulate at some parts of the plates, especially along the borders between them.

Turkey is a seismically very active region and most of the country is located along the tectonic plate boundaries as it is seen in Figure 2.1. The red and blue lines represent the plate boundaries (USGS, 2019).

Figure 2.1. Tectonic plate boundaries around Turkey

Earthquakes are the sudden or gradual release of this huge amount of accumulated energy by the shock waves which propagate from the epicenters through the surrounding soil and rock masses. While the waves move through the soil and the rock masses; they continuously keep losing their energy, in other words they are attenuated.

The earthquakes owe their hazardous capacity to two main factors, which are the acceleration of the ground and the waves that are caused by them. While the waves lead to strong vibrations on the structures, the ground acceleration make them exposed to the moment of inertia due to their own mass. Both of these loads, force the structures to lose their structural integrity. Besides those, the hazardous forces of earthquakes may cause landslides and liquefaction as well.

Although the geological researches allow scientists to detect the tectonic plate movements, the locations and the occurrence times of the earthquakes still remain random. Under this uncertainty; probabilistic methods allow us to make inferences by the existing information.

The very first step of conducting a probabilistic seismic hazard analysis, should be collecting data on the past seismic activity and then creating an earthquake catalog. Once the data about past seismic activities are compiled, the records are needed to be matched with the known seismic sources for understanding the seismicity of the considered region by detecting the distributions and the distribution parameters of the past earthquakes related to those sources.

2.2.1 Seismic Sources

Earthquakes are triggered due to the sudden or gradual transformations of the stored potential energy into the kinetic energy along the plate boundaries. The locations of the sources of the released energy; can be detected by processing the past earthquake records and the available geological data of the region of interest. By this process, seismic sources are modelled according to the specifications each which are related to one of the three main categories, namely, point sources, line (fault) sources or area sources.

2.2.1.1. Point Sources

Locally clustered past earthquake observations, especially when they are so far away from the researcher's area of interest and do not match with any of the well-defined faults around them, can practically be considered as if they were generated at a single location which is represented by a point. In some cases, even if the geological data is available, the dimensions of the source may not be of considerable importance due to its distance to the site and it can be treated as a point source as well.

2.2.1.2. Fault (Line) Sources

Fault sources are simply the geologically well-defined rupture paths, along which, the past earthquakes are observed and the new ones are expected to occur in the future. The three-dimensional forms of the faults can be identified in detail using the geological methods. These rupture paths are represented as the line segments with a defined trace coordinates on the geological maps.

2.2.1.3. Area Sources

In some cases; the locations of the past earthquake observations within the borders of the considered study region, may not match with the previously identified fault sources. Since they were observed in the study region, which means that they did not occur as far away as to be classified as the point sources as well, they require another classification approach.

These records, can be classified as the observations that belong to an area source, which extends through the whole study region. This area, represents the average seismicity of all of these non-matched observations. The seismicity of the area sources is assumed to be uniformly distributed along its surface. Area sources can be evaluated as the expected background seismicity of the region of interest. They behave like the default seismicity of the area.

Throughout the preparation process of the earthquake catalog; after the elimination of both the observations which match the fault sources, and, the earthquake clusters

outside the study region, the rest will be the ones which contribute to the area source. These remaining records belong to the background seismicity of the whole study area and they are the ones to be used for the estimation of the magnitude distribution there.

2.2.2. Modelling the Seismicity

2.2.2.1. Magnitude Scales

One of the initial steps of the probabilistic assessment of seismic demand is to have sufficient information about the occurrence likelihoods of the earthquakes, the magnitude of which, range from the minimum magnitude that is capable of causing structural damage on the network components to the maximum magnitude that the considered seismic source is able to generate.

Seismic events are recorded by the seismological observation stations which scatter around the world. There exist various magnitude scales for earthquake magnitude measurements, which represent the released energy by the earthquakes from different aspects briefly as follows.

Richter (1935), defined the local magnitude (M_L) using the earthquake records from the seismological observation stations which are located in close distance. Gutenberg and Richter (1936) and Gutenberg (1945a), developed the surface wave magnitude (M_S), by focusing on the surface wave amplitudes of the shallow teleseisms. Gutenberg (1945b, c), defined the body wave magnitude (m_B), by considering the amplitude/period ratio of the body waves of the shallow and the deep-focus teleseisms.

Each one of the various magnitude scales was derived for certain frequency ranges and the certain type of seismic signal. This situation, limits the use of three magnitude scales, ML, mb, and Ms.

ML, M_S and m_b magnitude scales are bounded from above although they are expected to be unbounded in principle (Hanks and Kanamori (1979)). According to them; the reason for that, was the incapability of the time domain amplitude measurements to measure the faulting characteristics of the large earthquakes due to being narrow-band.

Hanks and Kanamori (1979), proposed the relation below, for calculation of the moment magnitude (M_W):

$$M_W = \frac{2}{3}\log_{10}(M_0) - 10.7 \quad (2.1)$$

Where; M_0 is the seismic moment of the earthquake which is proposed by (Aki, 1966) and will be explained later.

The moment magnitude (M_W), is the most suitable earthquake magnitude measurement scale for this study because its validity is not limited only by certain frequency ranges.

Past seismic activities may be found as the records in different scales than the moment magnitude. In such cases; they need to be converted to a common scale for being able to obtain consistent results from the research. For this reason; such records will be converted into the moment magnitude, using the conversion equations that were proposed by Deniz and Yücemen (2010).

2.2.2.2. Magnitude Recurrence Relationships

The linear magnitude recurrence relationship was proposed by Richter (1958) to explain the relationship between the Richter magnitude "m" and the total number of earthquakes with magnitudes equal or greater than "m" (Öztürk, 2008) as seen in Equations (2.2) and (2.3) as follows:

$$\log N(m) = a - bm \quad (2.2)$$

$$N(m) = e^{\alpha - \beta m} \quad (2.3)$$

where

$\alpha = a(\ln 10)$

$\beta = b(\ln 10)$

N(m) : the number of earthquakes having magnitude equal or greater than "m"

a, b : constants depending on the seismic characteristics of the region

Magnitude recurrence equation combines the probability of the occurrence of an earthquake, the magnitude of which is greater than a predefined minimum hazardous magnitude (M_{min}), with the historical occurrence rate of such observations on the source as shown below:

$$V_m = V_{min} \int_M^{M_{max}} f_M(m)dm \quad (2.4)$$

where,

v_M : activity rate that represents the expected rate of the earthquakes to be generated with a magnitude greater than or equal to M, by a certain source

v_{min} : activity rate that represents the rate of the observed earthquakes with magnitude greater than or equal to M_{min}, on a certain source

$f_M(m)$: magnitude probability density function

M_{min} : the minimum magnitude that is considered as hazardous for the engineered structures included in this study

M_{max} : the maximum magnitude that a certain source is expected to be able to generate

The minimum magnitude (M_{min}) is decided to be 4.0 in moment magnitude scale as the common lower bound for all sources in this study, in order to cover even the smallest possible hazards. When it comes to the maximum magnitudes, estimations differ due to the type of the sources.

Because of the lack of well-defined specific geological data for point and area sources, the most practical way for a statistician, might be to assume the size of a future earthquake that expected to be generated by a point or an area source to be at most equal to the ones observed and recorded in the past.

Unlike point or area sources, historical records may not always give adequate information about the maximum magnitude of the fault sources. Besides this, for the fault sources, the amount of geological information and data that is sufficient enough

to model and estimate their behaviour is mostly available. In such cases, the maximum magnitude that a fault is expected to generate is estimated by the equations based on the rupture dimensions as shown below:

$$M = a + b(\log_{10})L \tag{2.5}$$

where,

M : earthquake magnitude

a , b : empirically determined coefficients

L : rupture length

2.2.2.3. Magnitude Distribution

The magnitude distribution function, $f_M(m)$, represents the likelihood of occurrences of different sized earthquakes over a seismic source. The parameters of a magnitude distribution function can be estimated by collecting the past earthquake records and then applying the proper estimation methods on them. But, the required paleoseismic data for the estimation process is usually unavailable for most of the faults.

In such cases; the slip rates of the faults can be used to estimate the frequency of the earthquake occurrences as an alternative way. Wallace (1970), proposed the very first use of the slip rates for the earthquake frequency estimation as below:

$$R = \frac{D}{S} \tag{2.6}$$

where;

R : the recurrence interval

D : the displacement per event

S : average seismic slip rate

This model only considers the earthquakes of size “D” and distributes the whole slip rate to these events.

The method proposed by (Aki, 1966), provides a better approach by using the seismic moment (M_0) as shown below:

$$M_0 = \mu A_r D \tag{2.7}$$

where;

μ : the rigidity or the shear modulus (~$3x10^{11}$ dyne/cm^2)

A_r : the rupture area on the fault plane (cm^2)

D : average displacement over the slip surface (cm2)

Once the fault slip rate is used to constrain the seismic moment rate on the fault, a model must be assumed for the manner in which the rate of moment release is distributed to earthquakes of various magnitudes (Youngs and Coppersmith, 1985).

2.2.2.3.1. Characteristic Earthquake Model

The characteristic earthquake model was proposed by Schwartz and Coppersmith (1984). In their research, they explored the same-size displacement occurrences along the same segments of Wasatch and San Andreas faults, due to the historical earthquakes. This means that the segments were generating same-size earthquakes consistently. The "same-size" means within about one-half magnitude unit (Youngs and Coppersmith, 1985).

(Youngs and Coppersmith, 1985), proposed the model below to represent the magnitude distribution of the earthquakes which are generated by the faults; the characteristics of which are mentioned above.

$$f_M(m) = \begin{cases} k\beta e^{-\beta(m-m_0)} & m_0 \le m \le m_1 - 0.5 \\ k\beta e^{-\beta\left(\left(m_1-\frac{3}{2}\right)-m_0\right)} & m_1 - 0.5 \le m \le m_1 \end{cases} \tag{2.8}$$

where,

k is the normalizing constant as follows:

$$k = \left[1 - e^{-\beta(m_1-0.5-m_0)} + \beta e^{-\beta\left(m_1-\frac{3}{2}-m_0\right)}0.5\right]^{-1} \tag{2.9}$$

2.2.2.3.2. Truncated Exponential Model

The truncated exponential model is widely used to represent the probability distributions of the earthquakes that is related to the area sources. Large regions, which typically contain a number of faults, usually display exponential recurrence behaviour (Youngs and Coppersmith, 1985). This model was derived from the following Gutenberg-Richter magnitude recurrence relationship (Gutenberg and Richter, 1944).

$$\log V_M = a - bM \tag{2.10}$$

where,

a, b : constants depending on the seismic characteristic of the region
M : Richter magnitude

V_M stands for the number of earthquakes with magnitude M or greater than M; in other words, the activity rate, and it is calculated as follows:

$$V_M = V_0 \exp(\beta M) \tag{2.11}$$

where,

$$v_0 = 10^a \tag{2.12}$$

$$\beta = b(\ln 10) \cong 2.3b \tag{2.13}$$

After deriving the β parameter, the exponential model that is truncated at M_{min} and M_{max} can be constructed as follows:

$$f_M(m) = \frac{\beta e^{-\beta(M - M_{min})}}{1 - e^{-\beta(M_{max} - M_{min})}} \tag{2.14}$$

2.2.2.4. Earthquake Activity Rates

Activity rate can be found by using different approaches. The simplest one is the use of past earthquake records. If sufficient information about the earthquakes that are recorded in an area, which is considered as related to a certain fault source, is available and clearly distinguishable from the rest of the records, then a reliable earthquake

catalog can be compiled for this source. After this process, the activity rate becomes simply available as the occurence rate of the earthquakes the magnitude of which are equal or greater than a predefined magnitude (which is $4.0\ M_w$ for this study) along the past records on the considered source.

If the source is an area, in this case, the records will not be spatially related with any one of the known faults. The best method is to fit the exponential model to the data in such situations. The exponential model should be truncated at the minimum hazardous magnitude ($4.0\ M_w$) and at the maximum magnitude that has ever recorded within the borders of the area. Seismic activities may include foreshocks and/or aftershocks beside the main shocks as well. It is better to consider only the main shocks in this process to be able to avoid double counting. Otherwise the frequency of that event artificially outweighs the rest of them and then increases the uncertainty that has been struggled to overcome. As stated by Weichert (1980), the b value can be calculated by using the maximum likelihood method as follows:

$$b = \frac{1}{(\ln 10)(M - M_{min})} \tag{2.15}$$

The seismicity of the segments which generate same-size earthquakes consistently is represented by the characteristic earthquake model. The activity rate for such a model can be computed based on the seismic moment (M_0).

The amount of the change in seismic moment (M_0) per time unit is called seismic moment rate (M_0') and obtained as follows:

$$M_0' = \mu A \frac{dD}{dt} = \mu A S \tag{2.16}$$

where,

S : average slip rate along the fault

D : average displacement over the rupture surface

After obtaining the seismic moment (M_0) as shown in Equation (2.1), the activity rate which represents the rate of the ground motions the magnitude of which is equal

to M_w or larger in a seismic source, can also be obtained from the following relationship:

$$V_M = \frac{M_0'}{M_0} = \frac{\mu AS}{10^{1.5M_W+16.05}} \quad (2.17)$$

2.2.2.5. The Renewal Models

One of the reasons for conducting a probabilistic seismic hazard assessment is to gather information on the expected time between main seismic shocks related to every single seismic source in the vicinity of the network components. Since the analysis is probabilistic, the time gap distribution between the occurrences of consecutive main shocks (inter-event times) needs to be identified. Then inferences can be made on the model parameters.

The hazard rate, which takes the time dependency into consideration, is dependent on the assumed probability distribution of interevent times. Hazard rate function is determined by the assumed probability distribution of interevent times. It is possible to derive the hazard rate from the hazard function (hazard rate function), h(t) as follows:

$$h(t) = \frac{f_T(t)}{1-F_T(t)} \quad (2.18)$$

where, $f_T(t)$ is the probability density function and $F_T(t)$, is the cumulative distribution function of the interevent times.

2.2.2.6. Ground Motion Prediction Equations

The shock waves of seismic events travel through the rocks and the soil mass and their energy may change throughout their paths due to the properties of the medium in which they propagate. Ground motion prediction equations (GMPE) predict the probability distribution of ground motion intensity as a function of many predictor variables such as the earthquake's magnitude, distance, faulting mechanism, the near-surface site conditions and the potential presence of directivity effects (Baker, 2008).

Even if they look similar, the magnitude and severity are two different concepts. Since the severity is observed based on the damage after the event, and the damage is the direct result of the acceleration of the ground; the ground motion prediction equations work like the link between the magnitude and the severity.

Those equations are constructed based on non-linear regression and the main components of them can be explored by their general form as follows:

$$\ln(Y) = c_0 + c_2 M + c_3 M^{c_4} + c_5 \ln(R) + f(F) + f(HW) + f(S') + \varepsilon \qquad (2.19)$$

where,

Y : ground motion parameter

c_0, c_1 , c_2, c_3, c_4, c_5 : regression parameters

M : magnitude

R : distance to the site from the source

S′ : site parameters

F : fault type parameters

HW : hanging wall parameters

There are many different ground motion prediction models in use. They are constructed according to the local properties of the considered regions in different studies and then fitted using the past earthquake records related to those regions.

In this thesis three different ground motion prediction equations will be used, namely:

- Boore, Joyner and Fumal (1997)
- Abrahamson and Silva (2008)
- Gülerce et al. (2015)

2.2.2.6.1. Boore, Joyner and Fumal (1997) Ground Motion Prediction Equation

Boore, Joyner and Fumal (1997) proposed a ground motion prediction equation in the following form:

$$\ln(Y) = b_1 + b_2(M-6) + b_3(M-6)^2 + b_5 \ln(r) + b_V \ln\left(\frac{V_S}{V_A}\right) \quad (2.20)$$

where,

$$r = \sqrt{r_{jb}^2 + h^2} \quad (2.21)$$

and

$$b_1 = \begin{cases} b_{1SS} & \text{for strike slip earthquakes} \\ b_{1RS} & \text{for reverse slip earthquakes} \\ b_{1ALL} & \text{if mechanism is not specified} \end{cases}$$

here,

Y : the ground motion parameter (peak horizontal acceleration or pseudo acceleration response in g)

M: moment magnitude

r_{jb} : Joyner-Boore distance (km)

V_S : average shear-wave velocity to 30 m (m/ sec)

h : fictitious depth which is determined by the regression

b_{1SS}, b_{1RS}, b_{1ALL}, b_2, b_3, b_5, h, b_V and V_A are the regression coefficients.

Boore, Joyner and Fumal (1997), defined and used a new horizontal distance variable called "Joyner-Boore Distance" (r_{jb}). The Joyner-Boore distance represents the closest horizontal distance from the station to a point on the earth's surface that lies directly above the rupture.

While they were developing their ground motion prediction equation, the magnitude scaling of other ground motion prediction equations were scaling the magnitudes smaller as the distance gets shorter. Since Boore, Joyner and Fumal (1997) investigated the scaling for shorter distances by Monte-Carlo simulation and did not

find any statistically significant difference compared to their approach, they preferred to use same magnitude scaling for all distances.

They fitted their regression equation on the data which was composed of the strike-slip and the reverse-slip earthquakes with only one exception. The only strike-slip earthquake included in the data set was the one that belongs to the Daly City Earthquake. This makes the Boore, Joyner and Fumal ground motion prediction equation more representative for strike-slip and the reverse-slip earthquakes than the normal-slip ones. More detailed information about this GMPE is available in Boore, Joyner and Fumal (1997).

2.2.2.6.2. Abrahamson and Silva (2008) Ground Motion Prediction Equation

Abrahamson and Silva (2008) ground motion prediction equation was derived within the context of the Next Generation Attenuation (NGA) Project. The project, let them use three classes of models. The simulations conducted by them, helped to construct a model with wide applicability limits like the magnitudes from 5 to 8.5, the distances from 0 to 200 km and the spectral periods from 0 to 10 seconds.

The base form of their ground motion prediction equation is as follows:

$$f_1\left(M, R_{rup}\right) = \begin{matrix} a_1 + a_4(M - c_1) + a_8(8.5 - M)^2 + (a_2 + a_3(M - c_1))\ln(R) & (M \leq c_1) \\ a_1 + a_5(M - c_1) + a_8(8.5 - M)^2 + (a_2 + a_3(M - c_1))\ln(R) & (M > c_1) \end{matrix} \quad (2.22)$$

$$R = \sqrt{R_{rup}^2 + c_4^2} \quad (2.23)$$

NGA models are intended to begin the transition from simple empirical models to full numerical simulations for specific source-site geometries. (Abrahamson and Silva (2008)). More detailed information about this GMPE is available in Abrahamson and Silva (2008).

2.2.2.6.3. Gülerce et al. (2015) Ground Motion Prediction Equation

The base ground motion prediction model which was proposed by Abrahamson and Silva (2008) was adjusted for Turkey by Gülerce et al. (2015). The model is called "TR-Adjusted NGA-W1" and the general form of it is similar to the one which was proposed by Abrahamson and Silva (2008) and given in Equation (2.22).

The ground motion prediction equations developed in the context of NGA project; were based on the shallow crustal earthquakes of Western US and they provided a model which is applicable for other shallow crustal earthquakes around the world. Gülerce et al. (2015), conducted a research to investigate the adaptability of the NGA-W1 ground motion prediction equations to the magnitude, distance and site effect scaling of the Turkish strong ground motions.

The NGA-W1 database, was constructed on the datasets including observations from seven to fifty two recordings of the earthquakes, which occurred in Turkey. The two fundamental reasons for using such small samples were stated by Gülerce et al. (2015) as below:

1. The magnitude constraint limitations in the NGA-W1 project.
2. Missing site information and missing strong ground motion data for Turkey during the database compilation period.

NGA-W1 ground motion prediction models were modified by Gülerce et al. (2015), for applicability to Turkey using the last 50 year's strong ground motion data, which was completed as part of the Turkish Strong Motion Database Project (Akkar et al., 2010). As a result, they constructed the TR-adjusted NGA-W1 models are useful for magnitude 4-8.0 events and distances up to 200 km. More detailed information about this GMPE is available in Gülerce et al. (2015).

2.3. Characterization of Ice and Wind Load on Electric Power Transmission Network

2.3.1. Wind Load

The power transmission in Turkey is mostly provided by the overhead transmission lines. The wide-spread spatial coverage of these lifeline systems; even in a local scale, make their components open to the various weather conditions. Wind is the most active atmospheric phenomenon amongst those. The moving air mass creates huge pressure on the structures and forces them to bend, break into pieces or even to be uprooted from their foundations.

The hazardous loads due to the extreme winds occur as a result of the cooperation of various factors. For example; the shape of the considered structure directly affects the wind load by the exposure area. The topographical properties of the considered region can also create additional wind load by causing turbulence and wind gusts around the structures. In this chapter, all of the factors that contribute to the characteristics of the wind force and the method suggested by American Society of Civil Engineers (ASCE) to consolidate all those factors will be explained.

2.3.1.1. Wind Load on Transmission Towers and Conductors

In this study, the wind force equation which is proposed in "ASCE Manuals and Reports on Engineering Practice No. 74, Guidelines for Electrical Transmission Line Structural Loading (2010)" document will be applied to the real life data. Since the measurement system is metric (SI units) in Turkey, the metric equivalents of the parameters and variables will be employed for the wind force calculations as follows:

$$F = \gamma_W Q K_Z K_{Zt} (V_{50})^2 G C_f A \tag{2.24}$$

$$F = Q K_Z K_{Zt} (V_{RP})^2 G C_f A \tag{2.25}$$

where,

F : the wind force in the direction of wind unless otherwise specified, in Newtons

γ_w : the load factor

V_{50} : basic wind speed, 50-year return period, 3-sec gust,in m/s

V_{RP} : the 3-sec gust design wind speed, in m/s, associated with the RP-return period

K_z : the velocity pressure exposure coefficient

K_{zt} : the topographic factor

Q : numerical constant

G : the gust response factor for conductors, ground wires, and structures

C_f : the force coefficient values

A : the area projected on a plane normal to the wind direction, in m^2

When the wind speed observations are unavailable for the considered return period; the load factor γ_w can be used for adjusting the force F, to the needed return period (see Equation (2.24)). The corresponding γ_w values for various return periods are provided in ASCE Manual No. 74 (2010). If the wind speed data is available for the considered return period (RP), the mean wind speed can be directly used in Equation (2.25) to obtain the wind force values.

The role of the velocity pressure exposure coefficient $K_{Z;}$ which is formulated below, is to adjust the wind speed with respect to the effects of various types of terrain and height:

$$K_Z = 2.01\left(\frac{Z_h}{Z_g}\right)^{\frac{2}{\propto}} \quad \text{for } 10.0554\ \text{m} \leq Z_h \leq Z_g \qquad (2.26)$$

where,

Z_h : the effective height (in meters)

Z_g : the gradient height (in meters)

α : the power law exponent

In ASCE Manual No. 74 (2010), the effective height of a structure is stated as the height above the ground to the center of pressure of the wind load while the gradient height is defined as the height above which the wind speed is assumed to be constant. ASCE Standard 7-05 (2006) classifies the roughness of the ground as three different

exposure categories. The gradient height and the power law exponent values for various terrain roughness categories are provided in ASCE Manual No. 74 (2010).

The topographic factor K_{Zt}, represents the wind speed acceleration effects of landforms such as escarpments, ridges, canyons, mountains and hills. The topographic factor can not be less than 1 and it is obtained from Equation (2.27) below. The topographic multiplier values are provided in ASCE Standard 7-05 (2006) as well.

$$K_{Zt} = (1 + K_1 K_2 K_3)^2 \tag{2.27}$$

where;

K_1 : factor to account for shape of topographic feature and maximum speed-up effect

K_2 : factor to account for reduction in speed-up with distance upwind or downwind of crest

K_3 : factor to account for reduction in speed-up with height above local terrain

The numerical constant Q; represents the mass density of air for the standard atmosphere conditions (15° C and sea level pressure of 29.92 inches of mercury, in other words, 101.325 kPa) (ASCE Manual No. 74, 2010).

The gust response factor is the adapted version of the original Davenport gust response factor to the 3-sec gust wind speed. Gust response factor values for wires (both conductor and ground wires) and the structures can be obtained by the following equations:

$$G_W = \frac{1+2.7E\sqrt{B_W}}{K_v^2} \tag{2.28}$$

$$G_t = \frac{1+2.7E\sqrt{B_t}}{K_v^2} \tag{2.29}$$

The value of E, B_w and B_t are calculated as follows:

$$E = 4.9\sqrt{\kappa}\left(\frac{10.0554}{Z_h}\right)^{\frac{1}{\propto_{FM}}} \tag{2.30}$$

$$B_W = \frac{1}{1+\frac{0.8S}{L_S}} \tag{2.31}$$

$$B_t = \frac{1}{1+\frac{0.56Z_h}{L_S}} \quad (2.32)$$

where;

Z_h : effective height of the wire for the calculation of G_w in meters

S : design wind span of the wires, in meters

K_v : 1.43, the ratio of the 3-sec gust wind speed to the 10-min average wind speed

α_{FM} : power law exponent

κ : surface drag coefficient

L_S : turbulence scale

The power law exponent, surface drag coefficient and turbulence scale values for different terrain roughness categories are provided in ASCE Manual No. 74 (2010).

The force coefficient C_f represents the effects of the shape and the physical characteristics of the network member on the wind force.

2.3.2. Ice Load

In real life; the accretion of ice on conductors don't have to be uniformly distributed along the considered wire. Formation of the ice may have different shapes besides having icicles attached. The ice density may vary from one point to another along the icy conductor as well.

ASCE; specifies the design ice thickness due to the freezing rain conditions, as an equivalent uniform radial thickness along the length of the wire in ASCE Manual No. 74 (2010).

Since the freezing rain is not seen often in Turkey due to the local meteorological conditions and the geographical properties; the provided equations in ASCE Manual No. 74 (2010) are not fully applicable for the electric power transmission networks installed in Turkey.

The most common type of ice accretion in Turkey is the one that occurs due to the humidity in the air. In this study; the design ice thickness will be calculated with the

method that is used by TEİAŞ. This approach will provide a more consistent and suitable calculations for climatic conditions of Turkey. According to this method, the design ice thickness is obtained based on the equations below:

$$d_b = \sqrt{d^2 + 2122q} \tag{2.33}$$

where;

db : icy diameter of wire (mm)
d : bare diameter of wire (mm)
q : unit ice load (kg/m)

$$g_b = q = k\sqrt{d} \tag{2.34}$$

where;

k : ice load coefficient

The ice load coefficient values for different ice regions are provided in TEİAŞ Elektrik Kuvvetli Akım Tesisleri Yönetmeliği (EKATY) document. Figure 2.2 illustrates the ice accretion zones map of Turkey (provided by Mr. Hüseyin Sağlam, TEİAŞ, 2018).

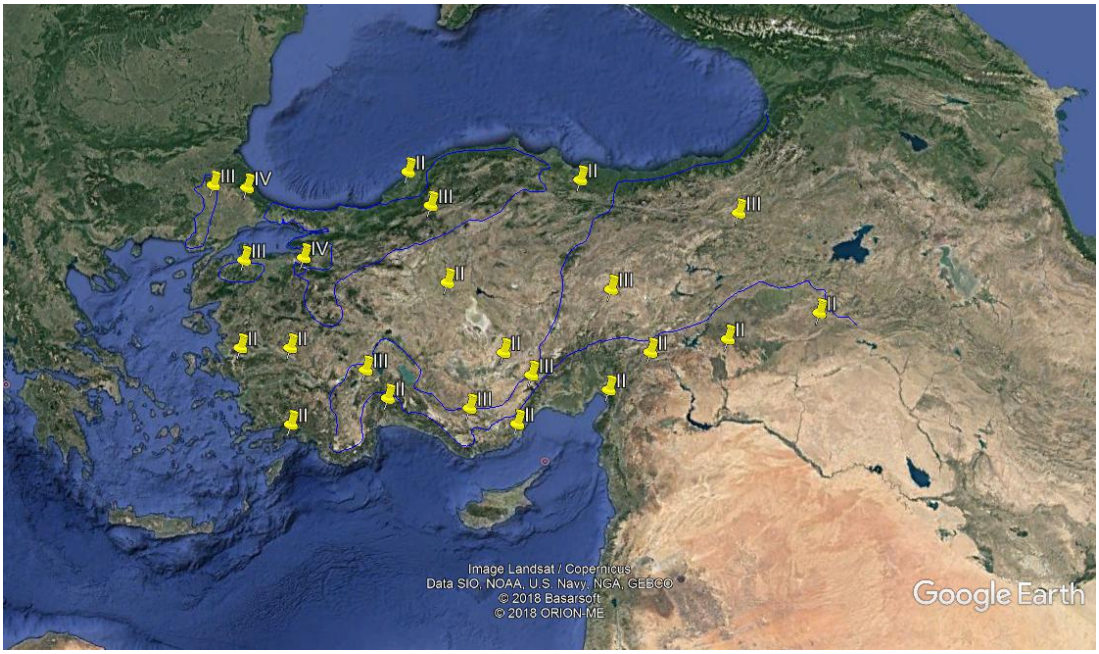

Figure 2.2. Map showing the ice accretion zones of Turkey provided by Mr. Hüseyin Sağlam (TEİAŞ, 2018)

2.4. Characterization of Corrosion and Wear Out Effects

The components of the overhead electric power transmission lines are subjected to various corrosive factors and harsh conditions over the years. These factors cause some parts of the components; especially the insulator casings of the conductors, to become defective gradually. Once the defects start appearing, the energy that flows through the wires starts ionizing the air around them and if this situation continues without any maintenance or repair, then these defects start causing arcs. The ionization of the air around such defective parts of the conductors is called the "corona effect".

Power transmission companies check transmission lines for such defects within certain time periods. Their method of performing this inspection is to use a helicopter which has both HD and UV cameras installed on board. While flying over the lines, the HD camera observes if there exist any unwanted objects around the components, such as a large tree growing under the overhead wires. Besides this, the UV camera

searches for possible corona discharges along the lines. The UV cameras can detect the ionized air due to the corona effect, as the firework-like sparks occur around the defective parts.

Any visual evidence of corona or the electric arcs (the traces of the burnt material, etc.) means that the failure risk of the conductor cable at the defective point is very high. Such risks will be evaluated as the decreasing mechanical resistance of the considered components.

The overhead lines are checked against the corona risks periodically. In this study; the random occurrences of the corona events over the different return periods, will be modeled by the Poisson distribution, the probability density function of which is given below:

$$P(X = x) = \frac{e^{-\lambda}\lambda^{x}}{x!} \tag{2.35}$$

where;

X : number of occurrences in a given time interval
λ : mean number of occurrences in a given time interval

CHAPTER 3

BEHAVIOUR OF ELECTRIC POWER TRANSMISSION NETWORK COMPONENTS UNDER MULTI-HAZARDS

The power transmission network considered in this study is composed of various types of components like transmission towers, conductor cables and transformer stations. Each one of them has a different architecture and design due to their expected role in power transmission. These differences lead them to react against environmental loads in various ways and within various tolerance limits. In this chapter, the mechanical resistance of each component under the mentioned loads will be investigated in terms of their fragility functions.

3.1. Fragility Functions

The probability distribution of the mechanical resistance capacities of the network components against various levels and types of environmental loads (seismic loads, wind pressure, tension due to the ice accretion, etc.) are defined by the fragility functions.

Fragility functions represent the corresponding cumulative probabilities of the resistance levels by which the considered component remains functional under the natural loads.

The lognormal cumulative distribution function (CDF) is one of the most common forms of a fragility function. The general form of this function is as follows:

$$F_d(X) = P(D \geq d|X = x) \tag{3.1}$$

$$F_d(X) = \Phi\left(\frac{\ln(x/\theta_d)}{\sigma_d}\right) \tag{3.2}$$

where;

D : uncertain damage state of a particular component

$\Phi(.)$: standard normal cumulative distribution function

θ_d : median capacity of the component to resist damage state d

σ_d : the standard deviation of the natural logarithm of the capacity of the component to resist damage state d

3.2. Behaviour of Substations Under Seismic Loads

Substations, which refer to the transformer stations in the context of this thesis, are complex facilities including one or more transformers, the technical specifications of which depend on the needs of the local distribution network paths that are fed by them.

Their role of being the main passage locations of the power flow from the previous parts of the network to the rest of them, requires them to be designed as durable as possible. Due to this importance, their critical components are designed to be backed up by the alternative ones that stand by in case of a need to intervene.

SYNER-G D 3.12 (2013) document states the reasons that may cause damage on the sub-stations due to the results of the hazardous forces. These conditions can cause problems by affecting the structural integrity of the sub-stations in various ways by leading individual or cascading hazards which are explained in detail in the document as well. The effects of the hazardous loads on the main vulnerable parts of the substations are classified in the considered document with respect to the affected parts of them as well.

Different percentage classes of the damage are also related to their corresponding damage states as complete, extensive, moderate and minor damage states. While the substations subjected to minor and moderate damage are considered to lose some of their power flow but remain operational without repair, the ones subjected to extensive damage needs to be repaired to be able to keep functioning properly. Since the level of the remaining power flow after the hazard is not investigated within the context of this thesis, the only focused damage state will be the complete damage state with zero

power flow. Since such a state represents the occurrence of complete failure in all four component classes, the substation totally loses its functions and can not become functional again even with a repair operation.

The individual probabilistic evaluation of the reliability of a transformer station under seismic load is a very complex task. It requires considering so many different types of sub-components and back-up procedures besides highly specified knowledge of electrical engineering. Such a task may need to be covered by an independent research itself.

Instead of doing this, it is preferred to approach the substations as the single individual components of the electric power transmission network by ignoring their inner complexity within the context of this study. In fact, this approach is quite fair since this reliability study pays attention to the significantly powerful seismic shocks, due to the damage of which, even the backup components can be expected to become damaged. In this study, the substations will be assumed to be affected only by seismic shocks.

The seismic demand handling capacity of the substations is proposed in the literature by the log-normal fragility function and the parameters of this function are classified with respect to the input voltage level that they are operated on. Since the substations are assumed to be single structures and their sub-components are ignored in this study, they will be assumed to survive as long as they do not lose their connectivity to the rest of the network due to the loss of their structural integrity.

A seismic fragility function, the parameters of which were derived by Oikawa et al. (2001) by estimating the median capacity of 8 transformer stations which are designed and manufactured for voltages higher than 187 kV will be used for the case study in Chapter 5. Table 3.1 shows the seismic fragility parameters of those 8 transformer stations and the overall parameters for transformer stations. Damage ratio is obtained

by dividing the number of failed equipment by the total number of equipment of the same type. Damage ratio in the parentheses, in other words the values 0.95 and 0.05, was regarded from the original values, 1 and 0 by Oikawa et al. (2001).

Table 3.1. *Seismic fragility parameters for transformer substations (Oikawa et al., 2001)*

Name of Substation	Observed or Estimated Peak Ground Acceleration [Gal]	Damage Ratio	Estimated Median Capacity [Gal]
Shin-Kobe	584	(0.95)	362
Itami	550	0.5	550
Nisi-Kobe	350	0.25	426
Yodogawa	300	(0.05)	483
Kobe	275	0.5	275
Kita-Toyonaka	250	(0.05)	403
Seidan	175	0.333	198
Nishi-Kyoto	129	(0.05)	208
Representative Median Capacity (Gal)			342
Logarithmic Standard Deviation			0.357

3.3. Behaviour of Transmission Towers Under Seismic and Ice-Wind Loads

Transmission towers are the support structures which are erected consecutively along the overhead power transmission lines. They are erected to carry the weight of conductor cables of high voltage overhead lines and keep them high enough from the ground to provide safe ground clearance.

Towers are designed in a variety of shapes and sizes to resist the expected natural forces in the considered region. They need to survive under different kinds of loads. The bodies of the towers are installed into the surface soil which means that they are vulnerable to the accelerations of the ground due to the seismicity. In addition, the whole body of them are open to the wind pressure which can bend or break the towers partially or can even uproot them in extreme cases. It is also possible to consider the expected atmospheric ice accretion on the towers as another hazardous condition. The accumulated ice extends the area which is subjected to the wind pressure besides

causing extra gravitational load. Since the fractional increase in overall projected area due to ice accretion is small for pole sections, as it is mentioned in ASCE No. 74 (2010), it will be ignored together with its additional effect on the total weight in this study.

Although the towers are designed as resistant as possible to the expected severity of the natural events, they are still vulnerable to the unexpected limit state exceedances. The transmission towers will be assumed to be vulnerable against seismic load and wind pressure in this study. The log-normal fragility function parameters given by Oikawa et al. (2001) after evaluation of the critical damage of transmission towers in Kobe region in each seismic intensity scale defined by the Japan Meteorological Agency (JMA) will be used for the seismic reliability evaluation of the transmission towers in the case study. The parameters for each seismic intensity scale and the overall parameters for the towers are given in Table 3.2. Damage ratio in the parentheses, in other words the values 0.95 and 0.05, was regarded from the original values, 1 and 0 by Oikawa et al. (2001).

Table 3.2. *Seismic fragility parameters for transmission towers (Oikawa et al. (2001)*

Seismic Intensity Scale Defined by the Japan Meteorological Agency	Number of Transmission Towers	Number of Damaged Towers	Damage Ratio	Estimated Peak Ground Acceleration	Estimated Median Capacity [Gal]
VII	53	0	(0.05)	800	1,354
VI	2,462	35	0.0142	400	807
V	94	0	(0.05)	250	423
Representative Median Capacity [Gal]					733
Logarithmic Standard Deviation					0.48

Although many different types of transmission towers are in use in and around Bursa region, it will be assumed that only one type of tower is erected along the paths of the

entire network. The “Single Circuit PB Type Suspension Tower” is amongst the most commonly used ones to carry the overhead lines in the transmission system of Turkey.

In this study, two different wind and ice related failure modes will be investigated. Extreme wind conditions without any ice accretion will be the first failure mode and the extreme wind force on icy surfaces of the transmission structures will be the second one. Detection of the wind pressure resistance limits of the mentioned towers (which are assumed to have 400 meters of wind span) against the wind pressure on the tower itself and the extra load applied on the towers due to the wind pressure on the conductor cables, requires a structural analysis to be conducted.

The structural analysis of the 154kV PB type suspension tower is conducted by Prof. Dr. Oğuzhan Hasançebi using PLS-TOWER (Power Line Systems Inc., 2015) software under extreme wind conditions both with and without ice accretion.

Figure 3.1 illustrates the structural analysis results when there is no ice accretion. The red colored elements are the ones which failed to resist and caused the whole structure to fail as soon as the wind pressure exceeded 72 kg/m^2. The analysis results of all the beams and elements of the tower are given in Table A1 in Appendix A.

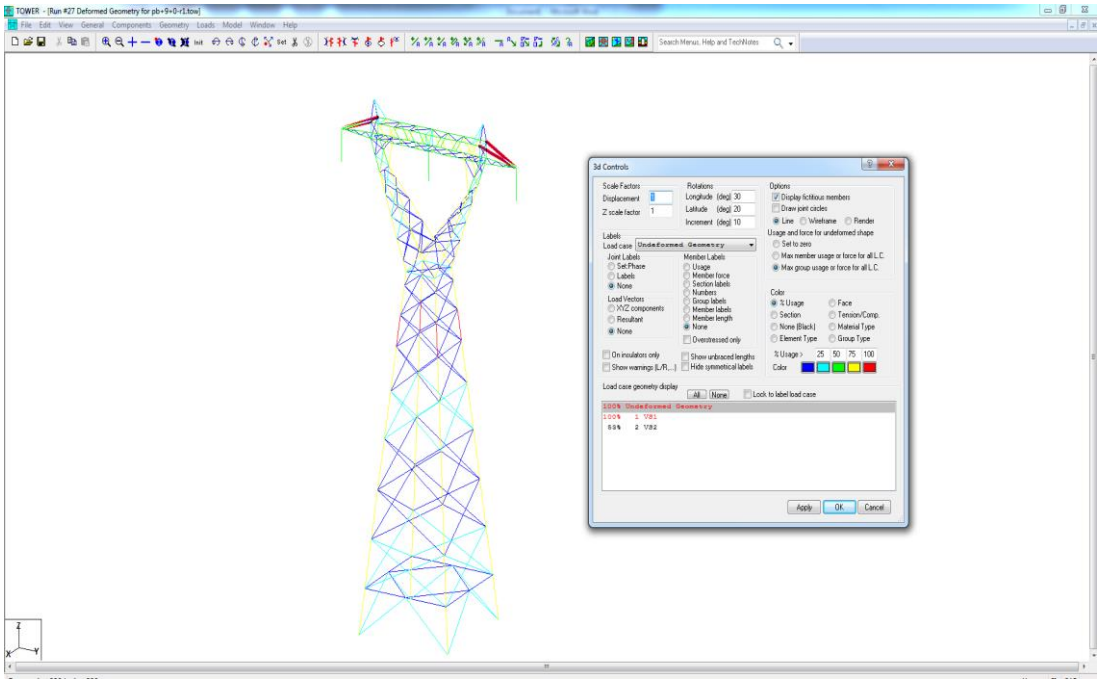

Figure 3.1. The structural analysis result of 154 kV PB type suspension tower under extreme wind conditions

Figure 3.2 illustrates the structural analysis results when there is ice accretion on both the tower itself and the conductor cables within 400 meters of wind span. Since these types of towers carry a single circuit, they support three conductor cables. Each of the conductor cables are assumed to be 1272 MCM Pheasant which is one of the most common conductor cable types in use for the overhead power transmission in Turkey. This type of conductors are resistant against almost 19 tons of tension and as a result of this, in both scenarios the towers failed before the cables break-off. Similar to the previous analysis, the red colored elements are the ones which failed to resist and caused the whole structure to fail as well, as soon as the wind pressure exceeded 30 kg/m^2. The analysis results of each element and beam is also available in Table A2 in Appendix A.

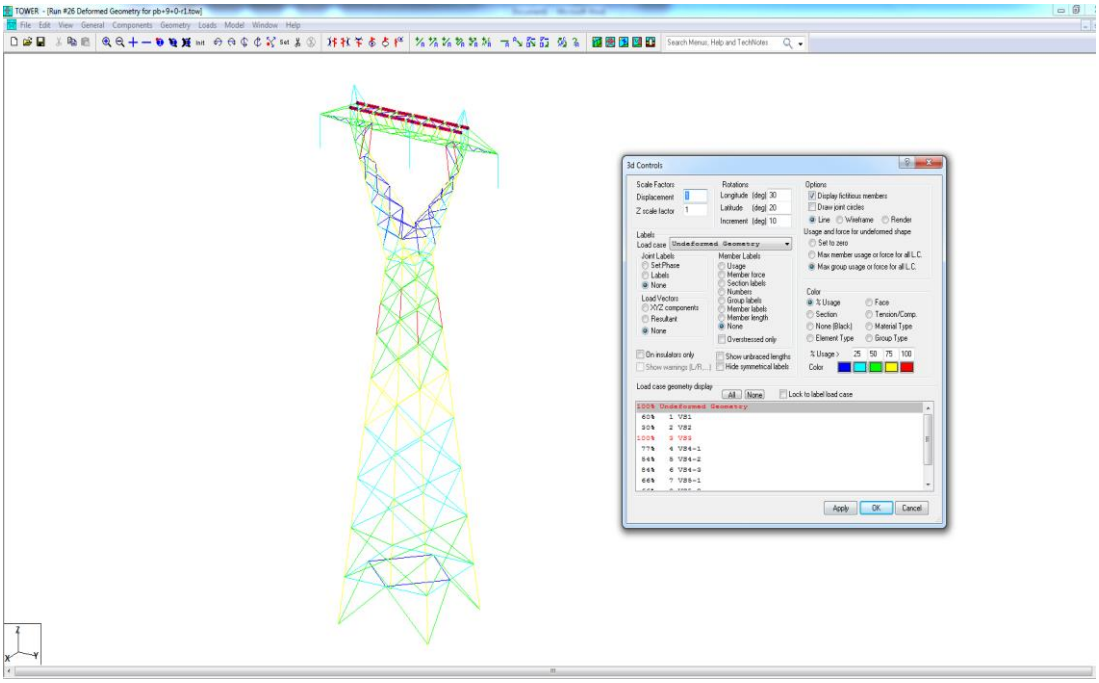

Figure 3.2. The structural analysis results of 154 kV PB type suspension tower under extreme wind and ice accretion conditions

3.4. Behaviour of Overhead Conductor Cables Under Ice-Wind Loads

Transmission of the high voltage electricity is provided by specifically designed aluminum core steel reinforced (ACSR) cables in Turkey. There are many different types of ACSR cables in the market, each one of which is designed specifically to meet different requirements.

The first thing that the cables should stand against, is their own weight. This weight create downward force due to the gravity effect on the lines. Long distance transmission means that the lines should pass through the regions with a variety of climatic conditions as well. Depending on these conditions (temperature, humidity, wind speed, etc.) the lines may be exposed also to ice accretion. The ice mass around the lines, causes two types of additional tension. The ice mass increase the total weight which must be handled by the cable. Besides this, the accreted ice increases the wind pressure by increasing the total area and causes extra wind force.

Since the ACSR cables are industrial products, the force that they can handle without breaking off is clearly calculated and available in product catalogs for every type of them. Comparison of these strength values with the force that they are expected to be exposed to, gives us a clear idea about the behaviour of the lines under the mentioned loads.

ASCE No. 74 (2010) provides information about the possible failure reasons of the transmission line components. These are classified as natural phenomena, man made causes, structural deficiencies, conductor, ground-wire and hardware deficiencies and construction related causes.

The hazardous natural loads are mainly caused by seismic activity (ground acceleration, liquefaction, landslides), atmospheric conditions (ice accretion, wind pressure, flooding due to extreme precipitation and combination of them) and mass movements (avalanches, ice movement, etc.). Two of them amongst those, namely wind pressure and atmospheric ice accretion will be considered as the potential hazards for the overhead conductor cables in this thesis.

The power grid components may also be damaged due to intentional or unintentional human activities. These types of failure occurrences are beyond the scope of this study. The research about the spatial distribution and intensity of such activities and the related predictions is itself an individual study field which overlaps with social sciences as well.

3.5. Behaviour of Transmission Lines Subjected to Corrosion and Wear Out

As the time passes, fatigue may occur on the structure of the conductors due to various factors like chemical contaminants, corrosion, long term environmental loads and the sudden and temporary flows of extra high level voltages.

Wear out yields to small defects on the conductors which cause them to lose their structural strength and to become weaker against the structural tension. Such defects also create ionisation around them and this phenomena is detectable by the ultraviolet

cameras. Figure 3.3 illustrates the corona effect which is seen as tiny sparks around the conductor as follows (https://www.ulirvision.co.uk, 2018):

Figure 3.3. UV image of a corona discharge on a power transmission line

In this study, such defects will be considered as a factor which decreases the resistance values of the conductor cables within spatial and temporal resolution. A hypothetical assumption will be established about the number of locations at which the corona discharges are detected within a year and within a certain distance. Then these discharges will be assumed to be distributed according to the Poisson distribution in spatio-temporal resolution with the rates obtained from the mentioned hypothetical data. The effect of increasing vulnerability on the overall reliability of the network will be investigated separately.

CHAPTER 4

ASSESSMENT OF RELIABILITY OF ELECTRIC POWER TRANSMISSION NETWORKS SUBJECTED TO MULTI-HAZARDS

4.1. Methods of Network System Reliability Analysis

Network reliability concept provides us a probabilistic measure to quantify the expected ability of the infrastructure network to remain operational under extreme loads within various return periods. The components of the infrastructure networks are built based on the type of materials and well engineered structural designs which satisfies the minimum design requirements as mentioned in Chapter 3. The cumulative probability distribution of the amount of maximum mechanical loads that these components can take without losing their structural integrity, also becomes available by the fragility functions as the result of their design processes.

The probabilistic characterization of the environmental forces; to which, the subcomponents are expected to be exposed to within different return periods, is considered in Chapter 2 as well. The probabilistic quantification of the resistances and the loads based on every single component, provides enough data to make a comparison and then obtain the component's failure and survival probabilities. Once these probability values are defined, the reliability of the whole network can be assessed by considering their joint behaviour.

4.1.1. Classical Reliability Approach

Reliability is a probabilistic measure of the expected resilience of a single structural unit or a network composed of many units under various expected load levels within various return periods. A network component remains functional as long as it is able to handle the load that is applied on it. Due to the inherent uncertainties in natural loads and the mechanical resistances of the components, both the resistances and the

loads are represented by random variables. As a result of this approach, the reliability assessment is carried out by quantifying the probabilities of the situations that the value of the random variable "resistance" exceeds the value of the random variable "load".

Reasons for each failure event of a structural unit due to a unique type of a load is classified into the failure modes. The probability distribution functions of loads and resistances which are specific for each failure mode are employed to cover the whole range of the probabilities in the analysis. The following logic is the main structure of the classical reliability approach. For a single failure mode and a specific direction of the forces; the following notation will be used:

R : resistance (capacity) : $R \geq 0$

S : load (demand) : $S \geq 0$

$f_{R,S}(r,s)$: the joint pdf of the random variables R and S

$M = R - S$: the safety margin

A network component remains functional as long as its load-specific resistance is greater than the load. When the load becomes equal or greater than the resistance, the component fails and can not remain functional anymore. Accordingly, the probability that the resistance is greater than the load is called "reliability" while the probability that the resistance is less than or equal to the load is called "risk" as shown below:

$$\Pr(\text{failure}) = \text{Risk} = p_f = \Pr(R \leq S), \qquad M = R - S \tag{4.1}$$

$$\Pr(\text{survival}) = \text{Reliability} = p_s = \Pr(R > S), \quad M = R - S > 0 \tag{4.2}$$

When the random variables load and resistance are not statistically independent, the failure probability of a component, is formulized by the integration of the probabilities in terms of the joint density functions as long as the resistance is less than the load within the whole range of the load domain as below:

$$p_f = \Pr(R \le S) = \iint_{\{\{r,s\};r<s\}} f_{R,S}(r,s)dsdr = \int_0^{\infty}\int_0^{s} f_{R,S}(r,s)drds \tag{4.3}$$

Similarly, when the random variables load and resistance are statistically independent, the failure probability of a component is expressed through the integration given below:

$$p_f = \Pr(R \le S) = \int_0^{\infty}\left(\int_0^{s} f_R(r)dr\right)f_S\, sds = \int_0^{\infty} F_R(s)f_S(s)ds \tag{4.4}$$

The failure probability of a network component can also be written with respect to the distribution function of the load as below:

$$p_f = \int_0^{\infty}\left[\int_r^{\infty} f_S(s)ds\right]f_R(r)dr = \int_0^{\infty}[1 - F_S(r)]f_R(r)dr \tag{4.5}$$

In probabilistic reliability assessment studies, both of the random variables resistance and load are often assumed to be normally distributed. In some cases, the resistance parameters of the component may also be available in the form of a Log-normal distribution parameters. When both the resistance and load are normally distributed random variables with means (μ_R, μ_S) and the standard deviations (σ_R, σ_S), the probabilities of survival and failure are evaluated by the standard normal cumulative distribution function as follows:

$$p_f = \Pr(R < S) = \Pr(R - S < 0) = \Pr(M < 0) \tag{4.6}$$

$$\Rightarrow \Pr\left[Z < \frac{0-(\mu_R-\mu_S)}{\sqrt{\sigma_R^2+\sigma_S^2}}\right] = \Pr\left[Z < -\left(\frac{\mu_R-\mu_S}{\sqrt{\sigma_R^2+\sigma_S^2}}\right)\right] = \Pr\left[Z \ge \frac{\mu_R-\mu_S}{\sqrt{\sigma_R^2+\sigma_S^2}}\right] \tag{4.7}$$

$$p_f = 1 - \Phi\left(\frac{\mu_R-\mu_S}{\sqrt{\sigma_R^2+\sigma_S^2}}\right) \quad \text{and} \quad p_S = \Phi\left(\frac{\mu_R-\mu_S}{\sqrt{\sigma_R^2+\sigma_S^2}}\right) \tag{4.8}$$

where;

Z : standard normal variable

Φ (.) : cumulative standard normal probability distribution function

When resistance (capacity) and load (demand) are normally distributed random variables, then the graphical representation of their density functions and the regions that represent the failure and the survival of the considered component is expected to be formed as follows (Özcan, 2016):

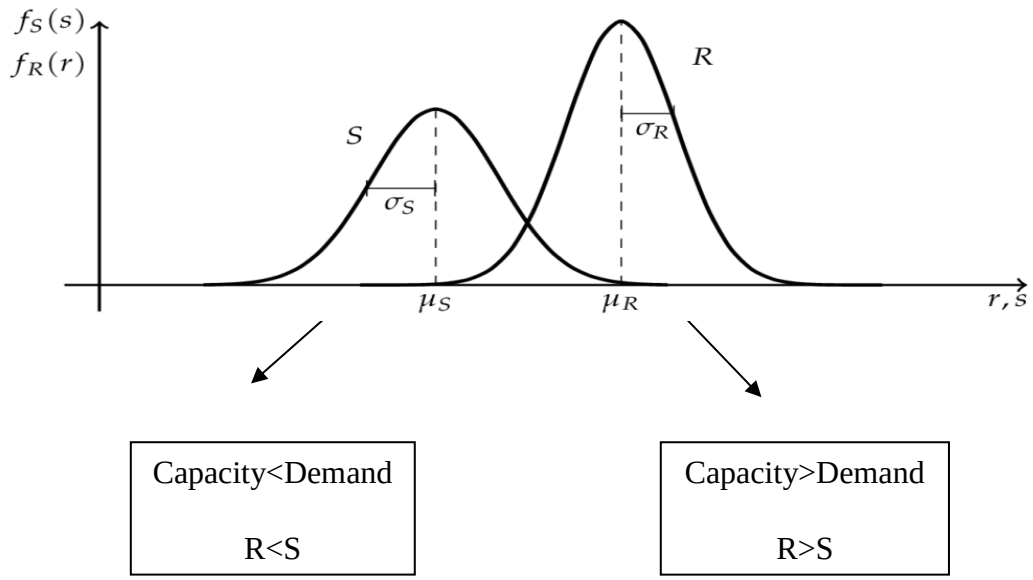

Figure 4.1. Survival and failure regions for capacity and demand which are normally distributed (Özcan, 2016)

When resistance and load are Log-normally distributed with means (λ_R, λ_S) and standard deviations (ξ_R, ξ_S), the probabilities of survival and failure are evaluated by the cumulative standard normal distribution similarly to the previous case, as follows:

$$p_f = \Pr(R \leq S) = \Pr(R - S \leq 0) = \Pr(M \leq 0) \tag{4.9}$$

$$p_f = \Pr(R \leq S) = \Pr\left(\frac{R}{S} \leq 1\right) = \Pr\left(\ln\frac{R}{S} \leq 0\right) = \Pr(\ln R - \ln S \leq 0) \tag{4.10}$$

$$p_f = 1 - \Phi\left(\frac{\lambda_R - \lambda_S}{\sqrt{\xi_R^2 + \xi_S^2}}\right) \tag{4.11}$$

4.2. Reliability of Structural Systems

4.2.1. Multiple Failure Modes

Lifeline networks and their components are subjected to various environmental harsh and hazardous conditions, under which, they have to keep functioning. Each type of the environmental load has the potential to force the components beyond their mechanical resistance capacities and lead them to fail by the loss of their structural integrity. The failures due to each type of those causes are called "failure modes". A component remains functional and reliable as long as it survives in all failure modes without any exceptions as follows:

$$p_S = \Pr(\bar{M}_1 \cap \bar{M}_2 \cap \dots \cap \bar{M}_k) \tag{4.12}$$

where;

p_S : survival probability

M_i : i^{th} failure mode

$\bar{M}_i$: survival in i^{th} failure mode

Conversely, the component failure occurs when it does not survive in at least one mode as follows:

$$p_f = \Pr(M_1 \cup M_2 \cup \dots \cup M_k) \tag{4.13}$$

Load effects on the component and capacities in different failure modes R_i, can be assumed to be statistically independent and be computed by integrating the probabilities as follows:

$$p_S = \int_0^\infty \left[\int_{C_1 S}^\infty \int_{C_2 S}^\infty \dots \int_{C_k S}^\infty f_{R_1 \dots R_k}(r_1, \dots, r_k) dr_1 \dots dr_k\right] f_S(s) ds \tag{4.14}$$

where;

$C_i S$: load effect in the i^{th} failure mode

Computing the component reliability based on different failure modes by a "k-fold" integration as above, may not always be the most practical way. Such an integration

requires complex mathematical operations. In addition, the distributional parameters for every single density function need to be identified before the calculation. The sufficient amount of data may not always be available for specifying the probability distributions for the basic parameters. Another and a practically more useful way is to establish probabilistic bounds instead of computing the exact probability values. These bounds are known as the "fundamental inequalities of reliability" and they can be established according to different assumptions as illustrated below.

4.2.1.1. Bounds on Component Reliability Considering k-Failure Modes

i) Failure Modes are Perfectly Correlated

When the failure modes are assumed to be perfectly correlated, the survival probability of the considered component is equal to the minimum survival probability amongst all failure modes:

$$p'_S = \min\{p_{S_1}, p_{S_2}, \dots, p_{S_k}\} \quad p'_S \geq p_S \tag{4.15}$$

where;

p_{S_i} : survival probability in the i^{th} mode

The survival probability of the component in i^{th} failure mode is computed by the equation below:

$$\Pr(\bar{M}_i) = \int_0^\infty \int_{C_i S}^\infty f_{R_i}(r_i) dr_i f_S(s) ds \tag{4.16}$$

Equation (4.16) represents the integration of the corresponding probabilities that the resistance exceed the load effect for the considered component in i^{th} failure mode under the whole range of the considered load effect.

ii) "k" Modal Resistances are Statistically Independent

Under the assumption of statistical independence of the modal resistances, the survival probability of the component equals to the integration of the multiplication of modewise probabilities, the resistances of which exceed the corresponding loads, under the whole range of load effects as follows:

$$p_S'' = \int_0^\infty \left[\int_{C_i S}^\infty f_{R_1}(r_1)dr_1 \int_{C_2 S}^\infty f_{R_2}(r_2) \dots \int_{C_k S}^\infty f_{R_k}(r_k)\right] f_S(s)ds \qquad (4.17)$$

iii) Modal Resistances and Modal Loads are Statistically Independent

When the modal resistances and the modal loads are assumed to be statistically independent, the survival probability of the component is computed by the following equation:

$$p_S^* = \prod_{i=1}^k \int_0^\infty \int_{C_1 S}^\infty f_{R_1}(r_1) f_S(s) dr_1 ds = p_{S_1} p_{S_2} \dots p_{S_k} = \prod_{i=1}^k p_{S_i} \qquad (4.18)$$

In such a case, the survival probability is equal to the multiplication of the modewise survival probabilities of the considered component.

iv) Fundamental Inequalities of Reliability

Finally, the probabilistic bounds on the component based survival probability, in other words the "fundamental inequalities of reliability" appear as follows (Yücemen, M. S., Unpublished Lecture Notes of CE589, (2018)):

$$p_S' \geq p_S \geq p_S'' \geq p_S^* \qquad (4.19)$$

$$p_f' \leq p_f \leq p_f'' \leq p_f^* \qquad (4.20)$$

where;

$$p_S^* = \prod p_{S_i} = \prod (1 - p_{f_i}) \qquad (4.21)$$

$$p_f^* = 1 - \prod (1 - p_{f_i}) = 1 - (1 - p_{f_1})(1 - p_{f_2}) \dots (1 - p_{f_k}) \qquad (4.22)$$

4.2.1.2. Reliability Considering the System Damage

Component reliability and network reliability concepts are applied based on a very similar logic. While the reliability of a single component is constructed on its survival in different failure modes, the reliability of the whole network is constructed on the survival of its components. The event of the failure of at least one element is called system damage. System damage does not always have to cause the whole network to collapse. The relation between the system failure and the failure of its elements (in other words, the system damage), depends on the interconnection types amongst the network elements.

i) Reliability of a Statically Determinate System (Series System)

If a system does not have any redundancy or any additional elements to support it in case of the failure of some components, then the network remains functional as long as all of its components are able to survive under the considered loads. Since there is no alternative path, the failure of even one of its elements causes the whole infrastructure to collapse. Such systems are called "statically determinate systems". The interconnection type which forms a single flow path by connecting the components consecutively without any redundancy is called "series connection". Series connection is an example of a statically determinate network as illustrated below:

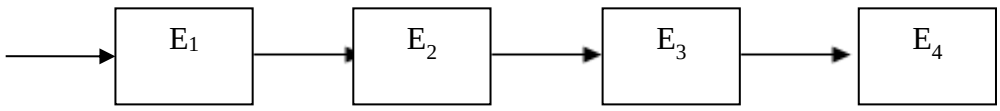

Figure 4.2. Series system

Since the failure of at least one of the components E_1, E_2, E_3 or E_4 causes the whole network to collapse, series systems are also called "weakest link systems", and the

system damage is equal to the system failure in statically determinate networks as follows:

$$p_{d_S} = p_{f_S} \tag{4.23}$$

where;

p_{d_S} : probability of system damage
p_{f_S} : probability of failure (collapse) of the system

ii) Reliability of a Statically Indeterminate System (Parallel System)

The networks that have redundant parts and/or alternative paths are called statically indeterminate systems. The components of such a system are interconnected in a way that they let the network to have alternative elements and /or paths which allow the whole system to remain functional in case of the collapse of some of their components. These types of systems are called "parallel systems. In Figure 4.3 elements E_2 and E_3 are connected in parallel:

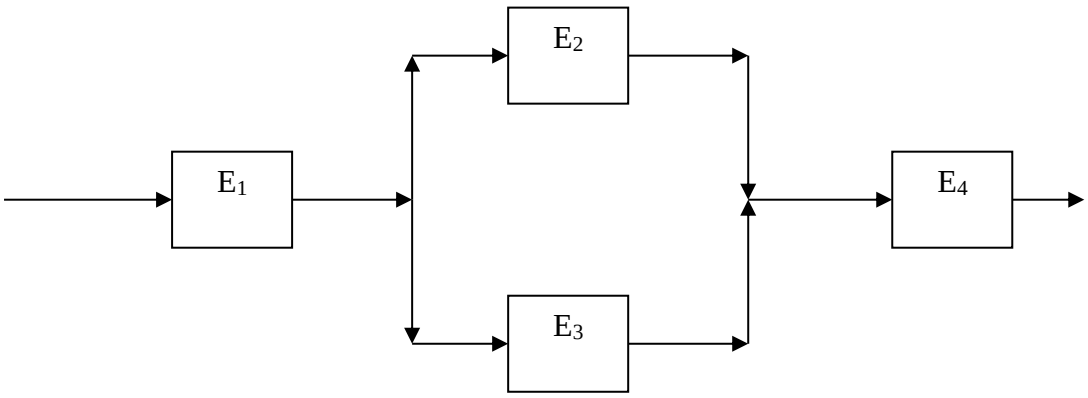

Figure 4.3. Parallel and series connections

In the network above, the collapse of one of the components E_2 and E_3, in other words the system damage, may reduce the flow, but does not interrupt it completely, and the system keeps functioning.

4.3. First Order Second Moment (FOSM) Method

Reliability of a structure is basically determined by the comparison of the load that a structure is exposed to and the mechanical resistance of it in the considered failure mode. The resistance and load variables in a specific failure mode are the components of the limit state of that mode. They are called "basic variables" and represented by the vector $\widetilde{X} = (X_1, \dots X_n)$. The balance between the load and the corresponding resistance, in other words the state of the system, can be explained by the limit state and denoted by the limit state function $g(\widetilde{X})$ as specified below:

$$M = g(\widetilde{X}) = g(X_1, \dots, X_n) \tag{4.24}$$

$g(\widetilde{X})$ is actually a mathematical equivalent of a surface that separates the safe region within which the state of the system, in other words the value of $g(\widetilde{X})$ is positive, from the failure region with the zero or negative values of $g(\widetilde{X})$.

When the safety margin $M = a_0 + a_1X_1 + \cdots + a_nX_n$ is linear, reliability of the structure in the considered failure mode can also be defined by a proportion called "reliability index" which is denoted by β_C (Cornell, 1969). As the value of the reliability index increases, the structure becomes more reliable.

$$\beta_C = \frac{\mu_M}{\sigma_M} \tag{4.25}$$

$$\mu_M = a_0 + a_1\mu_1 + \cdots + a_n\mu_n \tag{4.26}$$

$$\sigma_M^2 = a_1^2\sigma_1^2 + \cdots + a_n^2\sigma_n^2 + \sum_{i=1}\sum_{j=1_{i\neq j}} \rho_{ij}\, a_i a_j \sigma_i \sigma_j \tag{4.27}$$

where,

ρ_{ij} : the correlation coefficient between basic variables X_i and X_j .

$a_0, a_1, \ldots, a_n$: constants

μ_M : mean safety margin

σ_M^2 : variance of the safety margin

σ_i : standard deviation of i^{th} basic variable

μ_i : mean of i^{th} basic variable

When the limit state function is nonlinear, more advanced methods like the FOSM Approximation (Mean Value Method) are required for obtaining the mean safety margin μ_M, the standard deviation of safety margin σ_M and finally the reliability index β by the linearization of $g(\tilde{X})$.

FOSM approximation proposes that a nonlinear limit state function can be linearized and approximated by applying Taylor series expansion around the mean vector of its basic variables. For a nonlinear limit state function $M = g(\tilde{X}) \cong g(X_1, X_2, \ldots, X_n)$, Taylor series expansion is applied and evaluated at the mean vector $\tilde{\mu} = (\mu_1, \ldots, \mu_n)$ of basic variables as follows:

$$g(\tilde{X}) \cong g(X_1, \ldots, X_n) + \sum_{i=1}^{n}(X_i - \mu_i)\left(\frac{\partial g}{\partial X_i}\right)_{\tilde{\mu}} + \frac{1}{2}\sum_{i=1}^{n}\sum_{j=1}^{n}(X_i - \mu_i)(X_j - \mu_j)\left(\frac{\partial^2 g}{\partial X_i\, \partial X_j}\right)_{\tilde{\mu}} \quad (4.28)$$

Then by keeping only the first order terms, the approximate value of mean μ_M and variance σ_M^2 are calculated by Equations (4.29) and (4.30).

$$\mu_M \cong g(\mu_1, \ldots, \mu_n) \quad (4.29)$$

$$\sigma_M^2 \cong \sum_{i=1}^{n}\left(\frac{\partial g}{\partial X_i}\right)_{\tilde{\mu}}^2 + \sum_{i=1}^{n}\sum_{j=1}^{n}\left(\frac{\partial g}{\partial X_i}\right)_{\tilde{\mu}}\left(\frac{\partial g}{X_j}\right)_{\tilde{\mu}} \mathrm{Cov}(X_i, X_j) \quad (4.30)$$

When the basic variables are statistically independent, Equation (4.30) becomes:

$$\sigma_M^2 = \sum_{i=1}^{n}\left(\frac{\partial g}{\partial X_i}\right)_{\tilde{\mu}}^2 \sigma_i^2 \quad (4.31)$$

Equation (4.31) is also called the "Error Propagation Equation" with sensitivity coefficients $\left(\frac{\partial g}{\partial X_i}\right)^2_{\tilde{\mu}}$ and used for adding up the uncertainties coming from each basic variable taking into consideration of the failure function with respect to each basic variable.

4.4. Spatial Correlation

Random functions or in other words, stochastic processes can simply be defined as the families of random variables. The random variables which form such a process X(t), are identified as the individual members of that collection by the indexes that are elements of the index set T and denoted by t. Each fixed (or indexed) value of a random function with respect to a time and/or a space window defined within the index set (parameter space) T, in other words a single value of the metric t, yields a random variable.

In such a system, X(t) represents the state of the system, in other words a sample path, at a fixed value of a member "t" of the corresponding parameter space T. All possible values that X(t) can take form the state space E. Both the parameter space T and the state space E can be either discrete or continuous. Since they are the reduced forms of the random function into a state through an index, each sample path of the process behaves like a sample taken from a population and called "realization". As mentioned by (Yücemen, 1989(b)), random functions can be classified according to two criteria as follows:

i. Discrete or continuous character of the parameter t and the state of the random function X(t), which can be described as the outcome of the random variable associated with the parameter t.
ii. Dimensions of t and X. In other words whether t and X are scalars or vectors.

4.4.1. Spatial Processes

Spatial processes are the random functions, the index sets $\underset{\sim}{S} = [s_1, s_2, \ldots, s_d]$ of which are composed of spatial coordinates. When indexed by the members of the spatial coordinates set $D \subset \mathbb{R}^d$, they yield a spatial observation $Y(\underset{\sim}{S})$ at the considered location $\{\underset{\sim}{S} \in \mathbb{R}^d\}$. In such a state of a spatial process, while Y stands for the attribute of interest to be measured, $\underset{\sim}{S}=[x,y]^T$ represents the location of this observation. The stochastic processes, the dimension d of the parameter space T of which is greater than 1, are called "random fields".

Mainly, two types of effects, namely first order and second order effects determine the behaviour of the spatial processes. First order effects are the effects which cause changes in the mean of the whole process throughout the space. Differently, second order effects are the effects that cause changes in the values of the considered attributes, due to the changes which are measured in the locations within the close distance. Detection of such a tendency requires some level of correlation between the values of neighbouring locations to be considered. Mixture of these two types of effects is the reason of the deviations in the process from one location to another.

4.4.1.1. Stationarity and Isotropy

The spatial processes, the mean $E[Y(\underset{\sim}{S})]$ and the variance $V[Y(\underset{\sim}{S})]$ of which are constant throughout $\mathbb{R}$, in other words independent from the absolute location, are said to be "stationary" or "homogeneous".

Since the first order effects do not allow local interaction between the neighbouring sites as explained previously, in first order stationarity case, mean, variance and all higher moments are constant and the distribution functions do not change according to the direction or distance. Which means that they remain as they are under rotation and translation. First order stationarity is expressed mathematically as follows:

$$P\,[Y(\underset{\sim}{S}_1) \leq y_1, Y(\underset{\sim}{S}_2) \leq y_2, \ldots, Y(\underset{\sim}{S}_k) \leq y_k] = P\,[Y(\underset{\sim}{S}_1+\underset{\sim}{h}) \leq y_1, Y(\underset{\sim}{S}_2+\underset{\sim}{h}) \leq y_2, \ldots, Y(\underset{\sim}{S}_k+\underset{\sim}{h}) \leq y_k] \quad (4.32)$$

where;

$\underset{\sim}{h}$: lag vector

Differently, the second order effects are based on the local interactions. Besides that the constant mean and constant variance assumptions are still valid in this case, the covariance structure exist as well. In second order stationarity, the covariance structure depends on the distances between the sites and their relative directions with respect to each other but it is still independent from the absolute locations of the considered sites in $\mathbb{R}$ as follows:

$$E[Y(\underset{\sim}{S})] = \mu \text{ and } Cov[Y(\underset{\sim}{S}), Y(\underset{\sim}{S}+\underset{\sim}{h})] = C(\underset{\sim}{h}) \quad (4.33)$$

where,

Cov(.) : covariance function

C(.) : correlation function

When the covariance of a second order stationary spatial process is independent from the relative direction of the locations with respect to each other and only dependent on the distances amongst them, the process is called "isotropic". Isotropy is a widely used assumption in spatial modelling.

4.4.2. Moving Average Processes

While the properties and the variability within a (time and/or space oriented) domain is being analyzed, the aim is mostly to extract results which are representative for the overall investigation. As much as the details of the differences and the variabilities amongst the values of the attributes at different points are focused on, the smoothness of the analysis keeps disappearing. To reach smoother results, a bit more aggregative approach by averaging the attribute values throughout the domain can be employed. Such a method also guarantees the existence of the mean square derivatives of the random functions upon which level excursion and extreme value statistics depend (Vanmarcke, 1983).

When a random process X(t), with mean m_x and standard deviation σ_x, is integrated throughout a certain time and/or a space window T, it yields a local integral process $X_I(t)$ as follows:

$$X_I(t) = \int_{t-T/2}^{t+T/2} X(u)du \tag{4.34}$$

The local integral process which is averaged with respect to the window T, yields a moving average process $X_T(t)$ for a stationary one dimensional spatial process X(t) with a continuous parameter as below:

$$X_T(t) = \frac{1}{T}\int_{t-T/2}^{t+T/2} X(u)du \tag{4.35}$$

While the mean of the moving average process is $E(X_T)=m_x$, the variance of the process is defined by the variance function $\Gamma_x(.)$ of X(t) as:

$$V(X_t) = \Gamma_x(T)\sigma_x^2 \tag{4.36}$$

4.4.3. Variance Function and Scale of Fluctuation

The variance of the moving average process is dependent on the size of the averaging window T. To simplify the assessment of the correlation structure and providing homogeneity, the variance function and the scale of fluctuation concepts were proposed by Vanmarcke (1983). The operation of obtaining the moving average process from a local integral process causes the point variance σ_x^2 to be reduced and the amount of this reduction is represented by the variance function $\Gamma_x(T)$, the square root of which is the reduction factor for point standard deviation. The properties of the dimensionless variance function are as follows:

i. $\Gamma_x(T) \geq 0$
ii. $\Gamma_x(0) = 1$
iii. $\Gamma_x(T) = \Gamma_x(-T) = \Gamma_x(|T|)$

Autocorrelation is a measure which basically represents the level of correlation of a random variable with itself. In time domain it stands for the correlation between the values of a specific random variable at time t and time (t-h). In spatial domain,

similarly, it represents the correlation between the values at location i and its neighbouring location j. Triangular, Exponential and Gaussian correlation functions are amongst the many functions in use to describe the nature of the correlation structure that best describes the data. Although the forms and characteristics of these functions will not be explained within the context of this thesis, a vast amount of information is available in the related literature. The correlation function ρ_x of the spatial process may also be used to define the variance function as follows:

$$\Gamma_x(T) = \frac{1}{T^2}\int_0^T \int_O^T \rho_x(t_1 - t_2)dt_1 dt_2 \tag{4.37}$$

$$\Gamma_x(T) = \frac{2}{T}\int_0^T \left(1 - \frac{\tau}{T}\right)\rho_x(\tau)d\tau \tag{4.38}$$

where,

τ : distance between two locations

For notational convenience, a new function $\Delta(T)$ can be defined as:

$$\Delta(T) = T^2\Gamma_x(T) \tag{4.39}$$

After this simplification, the relation between the variance of the local integral process and the point variance σ_x^2 can also be derived as below:

$$V(X_I) = \sigma_x^2\Delta(T) \tag{4.40}$$

The scale of fluctuation measures the continuity of the strength of the spatial correlation structure with respect to the length of the interval T. If the random function is ergodic in the mean, its scale of fluctuation in terms of the variance function is defined as (Vanmarcke, 1983):

$$\lambda_x = \lim_{T\to\infty} T\Gamma_x(T) \tag{4.41}$$

or,

$$\Gamma_x(T) = \frac{\lambda_x}{T} \text{ when } T \to \infty \tag{4.42}$$

It is also possible to define the scale of fluctuation by the correlation function, but first, the Equations (4.41) and (4.42) should be processed as:

$$\Gamma_x(T) = \frac{2}{T}\left[\int_0^T \rho_x(\tau)d\tau - \frac{1}{T}\int_0^T \tau\rho_x(\tau)d\tau\right] \quad (4.43)$$

Considering that the first moment of the spatial correlation function $\rho_x(.)$ should be finite, by transforming the Equation (4.41), the scale of fluctuation is expressed by the spatial correlation function as follows:

$$\lambda_x = \int_{-\infty}^{\infty} \rho_x(\tau)d\tau \quad (4.44)$$

Table 4.1. shows some common correlation functions, variance functions and the scale of fluctuations (Vanmarcke, 1983).

Table 4.1. *Some common correlation functions, variance functions and scale of fluctuation (from Vanmarcke, 1983). (The table is adopted from (Akkaya, 1995))*

Correlation Function $\rho_x(\tau)$	Variance Function $\Gamma_x(T)$	Scale of Fluctuation λ_x
Triangular $1-\lvert\tau\rvert/a, \quad \lvert\tau\rvert \le a$ $0, \quad \lvert\tau\rvert \ge a$	$1-T/3a, \quad T \le a$ $(a/T)[1-a/3T], \quad T \ge a$	a
Exponential $\exp(-\lvert\tau\rvert/b)$	$2(b/T)^2\left(T/b-1+e^{-T/b}\right)$	2b
Gaussian (Squared Exponential) $\exp[-(\lvert\tau\rvert/c)^2]$	$(c/T)^2\left[(\pi)^{1/2}(T/c)E(T/c)+\exp(-(T/c)^2)-1\right]$	$\left[(\pi)^{1/2}c\right]$
Second Order Auto Regressive $[1+\lvert\tau\rvert/d]e^{-\lvert\tau\rvert/d}$	$2(d/T)\left[2+e^{-T/d}-3(d/T)\left(1-e^{-T/d}\right)\right]$	4d

Here, E(.)=2[F_N (.)-0.5] is the error function where F_N (.) is the standard Gaussian cumulative distribution function

CHAPTER 5

CASE STUDY

5.1. Introduction

In this chapter, a case study will be conducted to illustrate the application process of the theoretical information that has been mentioned in the previous chapters. The structural reliability of an electric power transmission network, the components of which are deployed in and around Bursa province, will be assessed probabilistically under various environmental loads and based on different return periods.

5.1.1. Power Transmission Network

The northern and the southern parts of the electric power transmission network in Bursa region are given in Figures 5.1a and 5.1b below. These two parts are connected at Bursa Industrial Zone Transformer Station.

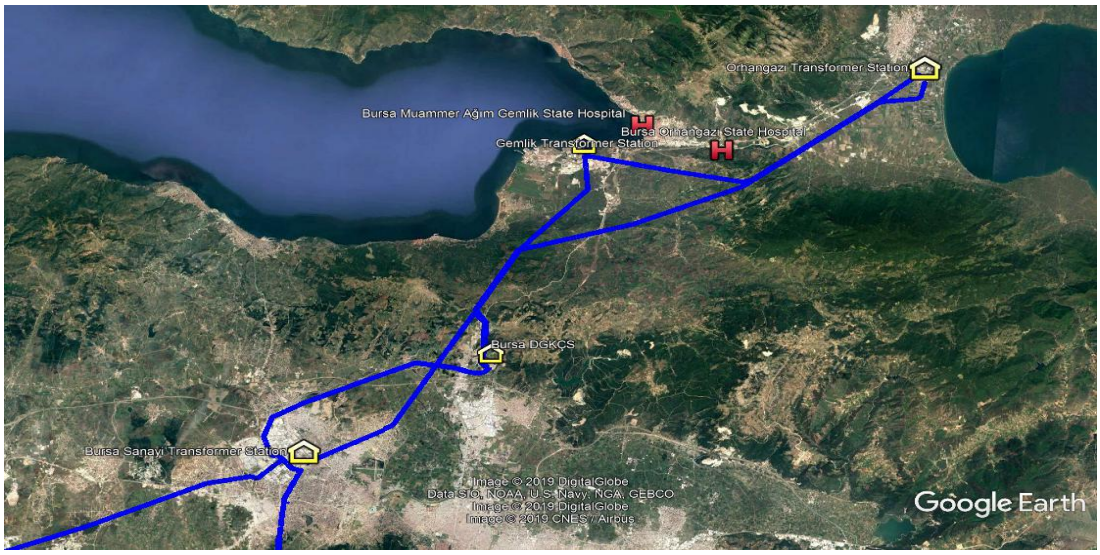

Figure 5.1.a The northern part of the electric power transmission network

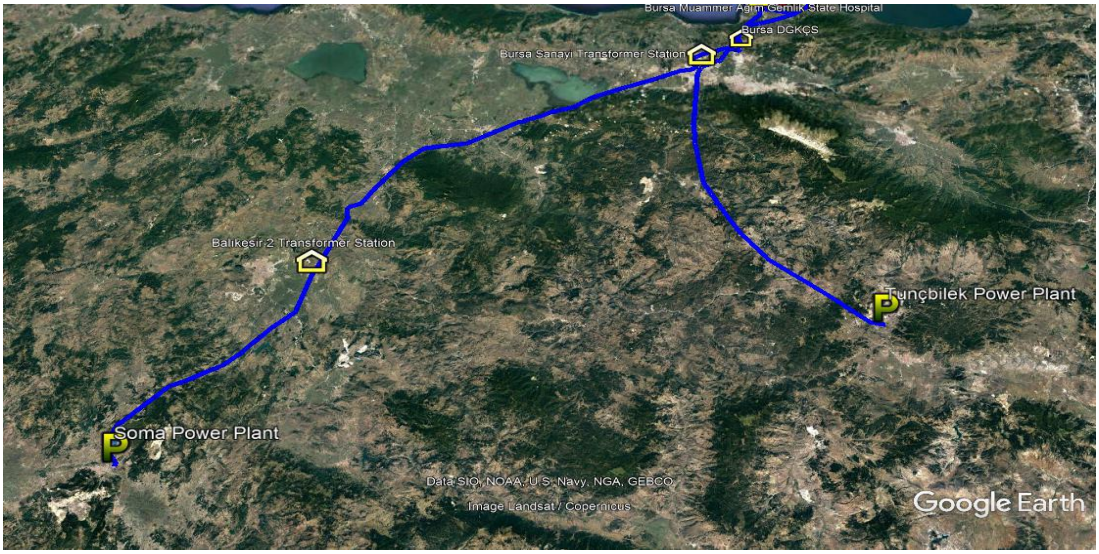

Figure 5.1.b The southern part of the electric power transmission network

This network is composed of five transformer stations (TS), namely, Bursa Industrial Zone, Balıkesir-2, Gemlik, Orhangazi and Bursa Natural Gas Combined Cycle Plant (NGCCP). These will be referred as "substations". The system is mainly fed by two thermic power plants, namely Soma and Tunçbilek. The electricity generated by Tunçbilek power plant is directly transmitted to the Bursa Industrial Zone TS by a 380 kV overhead transmission line. Similarly, the electricity generated by Soma power plant is first transmitted into Balıkesir-2 TS, and then into the Bursa Industrial Zone TS through an overhead 380 kV line as well. The rest of the overhead lines provide 154 kV overhead transmission. One of the transformer stations, Bursa NGCCP, operates both as a power plant and a transformer station. These power plants and transformer stations are interconnected to each other by seven different paths, which in other words are the power lines composed of serially connected 942 transmission towers and the conductor cables between each consecutive couples of them. These transmission towers are erected along the mentioned paths to support the conductor cables and to provide the required ground clearance for them. Table 5.1 shows the substations and the power plants at the beginning and the end points of each path.

Table 5.1. *Start and end points of the paths*

Path Number	Beginning Location	Ending Location
1	Tunçbilek Power Plant	Bursa Industrial Zone TS
2	Soma Power Plant	Balıkesir-2 TS
3	Bursa Industrial Zone TS	Bursa NGCCP
4	Bursa NGCCP	Orhangazi TS
5	Bursa NGCCP	Orhangazi TS (by Gemlik TS)
6	Balıkesir-2 TS	Bursa Industrial Zone TS
7	Bursa NGCCP	Bursa Industrial Zone TS

The components of the entire network are spread throughout 15 districts. Since the network is exposed to various levels of environmental loads due to its widespread coverage, large amount of data collection and processing are needed. But, before that, the geographical location of each network element is required to be detected to plan the borders of the area for which both meteorological and seismic data should be gathered.

Figure 5.2 below, represents the single-line diagram of the power transmission network in and around Bursa. Although there are many transformer stations and power plants in this diagram, the study will not be conducted on the entire network.

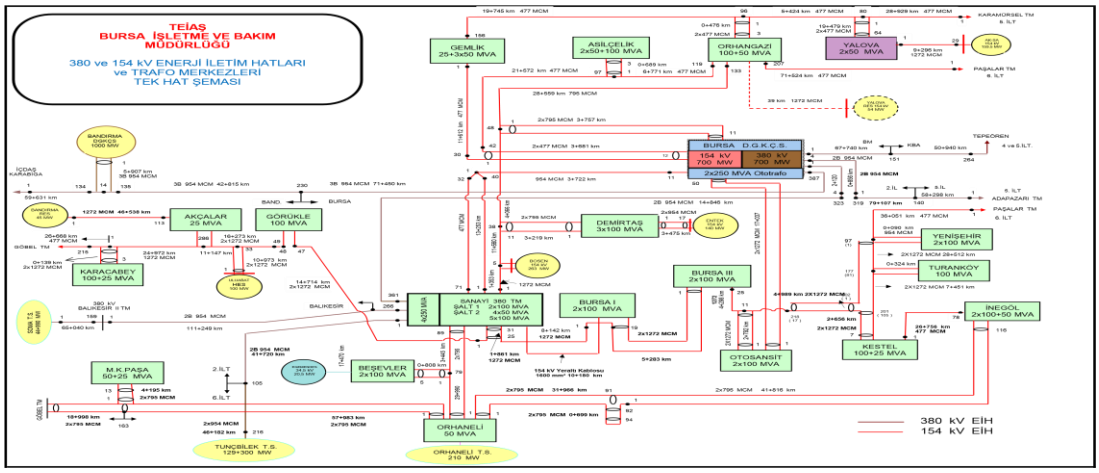

Figure 5.2. Single-line diagram of the power transmission network of Bursa (https://www.teias.gov.tr/bolge/bursa/, Last Access: 2017)

The map of the whole network is provided by TEİAŞ and the latitudes and longitudes of the locations of each transmission tower and transformer station are explored by using Google Earth. The lengths of the conductor segments between each consecutive tower couple are measured on Google Earth as well.

5.2. Data Base

5.2.1 Earthquake Data

The past earthquake records for the rectangular region which is bounded by the latitudes from 38.70°N to 42.10°N degrees and the longitudes from 25.90°E to 31.90°E degrees are taken from Disaster and Emergency Management Authority (AFAD) website. The seismic data is collected for the time interval 01.01.1900-16.05.2018. Once the data is obtained, the magnitudes of all earthquakes are converted into the moment magnitude (M_w) and the ones which are less than 4.0 are removed from the data. In this study, 4.0 is considered as the minimum potentially hazardous magnitude.

The location based peak ground acceleration values are computed by Ez-Frisk 7.52 (Risk Engineering, 2011) software. Figure 5.3 illustrates the fault sources in and around Bursa. The red colored lines represent the active faults.

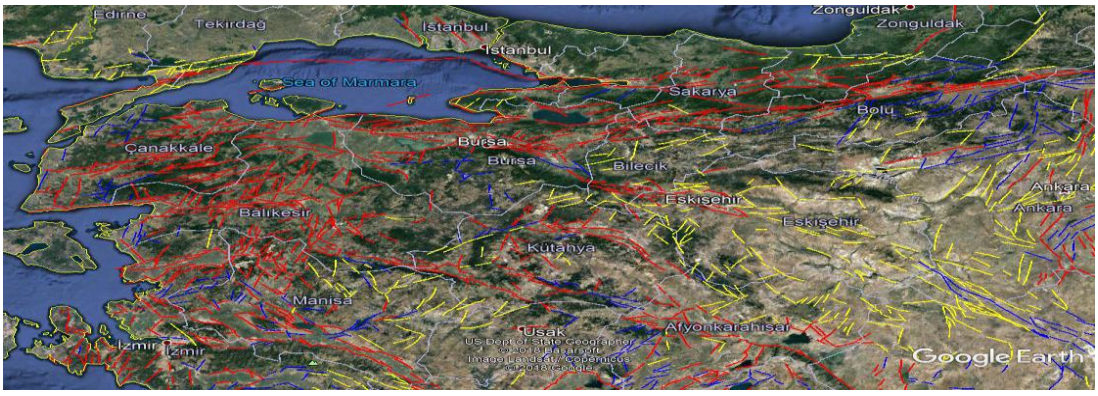

Figure 5.3. Map showing the faults around Bursa (provided by Prof. Dr. Sinan Akkar, Bogazici University Kandilli Observatory and Earthquake Research Institute, Department of Earthquake Engineering, 2018)

Among all of the faults delineated in the map, 135 different fault sources are considered to have seismic hazard potential to the components of the considered power transmission network. Emre et al., (2016) and Özcan, (2016) documented the seismicity parameters of these faults. The other information needed, are the trace coordinates of each fault. The names and the coding system of the faults provided in (Emre et al., 2016) matches with the coding system of the Active Fault Map of Turkey which was created by MTA (General Directorate of Mineral Research and Exploration). Figure 5.4 displays the Active Fault Map of Turkey provided by MTA, which formed the basis for identifying the faults to be considered in the study.

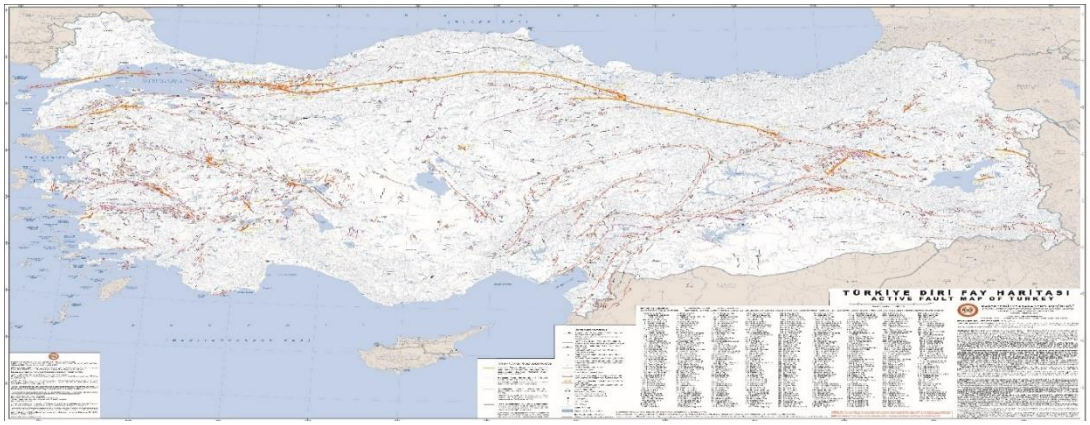

Figure 5.4. Active fault map of Turkey (MTA, 2017)

As the next step, the trace coordinates of each fault source, the names, codes and the seismicity parameters of which are defined in both (Emre et al., 2016) and the MTA map, are compiled. This task is achieved by superimposing the map in Figure 5.4 on to the map in Figure 5.3 using Google Earth as seen in Figure 5.5 as follows.

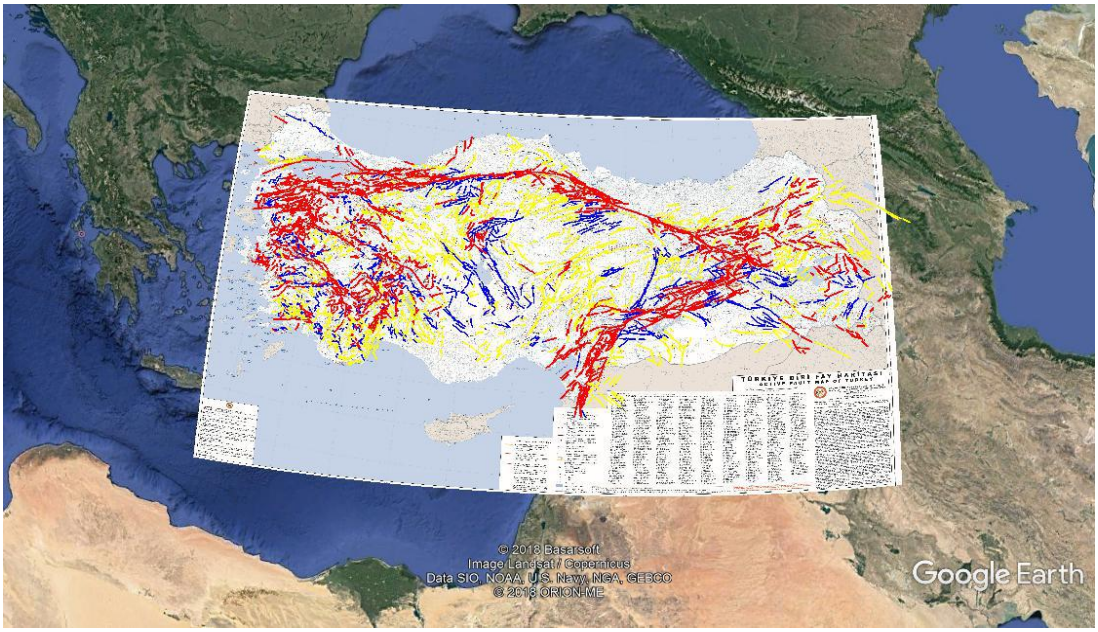

Figure 5.5. Superimposed fault maps (developed within the scope of this thesis)

Once the two maps were accurately overlaid (with approximately ±5 km deviation), then it was possible to detect the trace coordinates of each fault source. The trace coordinates which are found by the mentioned method are available in the Table B.1 in Appendix B.

Another type of seismic source, namely area source basically represents the expected background seismicity of the considered study region. The past earthquake records which do not match with any of the faults within the rectangular region that is bounded by the latitudes from 38.70°N to 42.10°N degrees and the longitudes from 25.90°E to 31.90°E are considered the records which belong to the background seismicity in this area. Before detecting the parameters of the area source, the past earthquake records should be matched with the faults. To achieve this, rectangular areas within 50 km's extension of each fault are created and then compared with the locations of the past records. Once this process is completed, then the locations of the past earthquakes can easily be compared with the extended area of each fault and the unmatched ones can be considered as the records which belong to the background seismicity and their

distributional parameters can be used to define an area source for the analysis. The analysis results are discussed in Section 5.3.2. The parameters of the area source computed by fitting a truncated exponential model to the unmatched records are as follows:

Table 5.2. *Area source parameters*

M_{min} (M_w)	M_{max} (M_w)	Total Area(km^2)	Activity Rate (#of earthquakes at $M_{min,}$ per year)	Activity Rate (# of earthquakes at $M_{min,}$ per year, per km^2)	β
4.0	6.0	174692.2	4.213	0.00002411	2.491

5.2.2. Wind Speed Data

Another equally important data collection process consists of gathering wind speed data for 15 districts, throughout which, the power is transmitted by the overhead lines. Daily-based maximum wind speed observations for the last 50 years are provided by the Turkish State Meteorological Institute for fifteen districts. Due to missing or unavailable records in the data, the wind speeds of some of the districts are completed using the ones from their geographically similar neighbours. After this operation, the remaining small gaps are completed using linear interpolation. The logic according to which the data is merged to complete the missing observations from the neighbour locations is explained below:

Wind speed data is partially available from two different meteorological stations for Balıkesir. Wind speed measurements are not available for the first one, which is Balıkesir Airport Station, up to 1998, while another station located in the city provided data from 1965 to 1996. The data from these two stations are merged to obtain a single dataset for Balıkesir.

Wind speed data for Orhaneli and Nilüfer districts is entirely missing and it is completed by using Osmangazi data, again due to geographical similarity. As it is seen in Figure 5.6, Orhaneli, Nilüfer and Osmangazi are not only neighbours of each other

but also they share same mountainous area which leads them to experience similar meteorological conditions.

Figure 5.6. Map of Orhaneli, Nilüfer and Osmangazi districts

The wind speed data for Mustafa Kemal Paşa district exists after the date 20.09.2006 and the missing part is completed by using the measurements of Nilüfer (which are originally obtained for Osmangazi). Figure 5.7 illustrates that Nilüfer and Mustafa Kemal Paşa districts are neighbours to each other and they share approximately the same portions of the Lake Ulubat and the mountainous area. Thus, they are assumed to have similar meteorological conditions.

Figure 5.7. Map of Mustafa Kemal Paşa and Nilüfer districts

Wind speed data for Karacabey district is missing between the dates 01.01.1968 and 17.11.2007. This missing part is completed by using wind speed data which is available for Bandırma. Bandırma and Karacabey are both located at the sea side and they have approximately the same length of shore to the Marmara Sea as seen in Figure 5.8 below. Besides, they both have similar amount of lake area and they also share a mountainous area on their north. Wind speed data from 1977 to March 1987, and from 2007 to 17.11.2007 are completed by using data available for Osmangazi district.

Figure 5.8. Map of Bandırma and Karacabey districts

As it is seen in Figure 5.9 below, Gemlik is geographically unique amongst other districts since it has a long shore line and it hosts a bay. Thus, only its own available data is used for Gemlik.

Figure 5.9. Map of Gemlik district

Wind speed data does not exist for Orhangazi. Related data for İznik district is used for Orhangazi as well since they both are elevated up to around 1100 meters and share similar meteorological conditions (see Figure 5.10). The wind speed data for İznik is available only for the last ten years.

Figure 5.10. Map of Orhangazi and İznik districts

Data is not available for Soma and Savaştepe districts and for their neighbouring districts as well. Since the nearest location is Balıkesir, the data available for Balıkesir is used for the wind pressure calculations of Soma and Savaştepe as well. Figure 5.11 illustrates the relative positions of Soma, Savaştepe and Balıkesir.

Figure 5.11. Map of Balıkesir, Savaştepe and Soma

Susurluk district has borders to both Balıkesir and Mustafa Kemal Paşa as seen in Figure 5.12. Amongst those two, Balıkesir data is preferred to be used to complete the missing part of the data of Susurluk due to geographical similarity.

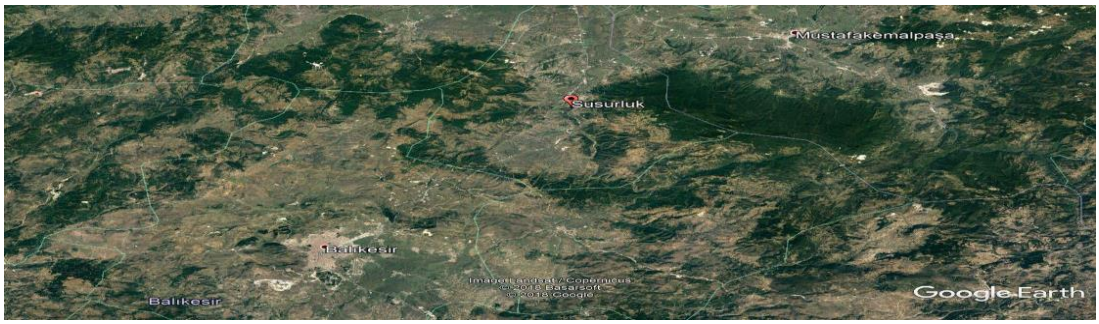

Figure 5.12. Map of Susurluk, Balıkesir and Mustafa Kemal Paşa

The data for Tavşanlı district is available starting from 1992. Since there is no neighboring location to complete the missing part of the data, its own available wind speed data is used in calculations. Wind speed data is not available for Harmacık district and Tavşanlı data is used for Harmancık district as well. These two districts are geographically close to each other as it is seen in Figure 5.13.

Figure 5.13. Map of Tavşanlı and Harmancık districts

5.3. Scenarios and Assessment of Failure Modes

Natural disasters are emergency situations which cause both structural and financial damage but more importantly, they are serious threats to human life. Health services provided by the state hospitals are crucial in such cases and these facilities are expected to remain fully functional as long as possible. Physical strength of those buildings will not be examined in this study and they will be assumed to be perfectly reliable. The functionality of them will be investigated in terms of being fed by electricity. Today almost every critical facility is supported by backup alternatives like diesel powered generators or parallel backup lines from the distribution grid to make sure that they continue operating under unexpected circumstances.

Figure 5.1a illustrates that there are two different state hospitals which are located in the vicinity of Gemlik and Orhangazi transformer stations. The case study will be conducted according to a scenario in which the access of these two hospitals to the power from the network under multi-hazard conditions is possible and this scenario will be evaluated probabilistically. To simplify the analysis, all backup procedures and equipment will be ignored and the hospitals will be assumed to get their energy only by the single transformer station within their vicinity. In this case, Bursa Muammer Ağım Gemlik State Hospital will be assumed to be connected to Gemlik TS and Bursa Orhangazi State Hospital will be assumed to be connected to Orhangazi TS and there is no alternative connection to provide power in case of any disconnection. With this assumption, the connectivity of Gemlik TS and Orhangazi TS to the system becomes crucial.

Four different failure modes, namely; earthquake, wind force without ice accretion, wind force on icy components and wear out due to the aging of the materials will initially be evaluated and then, as the final step, they will be consolidated to derive a multi hazard assessment. The study will be conducted for 50, 100, 500, 1000 and 2500 years return periods. There are two practical reasons for starting the evaluation from 50 years and proceeding through the periods which are multiples of 50 years. The

wind force computations are mainly based on 50 years average wind speed data and the gamma multiplier γ_w of the Equation (2.24) allows one to adapt the results to different return periods based on 50 years average wind speed. The other reason for choosing such a time scale is to cover the results of all failure modes as equally weighted as possible. While the effects of the extreme winds and ice accretion are mostly recognizable in shorter time periods, the earthquakes become more and more effective as the time goes on due to the accumulation of potential energy along the faults. By using the given return periods, a fair coverage of all these effects is provided.

5.3.1. Assessment of Wind Load

The power network considered in this study is composed of 942 transmission towers and they are of various types according to their location and purpose. Deriving the resistance parameters of every single type of tower is a very complicated and time consuming process besides being out of the context of this thesis. Thus, to provide computational simplicity, all transmission towers are assumed to be PB type suspension towers. ASCE No.74 (2010), suggests the numerical constant Q to be 0.613 for metric system. The velocity pressure exposure coefficient K_z is calculated for the α and Z_g parameters of exposure category C by considering the suggestion of ASCE No.74 (2010) which states that category C should be chosen unless it is exactly clear that the terrain structure represents one of the categories B with numerous closely spaced obstacles or D with unblocked flat areas. Detailed explanation about the categories are available in the document. The value of K_z is 1.094 for 22.9 meters transmission tower height and exposure category C. While calculating the topographic factor K_{zt} which represents the wind speed up effect of the terrain, K_1, K_2 and K_3 multipliers are chosen according to the values given in the document for two dimensional escarpments of category C. The value of it is calculated as 1.368. The gust response factor G_t is also computed with respect to category C and therefore the values of power law exponent α_{FM}, surface drag coefficient κ and turbulence scale L_S are chosen accordingly from the ones provided by the document as well. The value of G_t is found as 0.894. The values of the load factor γ_w for 100, 500, 1000 and 2500

years return periods are calculated by extrapolating the values provided in the document which yielded to 1.15, 1.4875, 1.6375 and 1.834375, respectively. Equation (2.24) gives the wind pressure values when the variables C_f and A are eliminated from it. Since the measurement system is metric in Turkey, the input values for the variables of Equation (2.24) are taken with their metric equivalents.

All wind speeds are converted into meters per second (m/s) unit to be used in the wind force formula given in Equation (2.24). The reliability assessment is conducted over the extreme load values, for each year, the maximum wind speed value is chosen as the maximum of the considered year. Then the 50 years average wind speeds are calculated over these series for each district. Table 5.3 below, gives the 50 years average wind speed data including the standard deviations for each of the 15 districts after completion of the missing parts in their data basis.

Table 5.3. *Statistical parameters obtained from the wind speed data for different districts*

Location	50 Years Mean Wind Speed (m/s)	Standard Deviation of 50 Years Maximum Wind Speed (m/s)
Bandırma	8.22	1.42
Karacabey	7.49	1.55
Balıkesir	6.30	0.97
Soma	6.30	0.97
Savaştepe	6.30	0.97
Susurluk	6.30	0.97
Mustafa Kemal Pasa	6.59	1.57
Osmangazi	6.57	1.22
Orhaneli	6.57	1.22
Nilüfer	6.57	1.22
Tavşanlı	5.39	0.96
Harmancık	5.39	0.96
Gemlik	8.86	2.05
İznik	7.07	2.61
Orhangazi	7.07	2.61

Having the same type of transmission towers throughout the entire network makes the variables of the wind force equation constant values except the mean wind speed. In this case, finding the standard deviations of the wind pressures of each return period requires a more advanced method which allows combining the variation of both constant part and the wind speed variable V. First Order Second Moment (FOSM) method is employed for this purpose. The coefficient of variation for the constant part of the wind pressure equation is assumed to be 0.15 for the purpose of considering and covering any possible measurement errors in the parameters consisting the constant part. The resulting mean wind pressure values and their standard deviations are given in Table 5.4 below. Table C.1 in Appendix C shows the wind pressure values for each transmission tower.

Table 5.4. *Mean (μ_w) and standard deviation (σ_w) of wind pressures corresponding to different return periods*

Return Period (years)	50		100		500		1000		2500	
Location	μ_w (kg/m^2)	σ_w (kg/m^2)	μ_w (kg/m^2)	σ_w (kg/m^2)	μ_w (kg/m^2)	σ_w (kg/m^2)	μ_w (kg/m^2)	σ_w (kg/m^2)	μ_w (kg/m^2)	σ_w (kg/m^2)
Bandırma	5.66	2.04	6.51	2.35	8.42	3.04	9.27	3.34	10.38	3.75
Karacabey	4.70	2.00	5.40	2.30	6.99	2.98	7.69	3.28	8.62	3.67
Balıkesir	3.32	1.07	3.82	1.23	4.95	1.60	5.45	1.76	6.10	1.97
Soma	3.32	1.07	3.82	1.23	4.95	1.60	5.45	1.76	6.10	1.97
Savaştepe	3.32	1.07	3.82	1.23	4.95	1.60	5.45	1.76	6.10	1.97
Susurluk	3.32	1.07	3.82	1.23	4.95	1.60	5.45	1.76	6.10	1.97
Mustafa Kemal Pasa	3.64	1.77	4.18	2.03	5.41	2.63	5.96	2.90	6.67	3.25
Osmangazi	3.62	1.39	4.16	1.60	5.38	2.07	5.93	2.28	6.64	2.55
Orhaneli	3.62	1.39	4.16	1.60	5.38	2.07	5.93	2.28	6.64	2.55
Nilüfer	3.62	1.39	4.16	1.60	5.38	2.07	5.93	2.28	6.64	2.55
Tavşanlı	2.43	0.90	2.80	1.03	3.62	1.34	3.98	1.47	4.46	1.65
Harmancık	2.43	0.90	2.80	1.03	3.62	1.34	3.98	1.47	4.46	1.65
Gemlik	6.58	3.12	7.56	3.59	9.78	4.64	10.77	5.11	12.07	5.72
İznik	4.18	3.12	4.81	3.59	6.23	4.64	6.85	5.11	7.68	5.73
Orhangazi	4.18	3.12	4.81	3.59	6.23	4.64	6.85	5.11	7.68	5.73

The next step is to calculate the survival probabilities for each transmission tower in both wind and wind-ice failure modes by using Reliability Index Calculator (RIC) software (Yücemen, M. S., CE589 unpublished class material, (2018)). RIC requires the knowledge of the statistical distribution of wind pressure. Since they are the most widely used distributions for the assessment of extreme values, Gamma, Weibull, Lognormal and Gumbel distributions are compared to find the best fit for wind pressure. Four different criteria namely, Coefficient of Determination (R^2), Kolmogorov-Smirnov Test Statistic (K-S), Akaike's Information Criterion (AIC) and Bayesian Information Criterion (BIC) are used to make a comparison amongst those four distributions for each district. The coefficient of determination values represent the level of fit of the wind pressure data of each district to the quantiles of each of four distributions and they are obtained through fitting the data to the distributions by using Q-Q plots. The values computed according to these four criteria are given in Table 5.5 for the wind pressure.

Table 5.5. *Goodness of fit statistics of wind pressures in different regions*

Region	Distribution	R^2	K-S Test Statistic	K-S D value	AIC	BIC
Bandırma	Gamma	0.92	0.10	0.19	208.99	212.81
	Weibull	0.88	0.12	0.19	219.95	223.78
	Lognormal	0.94	0.08	0.19	205.89	209.72
	Gumbel	0.95	0.08	0.19	205.48	209.31
Karacabey	Gamma	0.98	0.08	0.19	209.99	213.81
	Weibull	0.96	0.10	0.19	210.79	214.61
	Lognormal	0.97	0.11	0.19	213.62	217.45
	Gumbel	0.98	0.09	0.19	210.29	214.12
Balıkesir Soma Savaştepe Susurluk	Gamma	0.95	0.08	0.19	149.45	153.27
	Weibull	0.98	0.07	0.19	144.87	148.69
	Lognormal	0.92	0.10	0.19	152.82	156.65
	Gumbel	0.91	0.10	0.19	153.47	157.29
Mustafa Kemal Paşa	Gamma	0.89	0.12	0.19	193.77	197.59
	Weibull	0.86	0.13	0.19	203.14	206.96
	Lognormal	0.93	0.08	0.19	188.82	192.65
	Gumbel	0.91	0.10	0.19	191.51	195.33
Osmangazi Orhaneli Nilüfer	Gamma	0.96	0.09	0.19	170.08	173.86
	Weibull	0.96	0.11	0.19	172.18	175.96
	Lognormal	0.95	0.09	0.19	170.16	173.95
	Gumbel	0.95	0.09	0.19	170.69	174.48
Tavşanlı Harmancık	Gamma	0.82	0.11	0.25	67.06	69.58
	Weibull	0.78	0.17	0.25	74.65	77.17
	Lognormal	0.84	0.09	0.25	64.63	67.15
	Gumbel	0.85	0.08	0.25	64.21	66.72
Gemlik	Gamma	0.94	0.14	0.37	62.62	63.59
	Weibull	0.92	0.16	0.37	64.01	64.98
	Lognormal	0.96	0.14	0.37	61.93	62.90
	Gumbel	0.95	0.15	0.37	62.46	63.43
İznik Orhangazi	Gamma	0.76	0.29	0.40	51.22	51.82
	Weibull	0.74	0.29	0.40	52.78	53.38
	Lognormal	0.81	0.24	0.40	48.40	49.01
	Gumbel	0.76	0.27	0.40	51.71	52.31

As it is seen from Table 5.5, all of the four distributions give almost equivalent good fit results. Since in the literature Gumbel distribution is the most widely used one, in this study, the wind pressure data is assumed to have a Gumbel distribution. The standard deviation and the mean of the Gumbel distribution can be computed by the following equations, respectively.

$$\alpha = \frac{\pi}{\sqrt{6}\sigma} \tag{5.1}$$

$$u = \mu + \frac{\gamma}{\alpha} \tag{5.2}$$

where, $\gamma = 0.577$ is the Euler's constant. The parameters of wind pressure distribution for each district is given in Table 5.6.

Table 5.6. *The statistical parameters of wind pressure distribution (Gumbel) for each district corresponding to different return periods*

Return Period (years)	50		100		500		1000		2500	
Location	α	u	α	u	α	u	α	u	α	u
Bandırma	0.62	6.58	0.54	7.56	0.42	9.78	0.38	10.77	0.34	12.07
Karacabey	0.63	5.60	0.55	6.44	0.42	8.33	0.39	9.17	0.34	10.27
Balıkesir	1.18	3.81	1.03	4.38	0.79	5.67	0.72	6.24	0.64	6.99
Soma	1.18	3.81	1.03	4.38	0.79	5.67	0.72	6.24	0.64	6.99
Savaştepe	1.18	3.81	1.03	4.38	0.79	5.67	0.72	6.24	0.64	6.99
Susurluk	1.18	3.81	1.03	4.38	0.79	5.67	0.72	6.24	0.64	6.99
Mustafa Kemal Pasa	0.72	4.43	0.62	5.10	0.48	6.60	0.44	7.26	0.39	8.14
Osmangazi	0.92	4.24	0.80	4.88	0.61	6.31	0.56	6.95	0.50	7.79
Orhaneli	0.92	4.24	0.80	4.88	0.61	6.31	0.56	6.95	0.50	7.79
Nilüfer	0.92	4.24	0.80	4.88	0.61	6.31	0.56	6.95	0.50	7.79
Tavşanlı	1.42	2.84	1.23	3.26	0.95	4.22	0.86	4.65	0.77	5.21
Harmancık	1.42	2.84	1.23	3.26	0.95	4.22	0.86	4.65	0.77	5.21
Gemlik	0.41	7.98	0.35	9.18	0.27	11.87	0.25	13.07	0.22	14.64
İznik	0.41	5.59	0.35	6.43	0.27	8.32	0.25	9.16	0.22	10.26
Orhangazi	0.41	5.59	0.35	6.43	0.27	8.32	0.25	9.16	0.22	10.26

The substations are assumed to be one hundred percent reliable under wind related loads and are not considered here.

5.3.2. Assessment of Seismic Load

Seismic load is the most effective failure mode for all transmission towers and substations. Therefore, the peak ground acceleration (PGA) values at the coordinates that every single tower and substation are located, are computed by using Ez Frisk 7.52 (Risk Engineering, 2011) for each return period based on the assumptions and input data presented in Section 5.2.1. Peak ground acceleration is measured in terms of g (gravitational acceleration). It is possible to convert the g values into the moment magnitude (M_W) by using "Modified Mercalli Intensity Scale (MMIS)" charts. MMIS scales the intensity of the observer's experience about the severity of the considered earthquake. According to the MMIS charts, the relation between the gravitational acceleration g and the moment magnitude M_W, can be tabulated as seen in Table 5.7 (https://www.usgs.gov, 2019):

Table 5.7. *Gravitational acceleration intervals and the Corresponding moment magnitude (M_W) values*

Acceleration (g)	Moment Magnitude (M_W)
< 0.0017	1.0 - 3.0
0.0017 - 0.014	3.0 - 3.9
0.014 - 0.039	4.0 - 4.9
0.039 - 0.092	4.0 - 4.9
0.092 - 0.18	5.0 - 5.9
0.18 - 0.34	5.0 - 5.9
0.34 - 0.65	6.0 - 6.9
0.65 - 1.24	6.0 - 6.9
> 1.24	7.0 +

The PGA values besides the wind pressure values for each transmission tower of path 1 are given in Table C1 as an example in Appendix C. Since it requires a very large space, the data for 50, 500 and 1000 years return periods and the data for the other paths are not given but they are available upon request. Table 5.8 below, shows the PGA (g) values for each substation.

Table 5.8. *Statistical parameters of the PGA (g) values for substations corresponding to different return periods*

Return Periods (years)	50		100		500		1000		2500	
Substations	PGA (g)	σ_{PGA} (g)	PGA (g)	σ_{PGA} (g)	PGA (g)	σ_{PGA} (g)	PGA (g)	σ_{PGA} (g)	PGA (g)	σ_{PGA} (g)
Bursa Industrial Zone	0.128	0.045	0.195	0.068	0.452	0.158	0.626	0.219	0.931	0.325
Bursa DGKÇS	0.128	0.045	0.195	0.068	0.454	0.158	0.628	0.219	0.931	0.326
Gemlik	0.129	0.045	0.197	0.069	0.460	0.161	0.634	0.222	0.937	0.328
Orhangazi	0.127	0.044	0.194	0.068	0.452	0.158	0.626	0.219	0.931	0.325
Balıkesir 2	0.125	0.043	0.190	0.066	0.449	0.157	0.624	0.218	0.929	0.325

In this study, the coefficient of variation for peak ground acceleration is assumed as 35% (Lallemant et al., 2015).

5.3.3. Assessment of Wear Out

The overhead transmission lines are checked using both HD and UV cameras by the transmission companies each year as mentioned in Section 3.5. During these detections all the defects and potential risks like corona, overheated sections, overgrown trees under the lines, leftover waste from nearby constructions violating the ground clearance etc. are reported. Semi-hypothetical data of such a control on path 2, path 3, path 4 and part of path 5 are generated based on a series of personal communications. All the possible defects are checked and the ones which have potential to cause disconnection are distributed randomly to each path. Then the rate of such defects per year is calculated for each path and these rates are used as the mean

of a Poisson distribution to derive the probability that a transmission tower erected along the considered path faces disconnection due to such defects. Each year, the transmission companies replace damaged components after annual controls which in other words means that the paths start to the new year with zero failure probability and at the end of the year they are expected to face the same failure rate of previous year. Accordingly, the failure rates of each return period will be assumed to be the same. Since all three are 380 kV lines, the failure rate of path 2 is used for both path 1 and path 6. Besides the towers of both lines are erected very close to each other, in order to cover the possible effects of geographical similarity on wear out, the failure rate of path 3 is used for path 7 as well. Similarly, the failure rate of path 4 is also used for path 5. The failure rates of each path are given in Table 5.9 below.

Table 5.9. *Wear out failure rates (λ) (per path, per year) for each path corresponding to different return periods*

	Return Periods				
Paths	50 years	100 years	500 years	1000 years	2500 years
Path 1	0.29	0.29	0.29	0.29	0.29
Path 2	0.29	0.29	0.29	0.29	0.29
Path 3	0.09	0.09	0.09	0.09	0.09
Path 4	0.01	0.01	0.01	0.01	0.01
Path 5	0.01	0.01	0.01	0.01	0.01
Path 6	0.29	0.29	0.29	0.29	0.29
Path 7	0.09	0.09	0.09	0.09	0.09

5.3.4. Assessment of Reliability

The first step of reliability evaluation of the entire network is to define the survival probabilities of every single network component under multi-hazard conditions within the considered return periods. Survival probability and the reliability index β values (except wear out) of the transmission towers in each one of four failure modes are given in Table C2 in Appendix C for 1000 years return period as an example. The table also includes the upper and lower bounds of component survival probabilities in

other words the reliability bounds under multi-hazard. Since it requires a very large space, the data for 50, 100, 500 and 2500 years return periods and the data for the other paths are not given but they are available upon request. Values of the reliability index β, upper and lower bounds of survival probabilities under seismic load and within the considered return periods are given in Table 5.10 below for each substation. Once the component reliabilities are defined, the next step is to derive the reliability bounds of each of the seven different paths as presented in Table 5.11.

Table 5.10. *Reliability index, survival and failure probabilities of substations corresponding to different return periods*

	Return Periods (years)														
	50			100			500			1000			2500		
Substation	β_C	P_f	P_S	β_C	P_f	P_S	β_C	P_f	P_S	β_C	P_f	P_S	β_C	P_f	P_S
Bursa Industrial Zone	5.45	0.00	≦1	2.39	0.01	0.99	-0.64	0.74	0.26	-1.25	0.89	0.11	-1.79	0.96	0.04
Bursa DGKÇS	5.45	0.00	≦1	2.39	0.01	0.99	-0.64	0.74	0.26	-1.25	0.89	0.11	-1.79	0.96	0.04
Gemlik	5.45	0.00	≦1	2.39	0.01	0.99	-0.69	0.76	0.24	-1.28	0.90	0.10	-1.79	0.96	0.04
Orhangazi	5.45	0.00	≦1	2.39	0.01	0.99	-0.64	0.74	0.26	-1.25	0.89	0.11	-1.79	0.96	0.04
Balıkesir 2	5.45	0.00	≦1	2.39	0.01	0.99	-0.59	0.72	0.28	-1.25	0.89	0.11	-1.77	0.96	0.04

Table 5.11. *Survival probability bounds computed for each path corresponding to different return periods*

	Survival Probabilities									
Return Periods	50 years		100 years		500 years		1000 years		2500 years	
Paths	upper bound	lower bound	upper bound	lower bound	upper bound	lower bound	upper bound	lower bound	upper bound	lower bound
Path 1	0.78	0.00	0.78	0.00	0.78	0.00	0.72	0.00	0.29	0.00
Path 2	0.78	0.00	0.78	0.00	0.78	0.00	0.72	0.00	0.30	0.00
Path 3	0.92	0.01	0.92	0.01	0.92	0.00	0.72	0.00	0.29	0.00
Path 4	0.99	0.36	0.99	0.35	0.97	0.02	0.70	0.00	0.29	0.00
Path 5	0.99	0.34	0.99	0.34	0.96	0.02	0.70	0.00	0.29	0.00
Path 6	0.78	0.00	0.78	0.00	0.78	0.00	0.72	0.00	0.29	0.00
Path 7	0.92	0.02	0.92	0.02	0.92	0.01	0.72	0.00	0.29	0.00

The connectivity of Bursa Muammer Ağım Gemlik State Hospital and Orhangazi State Hospital are to be evaluated by the reliability of Gemlik and Orhangazi transformer stations. To achieve such an evaluation, the events which have the potential to disconnect these two transformer stations from the rest of the network are defined as failure cases. Definition of these events, requires path 5 to be considered as two sections. While the first section of path 5 is considered as the overhead line between Bursa NGCCP and Gemlik TS, in other words, the first 40 transmission towers of it, the rest of path 5, in other words the line between Gemlik TS and Orhangazi TS is called as section two. The alternative failure cases, each of which individually has the capability to disconnect Gemlik and Orhangazi transformer stations, are described in Table 5.12.

Table 5.12. *Failure scenarios for Gemlik and Orhangazi transformer stations*

Alternative Failure Cases	
Gemlik Transformer Station	Orhangazi Transformer Station
Gemlik TS fails	Orhangazi TS Fails
Path 5-Section 1 and Path 5-Section 2 fail	Path 4 and Path 5-Section 2 fail
Path 5-Section 1 and Path 4 fail	Path 4 and Path 5-Section 1 fail
Path 5-Section 1 and Orhangazi TS fail	Path 4 and Gemlik TS fail
Bursa NGCCP fails	Bursa NGCCP fails
Path 3 and Path 7 fail	Path 3 and Path 7 fail
Bursa Industrial Zone TS fails	Bursa Industrial Zone TS Fails
Path 2 and Path 1 fail	Path 2 and Path 1 fail
Path 6 and Path1 fail	Path 6 and Path 1 fail
Balıkesir 2 TS and Path 1 fail	Balıkesir 2 TS and Path 1 fail

The overall reliability bounds for Gemlik TS and Orhangazi TS, in other words for Bursa Muammer Ağım Gemlik State Hospital and Bursa Orhangazi State Hospital with respect to the failure cases are given respectively in Table 5.13 and Table 5.14 below.

Table 5.13. *Reliability bounds (survival probabilities, P_S) for the Gemlik TS and Bursa Muammer Ağım Gemlik State Hospital corresponding to different return periods for loads*

	Reliability Bounds									
Return Periods (years)	50		100		500		1000		2500	
Failure Cases	$P_{S_{max}}$	$P_{S_{min}}$	$P_{S_{max}}$	$P_{S_{min}}$	$P_{S_{max}}$	$P_{S_{min}}$	$P_{S_{max}}$	$P_{S_{min}}$	$P_{S_{max}}$	$P_{S_{min}}$
Gemlik TS fails	≅1.00	≅1.00	0.99	0.99	0.24	0.24	0.10	0.10	0.03	0.03
Path 5(from Bursa NGCCP to Gemlik) and Path 5 (from Orhangazi to Gemlik) fail	0.99	0.83	0.99	0.83	0.99	0.25	0.91	≅0.00	0.49	≅0.00
Path 5(from Bursa NGCCP to Gemlik) and Path 4 fail	0.99	0.77	0.99	0.77	0.99	0.20	0.91	≅0.00	0.49	≅0.00
Path 5(from Bursa NGCCP to Gemlik) and Orhangazi TS fail	≅1.00	≅1.00	0.99	0.99	0.97	0.40	0.73	0.10	0.31	0.03
Bursa NGCCP fails (probability that it survives from the event of its own failure)	≅1.00	≅1.00	0.99	0.99	0.26	0.26	0.10	0.10	0.03	0.03
Path 3 and Path 7 fail	0.99	0.03	0.99	0.03	0.99	0.01	0.92	≅0.00	0.49	≅0.00
Bursa Industrial Zone TS fails	≅1.00	≅1.00	0.99	0.99	0.26	0.26	0.10	0.10	0.03	0.03
Path 2 and Path 1 fail	0.95	≅0.00	0.95	≅0.00	0.95	≅0.00	0.92	≅0.00	0.49	≅0.00
Path 6 and Path1 fail	0.95	≅0.00	0.95	≅0.00	0.95	≅0.00	0.92	≅0.00	0.49	≅0.00
Balıkesir 2 TS and Path 1 fail	≅1.00	≅1.00	0.99	0.99	0.84	0.27	0.75	0.10	0.31	0.03
Reliability Bounds of Gemlik TS and Bursa Muammer Ağım Gemlik State Hospital	0.95	≅0.00	0.95	≅0.00	0.24	≅0.00	0.10	≅0.00	0.03	≅0.00

Table 5.14. *Reliability bounds (survival probabilities, P_S) for the Orhangazi TS and Bursa Orhangazi State Hospital corresponding to different return periods for loads*

	Reliability Bounds									
Return Periods (years)	50		100		500		1000		2500	
Failure Cases	$P_{S_{max}}$	$P_{S_{min}}$	$P_{S_{max}}$	$P_{S_{min}}$	$P_{S_{max}}$	$P_{S_{min}}$	$P_{S_{max}}$	$P_{S_{min}}$	$P_{S_{max}}$	$P_{S_{min}}$
Orhangazi TS Fails	≅1.00	≅1.00	0.99	0.99	0.26	0.26	0.10	0.10	0.03	0.03
Path 4 and Path 5 (from Orhangazi to Gemlik) fail	0.99	0.69	0.99	0.69	0.99	0.10	0.91	≅0.00	0.49	≅0.00
Path 4 and Path 5(from Bursa NGCCP to Gemlik) fail	0.99	0.77	0.99	0.77	0.99	0.20	0.91	≅0.00	0.49	≅0.00
Path 4 and Gemlik TS fail	≅1.00	≅1.00	0.99	0.99	0.97	0.25	0.73	0.10	0.31	0.03
Bursa NGCCP fails	≅1.00	≅1.00	0.99	0.99	0.26	0.26	0.10	0.10	0.03	0.03
Path 3 and Path 7 fail	0.99	0.03	0.99	0.03	0.99	0.01	0.92	≅0.00	0.49	≅0.00
Bursa Industrial Zone TS Fails	≅1.00	≅1.00	0.99	0.99	0.26	0.26	0.10	0.10	0.03	0.03
Path 2 and Path 1 fail	0.95	≅0.00	0.95	≅0.00	0.95	≅0.00	0.92	≅0.00	0.49	≅0.00
Path 6 and Path 1 fail	0.95	≅0.00	0.95	≅0.00	0.95	≅0.00	0.92	≅0.00	0.49	≅0.00
Balıkesir 2 TS and Path 1 fail	≅1.00	≅1.00	0.99	0.99	0.84	0.27	0.75	0.10	0.31	0.03
Reliability Bounds of Orhangazi TS and Bursa Orhangazi State Hospital	0.95	≅0.00	0.95	≅0.00	0.26	≅0.00	0.10	≅0.00	0.03	≅0.00

5.3.5. Assessment of Reliability Considering the Correlation Among Different Routes

The reliability (survival probability) bounds of the entire power transmission network are computed with respect to the scenarios based on Gemlik and Orhangazi transformer stations. The reason for defining the upper and lower bounds instead of computing a single probability value is to avoid conducting complicated integrations. Construction of these bounds requires the two extreme cases based on the similarities of the paths and the substations of the system to be considered, namely perfect correlation ($\rho=1$) and complete independence ($\rho=0$).

In real life, instead of perfect correlation or complete independence, some level of high but not perfect spatial correlation in between these two is expected. Since the soil conditions , seismic loads and the severity of the meteorological events do not differ much within small distances it is fair to expect a high correlation among the load levels at the locations of each component. Besides this, the use of similar materials and construction methods on the different paths of the whole system also contributes to the similarity of reactions of them to natural loads.

In this section, the effect of spatial correlation which is obtained from the common paths and substations followed by the power flow within different routes is illustrated. To achieve this, the minimum and maximum reliability indices obtained from the elements of each path are combined with the average correlation coefficient of the whole network to establish new reliability bounds for each path by using the following equation (Grigoriu and Turkstra (1979)):

$$\beta_{system} = \beta_e \sqrt{\frac{n}{1+\bar{\rho}(n-1)}} \tag{5.3}$$

where;

β_e = reliability of a single element

n = number of elements (in this case, routes)

$\bar{\rho}$ = average correlation coefficient among member failures

Nowak and Collins (2012) defined the average correlation coefficient in parallel networks with unequally correlated components as follows:

$$\bar{\rho} = \frac{1}{n(n-1)} \sum_{i}^{n} \sum_{j}^{n} \rho_{ij} \quad (5.4)$$

where;

$i \neq j$

The power transmission system in this study has three different power plants, namely, Soma, Tunçbilek power plants and Bursa Natural Gas Combined Cycle Plant. In this section, each possible combination of the paths and substations between those power plants and the two state hospitals (Bursa Muammer Ağım Gemlik State Hospital and Bursa Orhangazi State Hospital) is defined as "route". The average correlation coefficient is obtained by a correlation matrix which considers the common network sections amongst different routes. Tables 5.15 and 5.16 shows the possible power flow routes for Orhangazi and Gemlik transformer stations respectively. (The network sections covered by the corresponding route are given 1 while the others are given 0).

Table 5.15. *The network sections covered by each possible power flow route between the power plants and Orhangazi TS*

	Balıkesir 2 TS	Bursa Industrial Zone TS	Bursa NGCCP	Orhangazi TS	Gemlik TS	Path 1	Path 2	Path 3	Path 4	Path 5 (Section 1)	Path 5 (Section 2)	Path 6	Path 7
Route 1	1	1	1	1	0	0	1	1	1	0	0	1	0
Route 2	1	1	1	1	0	0	1	0	1	0	0	1	1
Route 3	1	1	1	1	1	0	1	1	0	1	1	1	0
Route 4	1	1	1	1	1	0	1	0	0	1	1	1	1
Route 5	0	1	1	1	0	1	0	1	1	0	0	0	0
Route 6	0	1	1	1	0	1	0	0	1	0	0	0	1
Route 7	0	1	1	1	1	1	0	1	0	1	1	0	0
Route 8	0	1	1	1	1	1	0	0	0	1	1	0	1
Route 9	0	0	1	1	0	0	0	0	1	0	0	0	0
Route 10	0	0	1	1	1	0	0	0	0	1	1	0	0

Table 5.16. *The network sections covered by each possible power flow route between the power plants and Gemlik TS*

	Balıkesir 2 TS	Bursa Industrial Zone TS	Bursa NGCCP	Orhangazi TS	Gemlik TS	Path 1	Path 2	Path 3	Path 4	Path 5 (Section 1)	Path 5 (Section 2)	Path 6	Path 7
Route 1	1	1	1	0	1	0	1	1	0	1	0	1	0
Route 2	1	1	1	0	1	0	1	0	0	1	0	1	1
Route 3	1	1	1	1	1	0	1	1	1	0	1	1	0
Route 4	1	1	1	1	1	0	1	0	1	0	1	1	1
Route 5	0	1	1	1	1	1	0	1	1	0	1	0	0
Route 6	0	1	1	1	1	1	0	0	1	0	1	0	1
Route 7	0	1	1	0	1	1	0	1	0	1	0	0	0
Route 8	0	1	1	0	1	1	0	0	0	1	0	0	1
Route 9	0	0	1	1	1	0	0	0	1	0	1	0	0
Route 10	0	0	1	0	1	0	0	0	0	1	0	0	0

Once the network sections that are covered by the different routes are defined, the next step before obtaining the correlation matrix is to calculate the number of common sections between the routes. Tables 5.17 and 5.18 illustrate the number of common paths and substations used by the different routes through Orhangazi TS and Gemlik TS respectively.

Table 5.17. *Number of common network sections in different routes from the power plants through the Orhangazi TS*

	Route 1	Route 2	Route 3	Route 4	Route 5	Route 6	Route 7	Route 8	Route 9	Route 10
Route 1	13	7	7	6	5	4	4	3	3	2
Route 2	7	13	6	7	4	5	3	4	3	2
Route 3	7	6	13	9	4	3	7	6	2	5
Route 4	6	7	9	13	3	4	6	7	2	5
Route 5	5	4	4	3	13	5	5	4	3	2
Route 6	4	5	3	4	5	13	4	5	3	2
Route 7	4	3	7	6	5	4	13	7	2	5
Route 8	3	4	6	7	4	5	7	13	2	5
Route 9	3	3	2	2	3	3	2	2	13	2
Route 10	2	2	5	5	2	2	5	5	2	13

Table 5.18. *Number of common network sections in different routes from the power plants through the Gemlik TS*

	Route 1	Route 2	Route 3	Route 4	Route 5	Route 6	Route 7	Route 8	Route 9	Route 10
Route 1	13	7	7	6	4	3	5	4	2	3
Route 2	7	13	6	7	3	4	4	5	2	3
Route 3	7	6	13	9	7	6	4	3	5	2
Route 4	6	7	9	13	6	7	3	4	5	2
Route 5	4	3	7	6	13	7	5	4	5	2
Route 6	3	4	6	7	7	13	4	5	5	2
Route 7	5	4	4	3	5	4	13	5	2	3
Route 8	4	5	3	4	4	5	5	13	2	3
Route 9	2	2	5	5	5	5	2	2	13	2
Route 10	3	3	2	2	2	2	3	3	2	13

Since path 5 is divided into two different parts, now the entire network is considered as composed of 13 different sections (5 substations and 8 paths). The correlation matrices with respect to Orhangazi and Gemlik transformer stations are constructed by dividing each number in tables 5.17 and 5.18 by 13 and given in Table 5.19 and Table 5.20 respectively.

Table 5.19. *Correlation matrix for the power transmission network with respect to Orhangazi TS*

Correlation	Route 1	Route 2	Route 3	Route 4	Route 5	Route 6	Route 7	Route 8	Route 9	Route 10
Route 1	1.00	0.53	0.53	0.46	0.38	0.30	0.30	0.23	0.23	0.15
Route 2	0.53	1.00	0.46	0.53	0.30	0.38	0.23	0.30	0.23	0.15
Route 3	0.53	0.46	1.00	0.69	0.30	0.23	0.53	0.46	0.15	0.38
Route 4	0.46	0.53	0.69	1.00	0.23	0.30	0.46	0.53	0.15	0.38
Route 5	0.38	0.30	0.30	0.23	1.00	0.38	0.38	0.30	0.23	0.15
Route 6	0.30	0.38	0.23	0.30	0.38	1.00	0.30	0.38	0.23	0.15
Route 7	0.30	0.23	0.53	0.46	0.38	0.30	1.00	0.53	0.15	0.38
Route 8	0.23	0.30	0.46	0.53	0.30	0.38	0.53	1.00	0.15	0.38
Route 9	0.23	0.23	0.15	0.15	0.23	0.23	0.15	0.15	1.00	0.15
Route 10	0.15	0.15	0.38	0.38	0.15	0.15	0.38	0.38	0.15	1.00

Table 5.20. *Correlation matrix for the power transmission network with respect to Gemlik TS*

Correlation	Route 1	Route 2	Route 3	Route 4	Route 5	Route 6	Route 7	Route 8	Route 9	Route 10
Route 1	1.00	0.53	0.53	0.38	0.30	0.23	0.38	0.30	0.15	0.23
Route 2	0.53	1.00	0.46	0.46	0.23	0.30	0.30	0.38	0.15	0.23
Route 3	0.53	0.46	1.00	0.61	0.53	0.46	0.30	0.23	0.38	0.15
Route 4	0.38	0.46	0.61	1.00	0.46	0.53	0.23	0.30	0.38	0.15
Route 5	0.30	0.23	0.53	0.46	1.00	0.53	0.38	0.30	0.38	0.15
Route 6	0.23	0.30	0.46	0.53	0.53	1.00	0.30	0.38	0.38	0.15
Route 7	0.38	0.30	0.30	0.23	0.38	0.30	1.00	0.38	0.15	0.23
Route 8	0.30	0.38	0.23	0.30	0.30	0.38	0.38	1.00	0.15	0.23
Route 9	0.15	0.15	0.38	0.38	0.38	0.38	0.15	0.15	1.00	0.15
Route 10	0.23	0.23	0.15	0.15	0.15	0.15	0.23	0.23	0.15	1.00

From Equation (5.4), the average correlation coefficient by considering the routes from the power plants to Orhangazi and Gemlik transformer stations are calculated as 0.3316 and 0.3264. Following the calculation of the average correlation coefficient, to construct the new reliability bounds of each path, the minimum and maximum reliability indices of the elements of each path are required. Since each transmission tower is evaluated under four failure modes, each tower has three different reliability indices coming from different failure modes and a failure probability computed for wear out. Besides this, the reliability indices of different failure modes are computed from different probability distributions which are Normal and Gumbel distributions. Because of these reasons, a different approach is needed to find a single beta value to represent each transmission tower. To obtain those values, the reliability bounds of each component are transformed into reliability indices by the following R code:

(-1)*qnorm((1-x), mean = 0, sd = 1, lower.tail = TRUE, log.p = FALSE) (5.5)

Table 5.21 illustrates the minimum and maximum reliability indices computed for each path.

Table 5.21. *Maximum and minimum reliability indices of each path*

Return Period	50 years		100 years		500 years		1000 years		2500 years	
	$\beta_{e_{max}}$	$\beta_{e_{min}}$	$\beta_{e_{max}}$	$\beta_{e_{min}}$	$\beta_{e_{max}}$	$\beta_{e_{min}}$	$\beta_{e_{max}}$	$\beta_{e_{min}}$	$\beta_{e_{max}}$	$\beta_{e_{min}}$
path1	0.77	0.77	0.77	0.77	0.77	0.69	0.58	0.15	-0.53	-0.75
path2	0.77	0.77	0.77	0.77	0.77	0.77	0.70	0.15	-0.48	-0.73
path3	1.38	1.38	1.38	1.38	1.38	1.22	0.58	0.41	-0.56	-0.63
path4	2.30	2.29	2.30	2.29	1.88	1.73	0.58	0.50	-0.56	-0.57
path5-1	2.30	2.29	2.30	2.29	1.88	1.65	0.58	0.50	-0.56	-0.57
path5-2	2.30	2.29	2.30	2.29	1.88	1.65	0.58	0.50	-0.56	-0.57
path6	0.77	0.77	0.77	0.77	0.77	0.69	0.58	0.15	-0.53	-0.75
path7	1.38	1.38	1.38	1.38	1.38	1.22	0.58	0.41	-0.56	-0.63

From Equation (5.3), the reliability indices (β_{system}) for each path are computed. The new maximum and minimum reliability indices for each path with respect to the

average correlation coefficients are given in Tables 5.22 and 5.23 for Orhangazi and Gemlik transformer stations, respectively.

Table 5.22. *Maximum and minimum reliability index values computed using the average correlation coefficient for Orhangazi TS*

Return Period	50 years		100 years		500 years		1000 years		2500 years	
	$\beta_{system_{max}}$	$\beta_{system_{min}}$	$\beta_{system_{max}}$	$\beta_{system_{min}}$	$\beta_{system_{max}}$	$\beta_{system_{min}}$	$\beta_{system_{max}}$	$\beta_{system_{min}}$	$\beta_{system_{max}}$	$\beta_{system_{min}}$
path1	1.22	1.22	1.22	1.22	1.22	1.10	0.93	0.25	-0.84	-1.20
path2	1.22	1.22	1.22	1.22	1.22	1.22	1.11	0.25	-0.76	-1.16
path3	2.19	2.19	2.19	2.19	2.19	1.94	0.93	0.66	-0.88	-1.00
path4	3.64	3.64	3.64	3.63	2.99	2.75	0.93	0.80	-0.88	-0.90
path5-1	3.64	3.64	3.64	3.63	2.99	2.62	0.93	0.80	-0.88	-0.90
path5-2	3.64	3.64	3.64	3.63	2.99	2.62	0.93	0.80	-0.88	-0.90
path6	1.22	1.22	1.22	1.22	1.22	1.10	0.93	0.25	-0.84	-1.20
path7	2.19	2.19	2.19	2.19	2.19	1.94	0.93	0.66	-0.88	-1.00

Table 5.23. *Maximum and minimum reliability index values computed using the average correlation coefficient for Gemlik TS*

Return Period	50 years		100 years		500 years		1000 years		2500 years	
	$\beta_{system_{max}}$	$\beta_{system_{min}}$	$\beta_{system_{max}}$	$\beta_{system_{min}}$	$\beta_{system_{max}}$	$\beta_{system_{min}}$	$\beta_{system_{max}}$	$\beta_{system_{min}}$	$\beta_{system_{max}}$	$\beta_{system_{min}}$
path1	1.23	1.23	1.23	1.23	1.23	1.11	0.93	0.25	-0.85	-1.20
path2	1.23	1.23	1.23	1.23	1.23	1.23	1.11	0.25	-0.77	-1.17
path3	2.20	2.20	2.20	2.20	2.20	1.95	0.93	0.66	-0.89	-1.00
path4	3.66	3.66	3.66	3.65	3.00	2.77	0.93	0.80	-0.89	-0.91
path5-1	3.66	3.66	3.66	3.65	3.00	2.64	0.93	0.80	-0.89	-0.91
path5-2	3.66	3.66	3.66	3.65	3.00	2.64	0.93	0.80	-0.89	-0.91
path6	1.23	1.23	1.23	1.23	1.23	1.11	0.93	0.25	-0.85	-1.20
path7	2.20	2.20	2.20	2.20	2.20	1.95	0.93	0.66	-0.89	-1.00

As the next step, the values that are given in Tables 5.22 and 5.23 are converted into survival probabilities by using the “pnorm( )” function of R. The new reliability bounds of each path that are computed according to the average correlation

coefficients of Orhangazi and Gemlik transformer station routes are given in Table 5.24 and Table 5.25 respectively.

Table 5.24. *The new reliability bounds (survival probabilities, P_S) for the paths with respect to the average correlation coefficient of Orhangazi TS routes*

Return Period	50 years		100 years		500 years		1000 years		2500 years	
	$P_{S_{max}}$	$P_{S_{min}}$	$P_{S_{max}}$	$P_{S_{min}}$	$P_{S_{max}}$	$P_{S_{min}}$	$P_{S_{max}}$	$P_{S_{min}}$	$P_{S_{max}}$	$P_{S_{min}}$
path1	0.88	0.88	0.88	0.88	0.88	0.86	0.82	0.59	0.19	0.11
path2	0.88	0.88	0.88	0.88	0.88	0.88	0.86	0.59	0.22	0.12
path3	0.98	0.98	0.98	0.98	0.98	0.97	0.82	0.74	0.18	0.15
path4	0.99	0.99	0.99	0.99	0.99	0.99	0.82	0.78	0.18	0.18
path5-1	0.99	0.99	0.99	0.99	0.99	0.99	0.82	0.78	0.18	0.18
path5-2	0.99	0.99	0.99	0.99	0.99	0.99	0.82	0.78	0.18	0.18
path6	0.88	0.88	0.88	0.88	0.88	0.86	0.82	0.59	0.19	0.11
path7	0.98	0.98	0.98	0.98	0.98	0.97	0.82	0.74	0.18	0.15

Table 5.25. *The new reliability bounds (survival probabilities, P_S) for the paths with respect to the average correlation coefficient of Gemlik TS routes*

Return Period	50 years		100 years		500 years		1000 years		2500 years	
	$P_{S_{max}}$	$P_{S_{min}}$	$P_{S_{max}}$	$P_{S_{min}}$	$P_{S_{max}}$	$P_{S_{min}}$	$P_{S_{max}}$	$P_{S_{min}}$	$P_{S_{max}}$	$P_{S_{min}}$
path1	0.89	0.89	0.89	0.89	0.89	0.86	0.82	0.59	0.19	0.11
path2	0.89	0.89	0.89	0.89	0.89	0.89	0.86	0.59	0.22	0.12
path3	0.98	0.98	0.98	0.98	0.98	0.97	0.82	0.74	0.18	0.15
path4	0.99	0.99	0.99	0.99	0.99	0.99	0.82	0.79	0.18	0.18
path5-1	0.99	0.99	0.99	0.99	0.99	0.99	0.82	0.79	0.18	0.18
path5-2	0.99	0.99	0.99	0.99	0.99	0.99	0.82	0.79	0.18	0.18
path6	0.89	0.89	0.89	0.89	0.89	0.86	0.82	0.59	0.19	0.11
path7	0.98	0.98	0.98	0.98	0.98	0.97	0.82	0.74	0.18	0.15

Once the new reliability bounds of the paths are obtained, the overall reliability bounds for Orhangazi and Gemlik transformer stations are established as illustrated in Table 5.26 and Table 5.27 respectively.

Table 5.26. *Overall reliability bounds (survival probabilities, P_S) of Orhangazi TS with respect to the average correlation coefficient*

	Reliability Bounds									
Return Periods	50 years		100 years		500 years		1000 years		2500 years	
Failure Cases	$P_{S_{max}}$	$P_{S_{min}}$	$P_{S_{max}}$	$P_{S_{min}}$	$P_{S_{max}}$	$P_{S_{min}}$	$P_{S_{max}}$	$P_{S_{min}}$	$P_{S_{max}}$	$P_{S_{min}}$
Orhangazi TS Fails	1.00	1.00	0.99	0.99	0.26	0.26	0.10	0.10	0.03	0.03
Path 4 and Path 5 (from Orhangazi to Gemlik) fail	1.00	1.00	1.00	1.00	1.00	0.99	0.96	0.95	0.33	0.33
Path 4 and Path 5(from Bursa NGCCP to Gemlik) fail	1.00	1.00	1.00	1.00	1.00	0.99	0.96	0.95	0.33	0.33
Path 4 and Gemlik TS fail	1.00	1.00	1.00	1.00	0.99	0.99	0.84	0.81	0.21	0.21
Bursa NGCCP fails	1.00	1.00	0.99	0.99	0.26	0.26	0.10	0.10	0.03	0.03
Path 3 and Path 7 fail	0.99	0.99	0.99	0.99	0.99	0.99	0.96	0.93	0.33	0.29
Bursa Industrial Zone TS Fails	1.00	1.00	0.99	0.99	0.26	0.26	0.10	0.10	0.03	0.03
Path 2 and Path 1 fail	0.98	0.98	0.98	0.98	0.98	0.98	0.97	0.83	0.37	0.22
Path 6 and Path 1 fail	0.98	0.98	0.98	0.98	0.98	0.98	0.96	0.83	0.35	0.21
Balıkesir 2 TS and Path 1 fail	1.00	1.00	0.99	0.99	0.92	0.90	0.84	0.64	0.28	0.20
Reliability Bounds of Orhangazi TS and Bursa Orhangazi State Hospital	0.98	0.97	0.98	0.94	0.26	0.01	0.10	0.00	0.03	0.00

Table 5.27. *Overall reliability bounds (survival probabilities, P_S) of Gemlik TS with respect to the average correlation coefficient*

	Reliability Bounds									
Return Periods	50 years		100 years		500 years		1000 years		2500 years	
Failure Cases	$P_{S_{max}}$	$P_{S_{min}}$	$P_{S_{max}}$	$P_{S_{min}}$	$P_{S_{max}}$	$P_{S_{min}}$	$P_{S_{max}}$	$P_{S_{min}}$	$P_{S_{max}}$	$P_{S_{min}}$
Gemlik TS fails	1.00	1.00	0.99	0.99	0.24	0.24	0.10	0.10	0.03	0.03
Path 5(from Bursa NGCCP to Gemlik) and Path 5 (from Orhangazi to Gemlik) fail	1.00	1.00	1.00	1.00	1.00	1.00	0.96	0.95	0.33	0.32
Path 5(from Bursa NGCCP to Gemlik) and Path 4 fail	1.00	1.00	1.00	1.00	1.00	1.00	0.96	0.95	0.33	0.32
Path 5(from Bursa NGCCP to Gemlik) and Orhangazi TS fail	1.00	1.00	1.00	1.00	0.99	0.99	0.84	0.81	0.21	0.21
Bursa NGCCP fails (probability that it survives from the event of its own failure)	1.00	1.00	0.99	0.99	0.26	0.26	0.10	0.10	0.03	0.03
Path 3 and Path 7 fail	0.99	0.99	0.99	0.99	0.99	0.99	0.96	0.93	0.33	0.28
Bursa Industrial Zone TS fails	1.00	1.00	0.99	0.99	0.26	0.26	0.10	0.10	0.03	0.03
Path 2 and Path 1 fail	0.98	0.98	0.98	0.98	0.98	0.98	0.97	0.83	0.37	0.22
Path 6 and Path1 fail	0.98	0.98	0.98	0.98	0.98	0.98	0.96	0.83	0.35	0.21
Balıkesir 2 TS and Path 1 fail	1.00	1.00	0.99	0.99	0.92	0.90	0.84	0.64	0.22	0.14
Reliability Bounds of Gemlik TS and Bursa Muammer Ağım Gemlik State Hospital	0.98	0.97	0.98	0.95	0.24	0.01	0.10	0.00	0.03	0.00

5.3.6. Assessment of Reliability Considering the Scale of Fluctuation

Scale of fluctuation is an important concept for probabilistic reliability assessment of infrastructural networks. The correlation coefficient corresponding to the scale of fluctuation of the area that the network is constructed on, can be used for evaluation of the reliability bounds of the entire system. In Tables 5.15 and 5.16, ten different routes which are defined between the power plants and each one of Orhangazi and Gemlik transformer stations are given. In this section, the average correlation coefficients with respect to the closeness of those routes to each other are calculated and the effects of them on the reliability bounds of two state hospitals are illustrated.

To achieve this, as a first step, distance matrices showing the distances (in meters) between the midpoints of each route are constructed. Table 5.28 and Table 5.29 show the corresponding distance matrices for Orhangazi TS and Gemlik TS, respectively.

Table 5.28. *Distances (in meters) between the midpoints of the routes which extend from the power plants through Orhangazi TS*

Routes	Route 1	Route 2	Route 3	Route 4	Route 5	Route 6	Route 7	Route 8	Route 9	Route 10
Route 1	0	217	1431	973	56592	56597	56603	56615	86304	85610
Route 2	217	0	1646	1191	56817	56800	56834	56843	86566	85831
Route 3	1431	1646	0	455	55173	55160	55191	55201	85038	84317
Route 4	973	1191	455	0	55632	55616	55649	55658	85441	84736
Route 5	56611	56817	55173	55632	0	221	1291	1089	40523	42243
Route 6	56597	56800	55160	55616	221	0	1513	1310	40744	42440
Route 7	56603	56834	55191	55649	1291	1513	0	205	39495	41119
Route 8	56615	56843	55201	55658	1089	1310	205	0	39653	41283
Route 9	86304	86566	85038	85441	40523	40744	39495	39653	0	4202
Route 10	85610	85831	84317	84736	42243	42440	41119	41283	4202	0

Table 5.29. *Distances (in meters) between the midpoints of the routes which extend from the power plants through Gemlik TS*

Routes	Route 1	Route 2	Route 3	Route 4	Route 5	Route 6	Route 7	Route 8	Route 9	Route 10
Route 1	0	170	18031	17818	66659	66717	64758	64807	92704	86495
Route 2	170	0	18200	17984	66825	66880	64885	64935	92863	86681
Route 3	18031	18200	0	216	48760	48812	48452	48555	74929	68623
Route 4	17818	17984	216	0	48973	49026	48624	48726	75206	68851
Route 5	66659	66825	48760	48973	0	154	18029	18431	33231	25925
Route 6	66717	66880	48812	49026	154	0	18185	18587	33117	25779
Route 7	64758	64885	48452	48624	18029	18185	0	407	49749	42567
Route 8	64807	64935	48555	48726	18431	18587	407	0	50120	42938
Route 9	92704	92863	74929	75206	33231	33117	49749	50120	0	7338
Route 10	86495	86681	68623	68851	25925	25779	42567	42938	7338	0

Once the distances are found, the next step is to construct the correlation matrices. The spatial correlation between the components of the network is expected to decrease exponentially with respect to the distance. Therefore, the exponential correlation function which is given in Table 4.1 is used for calculating the elements of the correlation matrices. In these calculations, the average distances 42757 meters and 44882 meters are assumed to be the scale of fluctuation values for Orhangazi TS and Gemlik TS based scenarios, respectively. Accordingly the "b" parameter in Table 4.1 will be 42757/2 ≅ 21000 meters and 44882/2 ≅ 22000 meters for Orhangazi TS and Gemlik TS based scenarios, respectively. Table 5.30 and Table 5.31 show the correlation matrices for Orhangazi TS and Gemlik TS, respectively.

Table 5.30. *Correlation matrix for Orhangazi TS*

Routes	Route 1	Route 2	Route 3	Route 4	Route 5	Route 6	Route 7	Route 8	Route 9	Route 10
Route 1	1.0000	0.9899	0.9352	0.9555	0.0707	0.0708	0.0708	0.0707	0.0176	0.0182
Route 2	0.9899	1.0000	0.9258	0.9458	0.0701	0.0701	0.0700	0.0700	0.0174	0.0180
Route 3	0.9352	0.9258	1.0000	0.9789	0.0750	0.0757	0.0756	0.0756	0.0187	0.0193
Route 4	0.9555	0.9458	0.9789	1.0000	0.0741	0.0741	0.0740	0.0740	0.0183	0.0189
Route 5	0.0707	0.0701	0.0750	0.0741	1.0000	0.9897	0.9413	0.9503	0.1502	0.1386
Route 6	0.0708	0.0701	0.0757	0.0741	0.9897	1.0000	0.9316	0.9405	0.1486	0.1373
Route 7	0.0708	0.0700	0.0756	0.0740	0.9413	0.9316	1.0000	0.9904	0.1576	0.1461
Route 8	0.0707	0.0700	0.0756	0.0740	0.9503	0.9405	0.9904	1.0000	0.1564	0.1449
Route 9	0.0176	0.0174	0.0187	0.0183	0.1502	0.1486	0.1576	0.1564	1.0000	0.8215
Route 10	0.0182	0.0180	0.0193	0.0189	0.1386	0.1373	0.1461	0.1449	0.8215	1.0000

Table 5.31. *Correlation matrix for Gemlik TS*

Routes	Route 1	Route 2	Route 3	Route 4	Route 5	Route 6	Route 7	Route 8	Route 9	Route 10
Route 1	1.0000	0.9924	0.4477	0.4520	0.0512	0.0511	0.0558	0.0556	0.0160	0.0211
Route 2	0.9924	1.0000	0.4444	0.4487	0.0509	0.0507	0.0555	0.0553	0.0159	0.0210
Route 3	0.4477	0.4444	1.0000	0.9904	0.1138	0.1135	0.1154	0.1149	0.0354	0.0469
Route 4	0.4520	0.4487	0.9904	1.0000	0.1127	0.1125	0.1145	0.1140	0.0350	0.0465
Route 5	0.0512	0.0509	0.1138	0.1127	1.0000	0.9931	0.4478	0.4398	0.2274	0.3149
Route 6	0.0511	0.0507	0.1135	0.1125	0.9931	1.0000	0.4447	0.4368	0.2286	0.3170
Route 7	0.0558	0.0555	0.1154	0.1145	0.4478	0.4447	1.0000	0.9820	0.1089	0.1500
Route 8	0.0556	0.0553	0.1149	0.1140	0.4398	0.4368	0.9820	1.0000	0.1071	0.1475
Route 9	0.0160	0.0159	0.0354	0.0350	0.2274	0.2286	0.1089	0.1071	1.0000	0.7210
Route 10	0.0211	0.0210	0.0469	0.0465	0.3149	0.317	0.1500	0.1475	0.7210	1.0000

From Equation (5.4), the average correlation coefficients for the routes through Orhangazi TS and Gemlik TS are calculated as 0.32 and 0.25. Similar to the previous section, Equation (5.3) is used to calculate the maximum and minimum reliability indices of each path by considering the correlation coefficients $\rho=0.32$ and $\rho=0.25$ together with the values that are given in Table 5.21, and then, these values are converted into the survival probabilities. Table 5.32 and Table 5.33 show the reliability bounds of each path with respect to the corresponding average correlation coefficients for Orhangazi TS and Gemlik TS, respectively.

Table 5.32. *The new reliability bounds (survival probabilities, P_S) for the paths with respect to the average correlation coefficient ρ=0.32 (calculated based on the distances between the midpoints of the routes from the power plants through Orhangazi TS)*

Return Periods	50 years		100 years		500 years		1000 years		2500 years	
Paths	$P_{S_{max}}$	$P_{S_{min}}$	$P_{S_{max}}$	$P_{S_{min}}$	$P_{S_{max}}$	$P_{S_{min}}$	$P_{S_{max}}$	$P_{S_{min}}$	$P_{S_{max}}$	$P_{S_{min}}$
Path 1	0.89	0.89	0.89	0.89	0.89	0.87	0.82	0.60	0.20	0.11
Path 2	0.89	0.89	0.89	0.89	0.89	0.89	0.87	0.60	0.22	0.12
Path 3	0.99	0.99	0.99	0.99	0.99	0.97	0.82	0.75	0.19	0.16
Path 4	≅1.00	≅1.00	≅1.00	≅1.00	≅1.00	≅1.00	0.82	0.79	0.19	0.18
Path 5-1	≅1.00	≅1.00	≅1.00	≅1.00	≅1.00	≅1.00	0.82	0.79	0.19	0.18
Path 5-2	≅1.00	≅1.00	≅1.00	≅1.00	≅1.00	≅1.00	0.82	0.79	0.19	0.18
Path 6	0.89	0.89	0.89	0.89	0.89	0.87	0.82	0.60	0.20	0.11
Path 7	0.99	0.99	0.99	0.99	0.99	0.97	0.82	0.75	0.19	0.16

Table 5.33. *The new reliability bounds (survival probabilities, P_S) for the paths with respect to the average correlation coefficient ρ=0.25 (calculated based on the distances between the midpoints of the routes from the power plants through Gemlik TS)*

Return Periods	50 years		100 years		500 years		1000 years		2500 years	
Paths	$P_{S_{max}}$	$P_{S_{min}}$	$P_{S_{max}}$	$P_{S_{min}}$	$P_{S_{max}}$	$P_{S_{min}}$	$P_{S_{max}}$	$P_{S_{min}}$	$P_{S_{max}}$	$P_{S_{min}}$
Path 1	0.91	0.91	0.91	0.91	0.91	0.89	0.85	0.61	0.17	0.09
Path 2	0.91	0.91	0.91	0.91	0.91	0.91	0.89	0.61	0.20	0.10
Path 3	0.99	0.99	0.99	0.99	0.99	0.98	0.85	0.77	0.16	0.13
Path 4	≅1.00	≅1.00	≅1.00	≅1.00	≅1.00	≅1.00	0.85	0.81	0.16	0.16
Path 5-1	≅1.00	≅1.00	≅1.00	≅1.00	≅1.00	≅1.00	0.85	0.81	0.16	0.16
Path 5-2	≅1.00	≅1.00	≅1.00	≅1.00	≅1.00	≅1.00	0.85	0.81	0.16	0.16
Path 6	0.91	0.91	0.91	0.91	0.91	0.89	0.85	0.61	0.17	0.09
Path 7	0.99	0.99	0.99	0.99	0.99	0.98	0.85	0.77	0.16	0.13

As the final step, the overall reliability bounds for the connectivity of Orhangazi and Gemlik transformer stations and the corresponding two state hospitals are calculated and displayed in Table 5.34 and Table 5.35 below.

Table 5.34. *Overall reliability bounds (survival probabilities, P_S) of Orhangazi TS and Bursa Orhangazi State Hospital with respect to the average correlation coefficient ρ=0.32*

	Reliability Bounds									
Return Periods	50 years		100 years		500 years		1000 years		2500 years	
Failure Cases	$P_{S_{max}}$	$P_{S_{min}}$	$P_{S_{max}}$	$P_{S_{min}}$	$P_{S_{max}}$	$P_{S_{min}}$	$P_{S_{max}}$	$P_{S_{min}}$	$P_{S_{max}}$	$P_{S_{min}}$
Orhangazi TS Fails	≅1.00	≅1.00	0.99	0.99	0.26	0.26	0.11	0.11	0.04	0.04
Path 4 and Path 5 (from Orhangazi to Gemlik) fail	≅1.00	≅1.00	≅1.00	≅1.00	≅1.00	≅1.00	0.97	0.96	0.34	0.33
Path 4 and Path 5 (from Bursa NGCCP to Gemlik) fail	≅1.00	≅1.00	≅1.00	≅1.00	≅1.00	≅1.00	0.97	0.96	0.34	0.33
Path 4 and Gemlik TS fail	≅1.00	≅1.00	≅1.00	≅1.00	≅1.00	≅1.00	0.84	0.81	0.22	0.21
Bursa NGCCP fails	≅1.00	≅1.00	0.99	0.99	0.26	0.26	0.11	0.11	0.04	0.04
Path 3 and Path 7 fail	≅1.00	≅1.00	≅1.00	≅1.00	≅1.00	≅1.00	0.97	0.94	0.34	0.29
Bursa Sanayi TS Fails	≅1.00	≅1.00	0.99	0.99	0.26	0.26	0.11	0.11	0.04	0.04
Path 2 and Path 1 fail	0.99	0.99	0.99	0.99	0.99	0.99	0.98	0.84	0.37	0.22
Path 6 and Path 1 fail	0.99	0.99	0.99	0.99	0.99	0.98	0.97	0.84	0.36	0.22
Balıkesir 2 TS and Path 1 fail	≅1.00	≅1.00	≅1.00	≅1.00	0.92	0.90	0.84	0.64	0.28	0.21
Reliability Bounds of Orhangazi TS and Bursa Orhangazi State Hospital	0.99	0.98	0.99	0.95	0.26	0.02	0.11	≅0.00	0.04	≅0.00

Table 5.35. *Overall reliability bounds (survival probabilities, P_S) of Gemlik TS and Bursa Muammer Ağım Gemlik State Hospital with respect to the average correlation coefficient ρ=0.25*

	Reliability Bounds									
Return Periods	50 years		100 years		500 years		1000 years		2500 years	
Failure Cases	$P_{S_{max}}$	$P_{S_{min}}$	$P_{S_{max}}$	$P_{S_{min}}$	$P_{S_{max}}$	$P_{S_{min}}$	$P_{S_{max}}$	$P_{S_{min}}$	$P_{S_{max}}$	$P_{S_{min}}$
Gemlik TS fails	≅1.00	≅1.00	0.99	0.99	0.24	0.24	0.10	0.10	0.04	0.04
Path 5(from Bursa NGCCP to Gemlik) and Path 5 (from Orhangazi to Gemlik) fail	≅1.00	≅1.00	≅1.00	≅1.00	≅1.00	≅1.00	0.98	0.96	0.30	0.29
Path 5(from Bursa NGCCP to Gemlik) and Path 4 fail	≅1.00	≅1.00	≅1.00	≅1.00	≅1.00	≅1.00	0.98	0.96	0.30	0.29
Path 5(from Bursa NGCCP to Gemlik) and Orhangazi TS fail	≅1.00	≅1.00	≅1.00	≅1.00	≅1.00	≅1.00	0.86	0.83	0.19	0.19
Bursa NGCCP fails (probability that it survives from the event of its own failure)	≅1.00	≅1.00	0.99	0.99	0.26	0.26	0.11	0.11	0.04	0.04
Path 3 and Path 7 fail	≅1.00	≅1.00	≅1.00	≅1.00	≅1.00	≅1.00	0.98	0.95	0.30	0.25
Bursa Sanayi TS fails	≅1.00	≅1.00	0.99	0.99	0.26	0.26	0.11	0.11	0.04	0.04
Path 2 and Path 1 fail	0.99	0.99	0.99	0.99	0.99	0.99	0.98	0.85	0.34	0.18
Path 6 and Path1 fail	0.99	0.99	0.99	0.99	0.99	0.99	0.98	0.85	0.32	0.18
Balıkesir 2 TS and Path 1 fail	≅1.00	≅1.00	≅1.00	≅1.00	0.94	0.92	0.86	0.65	0.21	0.13
Reliability Bounds of Gemlik TS and Bursa Muammer Ağım Gemlik State Hospital	0.99	0.98	0.99	0.96	0.24	0.01	0.10	≅0.00	0.04	≅0.00

After the evaluation of the reliability bounds for the connectivity of Gemlik and Orhangazi transformer stations and the two state hospitals that are fed by them, these bounds are compared to illustrate the changes according to the different correlation levels in Table 5.36 and Table 5.37 for Orhangazi TS and Gemlik TS, respectively. The first rows of each table represent the basic cases in which the individual reliability bounds of the system elements are established with respect to the fundamental inequalities of reliability. In these cases, the correlation between different paths and substations is not considered or involved in the calculations. The second rows represent the results when the average correlation coefficients are involved in addition to the basic first cases. In these cases, the average correlation coefficients are obtained based on the number of common segments between different routes. Finally, the third

rows represent the reliability bounds which are constructed based on the average correlation coefficients that are obtained by another approach. In these cases, the average correlation coefficients are calculated based on the concept of scale of fluctuation, where distances between the midpoints of different routes are taken into consideration.

Table 5.36. *Reliability bounds of Orhangazi TS and Bursa Orhangazi State Hospital for different correlation levels*

Return Periods	50 years		100 years		500 years		1000 years		2500 years	
Correlation Levels	Upper Bound	Lower Bound	Upper Bound	Lower Bound	Upper Bound	Lower Bound	Upper Bound	Lower Bound	Upper Bound	Lower Bound
With respect to the fundamental inequalities of reliability (ρ=1 and ρ=0)	0.95	≅0.00	0.95	≅0.00	0.26	≅0.00	0.10	≅0.00	0.03	≅0.00
Average correlation coefficient due to the route similarities (ρ=0.33)	0.98	0.97	0.98	0.94	0.26	0.01	0.10	≅0.00	0.03	≅0.00
Average correlation coefficient due to the distances between the routes (ρ=0.32)	0.99	0.98	0.99	0.95	0.26	0.02	0.11	0.00	0.04	≅0.00

Table 5.37. *Reliability bounds of Gemlik TS and Bursa Muammer Ağım Gemlik State Hospital for different correlation levels*

Return Periods	50 years		100 years		500 years		1000 years		2500 years	
Correlation Levels	Upper Bound	Lower Bound	Upper Bound	Lower Bound	Upper Bound	Lower Bound	Upper Bound	Lower Bound	Upper Bound	Lower Bound
With respect to the fundamental inequalities of reliability (ρ=1 and ρ=0)	0.95	≅0.0	0.95	≅0.00	0.24	≅0.00	0.10	≅0.00	0.03	≅0.00
Average correlation coefficient due to the route similarities (ρ=0.32)	0.98	0.97	0.98	0.95	0.24	0.01	0.10	≅0.00	0.03	≅0.00
Average correlation coefficient due to the distances between the routes (ρ=0.25)	0.99	0.98	0.99	0.96	0.24	0.01	0.10	≅0.00	0.04	≅0.00

From these tables, it is observed that the lower bound values are higher when low correlation exists in the random environment. Here, for illustrative purposes, the scale of fluctuation is arbitrarily assumed to be equal to the average distance between the midpoints of different routes. In future studies, a detailed sensitivity analysis should

be conducted to examine the sensitivity of the results to the magnitude of the scale of fluctuation.

CHAPTER 6

SUMMARY AND CONCLUSIONS

6.1. Summary and Conclusions

Probabilistic assessment of structural reliability of various types of infrastructural systems is getting more and more attention and the number of new studies is increasing every year. This study made additional contributions to the previous ones in certain aspects. First, the research is applied on the real data. Instead of assuming the overhead lines between the substations as the single segments, the coordinates of each component are detected one by one using Google Earth satellite map and the line drawings that are provided by TEİAŞ together. Another contribution is providing an example about the usage of ASCE No.74 (2010) document as the main guide for the wind pressure computations for a power transmission network in Turkey. Since this document is specifically prepared for the structural loading of the electric transmission lines, it provides specific and detailed information on the topic. The probabilistic evaluation of the network based on four different failure modes also demonstrates an example for the transmission system of Turkey. In addition, the effects of spatial correlation and the scale of fluctuation on the reliability bounds of the system are explained and illustrated in detail.

This study is conducted to investigate the structural reliability of lifeline networks under multi-hazard conditions. This is a significant contribution to the literature in this field of study. To achieve this, a network, the elements of which are scattered throughout large regions is selected. Since the study is based mostly on natural hazards, it is considered that the diversity and the variability of natural loads on the components increase as the area covered by the entire system enlarges. The choice of the lifeline system to be focused in the case study is decided to be done by selecting

the one which has wide coverage allowing the exposure of the loads from different natural conditions. Amongst the networks which satisfy this expectation, electric power transmission networks appeared to have an additional advantage. Power transmission is mostly operated by overhead lines in Turkey. This means that the network is expected to be open to both ground acceleration loads due to its components fixed to the ground and to the atmospheric loads due to its overhead design. Having this diversity also gives one a chance to investigate the methods of combining the damaging effects of all those disturbances and the behaviour of the system against them under an overall evaluation.

Estimation of structural resistance against external loads requires probability theory to be involved in the analysis. The loads investigated in this study occur as the consequences of nature based dynamic events. The magnitudes of them can be measured at the right moment of their occurrence but it is not possible to derive exact quantitative cause and result relations between their occurrence mechanism and the core reasons. Even sometimes they can't be measured with a hundred percent accuracy due to the measurement errors. The reason for such uncertainty is the large degree of randomness in everything related to the nature and real life. Probability theory is the field of science which focuses on explaining, measuring and handling uncertainty. With respect to that, probabilistic evaluation seems to be the best approach to deal with uncertainty and randomness in structural reliability evaluation.

This study is conducted with respect to four failure modes namely, seismic, wind, wind-ice and wear out. The wind speed data needed for computations of wind pressure with and without ice accretion is provided by Turkish State Meteorological Institute. The initial completion of the missing data is done with respect to the geographical similarities amongst the districts. After this process, yearly maximum values are obtained and they are used to create 50 years wind speed data set. Then the remaining lack of data is completed by linear interpolation as far as the data structure allowed. The ones which can not even be completed by interpolation are left as they are.

The past earthquake observations are gathered from the database of Disaster and Emergency Management Authority for the study area that extends through the latitudes from 38.70°N to 42.10°N and longitudes from 25.90°E to 31.90°E. All records are converted into moment magnitude M_w unit. Besides this, faults that are located within a close distance to the network elements are chosen and their trace coordinates are detected by using different maps comparatively. After these operations, the locations of the past earthquake records are compared with the delineated trace coordinates of the faults and the unmatched ones are used to construct the background seismicity by fitting the data to the truncated exponential distribution. Peak ground acceleration computations based on the locations of each network element are conducted using Ez Frisk 7.52 (Risk Engineering, 2011) software.

The survival probabilities of each network element is first evaluated under each failure mode one by one and then they are consolidated into an overall lower and upper bounds of reliability. The ways that results are used to derive the reliability bounds of the paths and the entire network is determined by the interconnection styles of the system elements. When a natural disaster occurs, the most important priority is always saving the human life and providing the proper treatment for those who need it. Hospitals have a crucial role on providing such services to the community. Because of this, it is very important to have an idea about their functionality under possible emergency conditions. To provide such an insight, as the last step of the study, a scenario based on the connectivity of two state hospitals is investigated. The aim for a scenario based evaluation is to demonstrate the reliability of two state hospitals with respect to receiving electricity supply under multi-hazard conditions. All these computations are conducted within five different return periods. The reliability calculations of each network element is conducted by using "Reliability Index Calculator" software.

As it is seen from the evaluation results which are presented in Table 5.13 and Table 5.14, both hospitals are expected to be highly reliable with respect to the supply of electricity during the first two return periods, namely within the first 50 and 100 years.

When it comes to 500 years, the results change dramatically. The main reason for this is the increasing dominance of the seismic load. Since the potential energy is accumulated more and more along the faults as time goes on unless it is released by an earthquake, the expected peak ground acceleration keeps increasing with time. Especially after 500 years return period it becomes more significant that the expected seismic load outweighs the mechanical resistances of the components and results in a decrease of their reliability which also reflects itself on the reliability of the two state hospitals, with respect to the continuity of electricity supply.

Wind load both with and without ice accretion might be thought as if it should have taken the lead amongst the loads due to the overhead deployment of the system. It is obvious that there may happen storms of various scales through the years and they are individually powerful enough to destroy the power network partially or even sometimes entirely. With respect to this reality of the daily life, the wind pressure results may seem a bit lower than expected at the first look. The main point here is to consider that the wind pressures are computed based on the 50 years mean wind speed values of yearly extremes. Since the unusually extreme climatic events like tornados and hurricanes are not observed up to the recent years, most of the measurements come from the years of mild weather conditions and the extreme values do not have enough weight to increase the 50 years mean wind speed by themselves. Since the long term local weather conditions are almost unpredictable, the values of the longer return periods are also derived based on 50 years mean wind speeds by using the gamma multiplier as the wind force formula of ASCE No. 74 (2010) indicates.

6.2 Future Work and Recommendations

It is possible to carry out this study further by extending it over some aspects that are not applied due to the limited time and the pre-specified scope of this work. Some details which are not considered and open to be processed are as follows.

Since the power transmission networks extend throughout large regions, there are various types of transmission towers in use. The types of them are chosen due to their

pre planned location and their expected function. Some of them might be the ones that end the line before the transformer stations while some others might be the towers that are specifically designed for river or valley crossings. Even the same type of towers may be designed with different heights sometimes. Each tower type changes the values of the parameters of the wind force formula as explained before. Gathering tower type data and using the actual dimensions of each tower may yield results which represent the real conditions better.

In addition to this, the topography of each transmission tower's location can be carefully investigated and defined. Such a definition process may help to choose the terrain based exposure categories and then the values of topography based parameters of the wind force formula provided by ASCE No.74 (2010) more realistically.

Reliability of the system components under seismic failure mode is conducted by assuming that the seismic load is distributed according to the normal distribution. Since there are too many components in the network, it is not possible to detect the distribution of the seismicity at each location one by one due to the limited time and the complexity of the process. As another study, the distribution of seismicity at each location can be assessed and used in reliability computations.

Similarly, distributions of wind pressures of each district are comparatively given in Table 5.5. The wind pressures of all districts are assumed to have Gumbel distribution as explained before. As a further study, the reliability of each network component in wind and wind-ice failure modes can be evaluated according to the corresponding distribution valid at their exact location.

REFERENCES

Abrahamson, N. A., and Silva, W. J. 2008. Summary of the Abrahamson & Silva NGA Ground-Motion Relations, *Earthquake Spectra*, *24*(1), 67-97.

Adachi, T. 2007. Impact of Cascading Failures on Performance Assessment of Civil Infrastructure Systems. Georgia Institute of Technology, PhD Dissertation.

Adachi, T., Ellingwood, B. R. 2009. "Serviceability assessment of electrical power transmission systems under probabilistically stated seismic hazards: case study for Shelby County, Tennessee." Struct. and Infrastruct. Engrg. 5(5):343-354

AFAD. 2018. Internet page of the Earthquake Research Department, Disaster and Emergency Management Presidency, Republic of Turkey, The Ministry of Interior, 1900 - 20xx Earthquake Catalog (M >= 4.0), https://deprem.afad.gov.tr/, Last access : 2018.

Aki, K. 1966. Generation and Propagation of G Waves from the Niigata Earthquake of June 16, 1964: Part 1. A statistical analysis.

Akkar, S. 2018. Personal Communication, Kandilli Observatory and Earthquake Research Institute, Boğaziçi University, İstanbul.

Akkar, S., Çağnan, Z., Yenier, E., Erdoğan, Ö., Sandıkkaya, A., Gülkan, P., 2010. The recently compiled Turkish strong motion database: preliminary investigation for seismological parameters. Journal of Seismology 14, 457– 479.

Akkaya, A. D. 1995. Stochastic Modelling of Earthquake Occurrences and Estimation of Seismic Hazard: A Random Field Approach, METU, PhD Dissertation.

ASCE Manuals and Reports on Engineering Practice No. 74. 2010. Guidelines for Electrical Transmission Line Structural Loading. American Society of Civil Engineers, Reston, Virginia.

ASCE Standard ASCE/SEI 7-05 Including Supplement No. 1. 2006. Minimum Design Loads for Buildings and Other Structures. American Society of Civil Engineers, Reston, Virginia.

Atkinson, G., and D. Boore (1995). New Ground Motion Relations for Eastern North America, Bull. Seism. Soc. Am. 85, 17–30.

Baker, J. W. 2008. An Introduction to Probabilistic Seismic Hazard Analysis (PSHA), White paper, version 1, 72.

Boore, D. M., Joyner, W. B., Fumal, T. E. 1997. Equations for Estimating Horizontal Response Spectra and Peak Acceleration from Western North American Earthquakes: A Summary of Recent Work. Seismological Research Letters, 68(1), 128-153.

Cornell, C. A. 1969. A Normative Second Moment Reliability Theory for Structural Design: Seminar No. 6, December 15, 1969. Solid Mechanics Division, University of Waterloo.

Deniz, A., Yücemen, M. S. 2010. Magnitude Conversion Problem for the Turkish Earthquake Data. Natural hazards, 55(2), 333-352.

Ellingwood, B. R., Tekie, P. B. 1999. Wind Load Statistics for Probability-Based Structural Design. Journal of Structural Engineering, 125(4), 453-463.

Emre, Ö., Duman, T. Y., Özalp, S., Şaroğlu, F., Olgun, Ş., Elmacı, H., Çan, T. 2016. Active Fault Database of Turkey, Bull Earthquake Eng., Springer Science+Business Media Dordrecht 2016.

Fırat, F. K. 2007. Development of Load and Resistance Factors for Reinforced Concrete Structures in Turkey. Middle East Technical University, PhD Dissertation.

Grigoriu, M., & Turkstra, C. (1979). Safety of Structural Systems with Correlated Resistances. *Applied Mathematical Modelling*, *3*(2), 130-136.

Gutenberg, B. 1945a. Amplitudes of Surface Waves and Magnitude of Shallow Earthquakes, Bull. Seismol. Soc. Amer., 35, 3-12.

Gutenberg, B. 1945b. Amplitudes of P, PP, and S and Magnitude of Shallow Earthquakes, Bull. Seismol. Soc. Amer., 35, 57-69.

Gutenberg, B. 1945c. Magnitude Determination for Deep-focus Earthquakes, Bull. Seismol. Soc. Amer., 35, 117-130.

Gutenberg, B., Richter, C. F. 1936. On Seismic Waves (third paper), Gerlands Beitrage zur Geophysik, 47, 73-131.

Gutenberg, B., Richter, C. F. 1944. Frequency of Earthquakes in California. Bulletin of the Seismological Society of America, 34(4), 185-188.

Gülerce, Z., Kargioglu, B., Abrahamson, N. A. 2015. Turkey-Adjusted NGA W1 Horizontal Ground Motion Prediction Models. Earthquake Spectra.

Güven, N. 2017. Personal Communication, Electrical and Electronics Engineering Department, METU, Ankara

Hanks, T. C., Kanamori, H. 1979. A Moment Magnitude Scale. Journal of Geophysical Research B, 84(B5), 2348-2350.

Hasançebi, O. 2019. Personal Communication, Civil Engineering Department, METU, Ankara.

Koçak, A. 2018. Personal Communication, Kaan Havacılık A.Ş., İstanbul.

Lallemant, D., Kiremidjian, A., Burton, H. 2015. Statistical Procedures for Developing Earthquake Damage Fragility Curves. Earthquake Engineering & Structural Dynamics, 44(9), 1373-1389.

Liu, Gee-Yu., Liu, Chih-Wen., Wang, Yi-Jen., Jean, Wen-Ju. 2004. Seismic Risk Analysis of Electric Power Networks Using Hazard-Consistent Scenario Earthquakes. In Proceedings of The Thirteenth World Conference on Earthquake Engineering. Vancouver, B. C., Canada.

Nowak, A. S., & Collins, K. R. 2012. Reliability of Structures. CRC Press.

Oikawa, T., Fukushima, S., Takase, H., Uchiyama, T., and Muramatsu, K. 2001. Seismic Reliability Evaluation of Electrical Power Transmission Systems and its Effect on Core Damage Frequency. Transactions SMIRT 16., Washington DC.

Power Line Systems Inc. 2015. PLS-TOWER Manual: Analysis and design of steel latticed towers used in transmission and communication facilities. USA: Power Line Systems Inc.

Richter, C. F. 1935. An Instrumental Magnitude Scale, Bull. Seismol. Soc. Amer., 25, 1-32.

Richter, C. F. 1958. Elementary Seismology, W.H. Freeman and Company, San Francisco.

Risk Engineering Inc. 2011. EZ-FRISK: 2005, User's Manual, Version 7.52, Colorado.

Sağlam, H. 2018. Personal Communication, TEİAŞ (Turkish Electricity Transmission Corporation), Ankara.

Salman, A. 2016. Risk-Based Assessment and Strengthening of Electrical Power Systems Subjected to Natural Hazards, Open Access Dissertation, Michigan Technological University.

Salman, A. M., Li, Y. 2016. Age-dependent Fragility and Life-cycle Cost Analysis of Wood and Steel Power Distribution Poles Subjected to Hurricanes. Structure & Infrastructure Engineering, 12(8), 890-903.

Schwartz, D. P., Coppersmith, K. J. 1984. Fault Behavior and Characteristic Earthquakes: Examples from the Wasatch and San Andreas Fault Zones. Journal of Geophysical Research: Solid Earth (1978–2012), 89(B7), 5681-5698.

Selçuk, A. S. 1996. A Probabilistic Model for the Evaluation of Reliability of Lifeline Networks Under Seismic Hazard. METU, PhD Dissertation.

SYNER-G D 3.12 Deliverable. 2013. SYNER-G Fragility Curves for All Elements at Risk. Project No:244061. European Community's Seventh Framework Programme (FP7/2007-2013).

Şaroğlu, F., Emre, Ö., Kuşçu, İ., 1992. Active Fault Map of Turkey. General Directorate of Mineral Research and Exploration. Ankara-Turkey.

TEİAŞ. Internet page of Turkish Electricity Transmission Corporation, Bursa Regional Office, Single Line Diagram of 380 and 154 kV Power Transmission Lines and Transformer Stations, https://www.teias.gov.tr/bolge/bursa/, Last Access: 2017.

TEİAŞ. 2000. EKATY (Elektrik Kuvvetli Akım Tesisleri Yönetmeliği), Legal Gazette of Turkey, 24246.

Topkara-Özcan, N. 2016. Reliability of Transportation Lifeline Systems Subjected to Earthquake Loads. Middle East Technical University, Master Thesis.

ULIRVISION. 2018. Internet page of Zhejiang Ulirvision Technology Co., LTD., UV image of a corona discharge, https://www.ulirvision.co.uk/., last Access: 2018.

USGS. 2019. Internet page of U.S. Geological Survey. Tectonic Plate Boundaries, https://earthquake.usgs.gov/learn/kml.php, last access:2019.

Vanmarcke, E. H. 1983. Random Fields : Analysis and Synthesis, MIT Press, Cambridge, Mass.

Wallace, R. E. 1970. “Earthquake Recurrence Intervals on the San Andreas Fault”. Geol. Soc. Am. Bull. 1970; 81: 2875-2890.

Weichert, D. H. 1980. Estimation of the Earthquake Recurrence Parameters for Unequal Observation Periods for Different Magnitudes. Bulletin of the Seismological Society of America, Vol. 70, No. 4, pp. 1337-1346.

Yavuz, E. A. 2013. Reliability Based Safety Assessment of Buried Continuous Pipelines Subjected to Earthquake Effects. Middle East Technical University, Master Thesis.

Yılmaz-Öztürk, N. 2008. Probabilistic Seismic Hazard Analysis: A Sensitivity Study With Respect to Different Models. Middle East Technical University, PhD Dissertation.

Yoo, Y. B., Deo N. 1988. A Comparison of Algorithms for Terminal Pair Reliability. IEEE Transactions on Reliability, 37, 210-215.

Youngs, R. R., Coppersmith, K. J. 1985. Implications of Fault Slip Rates and Earthquake Recurrence Models to Probabilistic Seismic Hazard Estimates. Bulletin of the Seismological Society of America, 75(4), 939-964.

Yücemen, M. S. 1989(b). Unpublished Lecture Notes of Stat 634, Theory of stationary random Functions, METU, Ankara.

Yücemen, M. S. 2018. Unpublished Lecture Notes of CE 589, Structural Reliability, METU, Ankara.

Yücemen, M. S. 2018. Unpublished Class Material of CE 589, Structural Reliability, RIC (Reliability Index Calculator).

APPENDICES

A.1. Structural Analysis Output of 154 kV PB Type Suspension Tower Under Wind Load (The values given in member forces of Figure 3.1 are supplied by Prof. Dr. Oğuzhan Hasançebi)

Table A.1 *Structural Analysis Output of 154 kV PB Type Suspension Tower Under Extreme Wind Conditions*

Row #	Group Label	Group Description	Angle Type	Angle Size (mm)	Steel Strength (MPa)	Max Usage %	Usage Control	Max Usage In Comp. %
1	DUM	D	DUM	1*1*1	355	0		0
2	1	L	SAE	50*50*5	235	18.55	Comp	18.55
3	2	L	SAE	50*50*5	235	41.88	Comp	41.88
4	3	W	SAE	70*70*7	235	52.88	Comp	52.88
5	4	W	SAE	70*70*7	235	75.07	Comp	75.07
6	5	W	SAE	65*65*6	235	66.26	Tens	10.95
7	6	W	SAE	60*60*5	235	58.09	Comp	58.09
8	7	W	SAE	40*40*4	235	30.52	Comp	30.52
9	8	L	SAE	35*35*3	235	42.47	Tens	0
10	9	L	DAE	100*100*10	235	5.67	Comp	5.67
11	10	L	SAE	35*35*3	235	37.02	Comp	37.02
12	11	L	SAE	100*100*8	235	30.47	Tens	0
13	12	W	SAE	40*40*4	235	20.35	Tens	12.99
14	13	W	SAE	60*60*5	235	88.5	Comp	88.5
15	14	W	SAE	50*50*5	235	76.99	Tens	28.27
16	15	W	SAE	45*45*4	235	83.84	Comp	83.84
17	16	W	SAE	45*45*4	235	71.74	Tens	12.88
18	17	W	SAE	45*45*4	235	83.46	Comp	83.46
19	18	H	SAE	45*45*4	235	71.72	Tens	13.76
20	19	H	SAE	45*45*4	235	81.42	Comp	81.42
21	20	L	SAE	40*40*4	235	12.93	Tens	3.03
22	21	L	SAE	40*40*4	235	24.27	Comp	24.27
23	22	W	SAE	40*40*4	235	14.26	Comp	14.26
24	23	W	SAE	40*40*4	235	0		0
25	24	W	SAE	65*65*6	235	51.03	Tens	0

**The last two columns represent the usage percentage of the capacity of the corresponding element under compression or tension.*

Table A.1 (Continued) *Structural Analysis Output of 154 kV PB Type Suspension Tower Under Extreme Wind Conditions*

Row #	Group Label	Group Description	Angle Type	Angle Size (mm)	Steel Strength (MPa)	Max Usage %	Usage Control	Max Usage In Comp. %
26	25	W	SAE	65*65*7	235	52.61	Comp	52.61
27	26	W	SAE	40*40*4	235	25.88	Comp	25.88
28	27	W	SAE	40*40*4	235	24.47	Comp	24.47
29	28	W	SAE	40*40*4	235	21.13	Comp	21.13
30	29	W	SAE	50*50*5	235	26.32	Tens	20.39
31	30	W	SAE	40*40*4	235	38.14	Comp	38.14
32	31	W	SAE	40*40*4	235	30.42	Tens	23.55
33	32	L	SAE	40*40*4	235	26.61	Comp	26.61
34	33	L	SAE	40*40*4	235	22.65	Tens	20.05
35	34	L	SAE	40*40*4	235	20.22	Comp	20.22
36	35	L	SAE	40*40*4	235	13.81	Comp	13.81
37	36	W	SAE	60*60*6	235	29.72	Comp	29.72
38	37	W	SAE	50*50*5	235	96.94	Tens	84.29
39	38	W	SAE	65*65*6	235	85.39	Comp	85.39
40	39	W	SAE	65*65*6	235	92.07	Comp	92.07
41	40	W	SAE	40*40*4	235	6.5	Comp	6.5
42	41	W	SAE	65*65*6	235	2.69	Comp	2.69
43	42	H	SAE	40*40*4	235	37.21	Tens	0
44	43	H	SAE	50*50*5	235	7.16	Comp	7.16
45	44	L	SAE	80*80*8	235	82.71	Comp	82.71
46	45	L	SAE	80*80*8	235	94.34	Comp	94.34
47	46	W	SAE	80*80*8	235	100.38	Comp	100.38
48	47	W	SAE	80*80*10	235	82.79	Comp	82.79
49	48	W	SAE	80*80*10	235	88.38	Comp	88.38
50	49	W	SAE	80*80*10	235	92.7	Comp	92.7
51	50	W	SAE	80*80*10	235	95.12	Comp	95.12
52	51	W	SAE	80*80*10	235	97.28	Comp	97.28
53	52	W	SAE	80*80*10	235	0		0
54	53	W	SAE	50*50*6	235	21.14	Comp	21.14
55	54	W	SAE	50*50*6	235	20.28	Comp	20.28
56	55	W	SAE	50*50*5	235	20.22	Tens	19.87
57	56	L	SAE	50*50*5	235	24.83	Comp	24.83
58	57	L	SAE	50*50*4	235	30.3	Comp	30.3
59	58	L	SAE	60*60*5	235	22.91	Comp	22.91
60	59	W	SAE	60*60*5	235	20.48	Comp	20.48
61	60	W	SAE	60*60*5	235	31.31	Comp	31.31

Table A.1 (Continued) *Structural Analysis Output of 154 kV PB Type Suspension Tower Under Extreme Wind Conditions*

Row #	Group Label	Group Description	Angle Type	Angle Size (mm)	Steel Strength (MPa)	Max Usage %	Usage Control	Max Usage In Comp. %
62	61	W	SAE	65*65*6	235	0		0
63	62	W	SAE	45*45*4	235	1.73	Comp	1.73
64	63	W	SAE	45*45*4	235	1.22	Tens	0
65	64	W	SAE	50*50*5	235	2.89	Comp	2.89
66	65	W	SAE	45*45*4	235	4.17	Tens	0.25
67	66	H	SAE	65*65*7	235	7.24	Comp	7.24
68	101	W	SAE	80*80*8	235	0		0
69	102	W	SAE	80*80*8	235	0		0
70	103	W	SAE	80*80*8	235	0		0
71	104	L	SAE	80*80*8	235	0		0
72	105	W	SAE	80*80*8	235	0		0
73	110	W	SAE	50*50*5	235	0		0
74	111	W	SAE	50*50*4	235	0		0
75	112	W	SAE	50*50*4	235	0		0
76	113	W	SAE	50*50*5	235	0		0
77	114	W	SAE	50*50*5	235	0		0
78	115	W	SAE	50*50*6	235	0		0
79	116	L	SAE	45*45*4	235	0		0
80	201	W	SAE	80*80*10	235	0		0
81	202	W	SAE	80*80*10	235	0		0
82	203	W	SAE	80*80*10	235	0		0
83	204	L	SAE	80*80*10	235	0		0
84	205	W	SAE	80*80*10	235	0		0
85	210	W	SAE	50*50*5	235	0		0
86	211	W	SAE	50*50*4	235	0		0
87	212	W	SAE	50*50*4	235	0		0
88	213	W	SAE	50*50*5	235	0		0
89	214	W	SAE	50*50*5	235	0		0
90	215	W	SAE	50*50*5	235	0		0
91	216	L	SAE	50*50*5	235	0		0
92	301	W	SAE	80*80*10	235	0		0
93	302	W	SAE	80*80*10	235	0		0
94	303	W	SAE	80*80*10	235	0		0

Table A.1 (Continued) *Structural Analysis Output of 154 kV PB Type Suspension Tower Under Extreme Wind Conditions*

Row #	Group Label	Group Description	Angle Type	Angle Size (mm)	Steel Strength (MPa)	Max Usage %	Usage Control	Max Usage In Comp. %
95	304	L	SAE	80*80*10	235	0		0
96	305	W	SAE	80*80*10	235	0		0
97	310	W	SAE	60*60*5	235	0		0
98	311	W	SAE	50*50*4	235	0		0
99	312	W	SAE	60*60*5	235	0		0
100	313	W	SAE	60*60*5	235	0		0
101	314	W	SAE	60*60*5	235	0		0
102	315	W	SAE	60*60*5	235	0		0
103	316	L	SAE	50*50*4	235	0		0
104	401	W	SAE	80*80*10	235	0		0
105	402	W	SAE	80*80*10	235	0		0
106	403	W	SAE	80*80*10	235	0		0
107	404	L	SAE	80*80*10	235	0		0
108	405	W	SAE	80*80*10	235	0		0
109	410	W	SAE	65*65*6	235	0		0
110	411	W	SAE	50*50*4	235	0		0
111	412	W	SAE	60*60*5	235	0		0
112	413	W	SAE	60*60*5	235	0		0
113	414	W	SAE	60*60*5	235	0		0
114	415	W	SAE	60*60*5	235	0		0
115	416	L	SAE	50*50*5	235	0		0
116	501	W	SAE	80*80*10	235	0		0
117	502	W	SAE	80*80*10	235	0		0
118	503	W	SAE	80*80*10	235	0		0
119	504	L	SAE	80*80*10	235	0		0
120	505	W	SAE	80*80*10	235	0		0
121	510	W	SAE	50*50*4	235	0		0
122	511	W	SAE	50*50*4	235	0		0
123	512	W	SAE	50*50*4	235	0		0
124	513	W	SAE	50*50*4	235	0		0
125	514	W	SAE	60*60*5	235	0		0
126	515	W	SAE	60*60*5	235	0		0
127	516	L	SAE	50*50*6	235	0		0

Table A.1 (Continued) *Structural Analysis Output of 154 kV PB Type Suspension Tower Under Extreme Wind Conditions*

Row #	Group Label	Group Description	Angle Type	Angle Size (mm)	Steel Strength (MPa)	Max Usage %	Usage Control	Max Usage In Comp. %
128	601	W	SAE	80*80*10	235	0		0
129	602	W	SAE	80*80*10	235	97.54	Comp	97.54
130	603	W	SAE	80*80*10	235	0		0
131	604	L	SAE	80*80*10	235	0		0
132	605	W	SAE	80*80*10	235	0		0
133	610	W	SAE	50*50*4	235	23.3	Comp	23.3
134	611	W	SAE	50*50*5	235	0		0
135	612	W	SAE	50*50*4	235	31.56	Comp	31.56
136	613	W	SAE	50*50*4	235	0		0
137	614	W	SAE	60*60*5	235	0		0
138	615	W	SAE	60*60*5	235	0		0
139	616	L	SAE	50*50*6	235	2.53	Comp	2.53
140	701	W	SAE	80*80*10	235	0		0
141	702	W	SAE	80*80*10	235	0		0
142	703	W	SAE	80*80*10	235	0		0
143	704	L	SAE	80*80*10	235	0		0
144	705	W	SAE	80*80*10	235	0		0
145	706	W	SAE	80*80*10	235	0		0
146	707	W	SAE	80*80*10	235	0		0
147	710	W	SAE	50*50*5	235	0		0
148	711	W	SAE	60*60*5	235	0		0
149	712	W	SAE	50*50*4	235	0		0
150	713	W	SAE	50*50*4	235	0		0
151	714	W	SAE	60*60*5	235	0		0
152	715	W	SAE	60*60*5	235	0		0
153	716	L	SAE	60*60*5	235	0		0
154	717	L	SAE	60*60*5	235	0		0
155	718	L	SAE	60*60*5	235	0		0

A.2. Structural Analysis Output of 154 kV PB Type Suspension Tower Under Wind and Ice loads (The values given in member forces of Figure 3.2 are supplied by Prof. Dr. Oğuzhan Hasançebi)

Table A.2 *Structural Analysis Output of 154 kV PB Type Suspension Tower Under Extreme Wind and Ice Conditions*

Row #	Group Label	Group Description	Angle Type	Angle Size (mm)	Steel Strength (MPa)	Max Usage %	Usage Control	Max Usage In Comp. %
1	DUM	D	DUM	1*1*1	355	0		0
2	1	L	SAE	50*50*5	235	41.06	Comp	41.06
3	2	L	SAE	50*50*5	235	91.89	Comp	91.89
4	3	W	SAE	70*70*7	235	83.47	Comp	83.47
5	4	W	SAE	70*70*7	235	87.35	Comp	87.35
6	5	W	SAE	65*65*6	235	77.37	Tens	26.31
7	6	W	SAE	60*60*5	235	58.96	Comp	58.96
8	7	W	SAE	40*40*4	235	43.46	Comp	43.46
9	8	L	SAE	35*35*3	235	59.9	Tens	0
10	9	L	DAE	100*100*10	235	30.38	Tens	28.33
11	10	L	SAE	35*35*3	235	41.25	Comp	41.25
12	11	L	SAE	100*100*8	235	46	Tens	0
13	12	W	SAE	40*40*4	235	21.11	Tens	9.86
14	13	W	SAE	60*60*5	235	100.12	Comp	100.12
15	14	W	SAE	50*50*5	235	85.4	Tens	7.2
16	15	W	SAE	45*45*4	235	97.63	Comp	97.63
17	16	W	SAE	45*45*4	235	83.59	Tens	0
18	17	W	SAE	45*45*4	235	97.22	Comp	97.22
19	18	H	SAE	45*45*4	235	83.59	Tens	0
20	19	H	SAE	45*45*4	235	94.59	Comp	94.59
21	20	L	SAE	40*40*4	235	14.23	Tens	1.47
22	21	L	SAE	40*40*4	235	61.47	Comp	61.47
23	22	W	SAE	40*40*4	235	58.3	Comp	58.3
24	23	W	SAE	40*40*4	235	0		0
25	24	W	SAE	65*65*6	235	77.06	Tens	0
26	25	W	SAE	65*65*7	235	76.17	Comp	76.17
27	26	W	SAE	40*40*4	235	32.69	Comp	32.69
28	27	W	SAE	40*40*4	235	50.12	Comp	50.12
29	28	W	SAE	40*40*4	235	65.19	Comp	65.19
30	29	W	SAE	50*50*5	235	81.03	Tens	74.27

**The last two columns represent the usage percentage of the capacity of the corresponding element under compression or tension.*

Table A.2 (Continued) *Structural Analysis Output of 154 kV PB Type Suspension Tower Under Extreme Wind and Ice Conditions*

Row #	Group Label	Group Description	Angle Type	Angle Size (mm)	Steel Strength (MPa)	Max Usage %	Usage Control	Max Usage In Comp. %
31	30	W	SAE	40*40*4	235	67.46	Comp	67.46
32	31	W	SAE	40*40*4	235	53.85	Tens	52.41
33	32	L	SAE	40*40*4	235	44.29	Comp	44.29
34	33	L	SAE	40*40*4	235	41.1	Comp	41.1
35	34	L	SAE	40*40*4	235	35.08	Tens	33.79
36	35	L	SAE	40*40*4	235	17.39	Comp	17.39
37	36	W	SAE	60*60*6	235	55.04	Comp	55.04
38	37	W	SAE	50*50*5	235	97.37	Tens	70.94
39	38	W	SAE	65*65*6	235	82.95	Comp	82.95
40	39	W	SAE	65*65*6	235	88.74	Comp	88.74
41	40	W	SAE	40*40*4	235	23.57	Comp	23.57
42	41	W	SAE	65*65*6	235	2.26	Comp	2.26
43	42	H	SAE	40*40*4	235	53.62	Tens	0
44	43	H	SAE	50*50*5	235	86.92	Comp	86.92
45	44	L	SAE	80*80*8	235	85.04	Comp	85.04
46	45	L	SAE	80*80*8	235	96.01	Comp	96.01
47	46	W	SAE	80*80*8	235	100.68	Comp	100.68
48	47	W	SAE	80*80*10	235	82.39	Comp	82.39
49	48	W	SAE	80*80*10	235	86.57	Comp	86.57
50	49	W	SAE	80*80*10	235	90.04	Comp	90.04
51	50	W	SAE	80*80*10	235	91.16	Comp	91.16
52	51	W	SAE	80*80*10	235	92.47	Comp	92.47
53	52	W	SAE	80*80*10	235	0		0
54	53	W	SAE	50*50*6	235	75.77	Comp	75.77
55	54	W	SAE	50*50*6	235	67.64	Comp	67.64
56	55	W	SAE	50*50*5	235	69.29	Comp	69.29
57	56	L	SAE	50*50*5	235	66.37	Comp	66.37
58	57	L	SAE	50*50*4	235	88	Comp	88
59	58	L	SAE	60*60*5	235	47.08	Comp	47.08
60	59	W	SAE	60*60*5	235	46.07	Comp	46.07
61	60	W	SAE	60*60*5	235	49.32	Comp	49.32
62	61	W	SAE	65*65*6	235	0		0
63	62	W	SAE	45*45*4	235	1.09	Comp	1.09
64	63	W	SAE	45*45*4	235	1.51	Tens	0
65	64	W	SAE	50*50*5	235	4.5	Comp	4.5
66	65	W	SAE	45*45*4	235	8.67	Tens	5.56

Table A.2 (Continued) *Structural Analysis Output of 154 kV PB Type Suspension Tower Under Extreme Wind and Ice Conditions*

Row #	Group Label	Group Description	Angle Type	Angle Size (mm)	Steel Strength (MPa)	Max Usage %	Usage Control	Max Usage In Comp. %
67	66	H	SAE	65*65*7	235	15.28	Comp	15.28
68	101	W	SAE	80*80*8	235	0		0
69	102	W	SAE	80*80*8	235	0		0
70	103	W	SAE	80*80*8	235	0		0
71	104	L	SAE	80*80*8	235	0		0
72	105	W	SAE	80*80*8	235	0		0
73	110	W	SAE	50*50*5	235	0		0
74	111	W	SAE	50*50*4	235	0		0
75	112	W	SAE	50*50*4	235	0		0
76	113	W	SAE	50*50*5	235	0		0
77	114	W	SAE	50*50*5	235	0		0
78	115	W	SAE	50*50*6	235	0		0
79	116	L	SAE	45*45*4	235	0		0
80	201	W	SAE	80*80*10	235	0		0
81	202	W	SAE	80*80*10	235	0		0
82	203	W	SAE	80*80*10	235	0		0
83	204	L	SAE	80*80*10	235	0		0
84	205	W	SAE	80*80*10	235	0		0
85	210	W	SAE	50*50*5	235	0		0
86	211	W	SAE	50*50*4	235	0		0
87	212	W	SAE	50*50*4	235	0		0
88	213	W	SAE	50*50*5	235	0		0
89	214	W	SAE	50*50*5	235	0		0
90	215	W	SAE	50*50*5	235	0		0
91	216	L	SAE	50*50*5	235	0		0
92	301	W	SAE	80*80*10	235	0		0
93	302	W	SAE	80*80*10	235	0		0
94	303	W	SAE	80*80*10	235	0		0
95	304	L	SAE	80*80*10	235	0		0
96	305	W	SAE	80*80*10	235	0		0
97	310	W	SAE	60*60*5	235	0		0
98	311	W	SAE	50*50*4	235	0		0
99	312	W	SAE	60*60*5	235	0		0
100	313	W	SAE	60*60*5	235	0		0
101	314	W	SAE	60*60*5	235	0		0
102	315	W	SAE	60*60*5	235	0		0

Table A.2 (Continued) *Structural Analysis Output of 154 kV PB Type Suspension Tower Under Extreme Wind and Ice Conditions*

Row #	Group Label	Group Description	Angle Type	Angle Size (mm)	Steel Strength (MPa)	Max Usage %	Usage Control	Max Usage In Comp. %
103	316	L	SAE	50*50*4	235	0		0
104	401	W	SAE	80*80*10	235	0		0
105	402	W	SAE	80*80*10	235	0		0
106	403	W	SAE	80*80*10	235	0		0
107	404	L	SAE	80*80*10	235	0		0
108	405	W	SAE	80*80*10	235	0		0
109	410	W	SAE	65*65*6	235	0		0
110	411	W	SAE	50*50*4	235	0		0
111	412	W	SAE	60*60*5	235	0		0
112	413	W	SAE	60*60*5	235	0		0
113	414	W	SAE	60*60*5	235	0		0
114	415	W	SAE	60*60*5	235	0		0
115	416	L	SAE	50*50*5	235	0		0
116	501	W	SAE	80*80*10	235	0		0
117	502	W	SAE	80*80*10	235	0		0
118	503	W	SAE	80*80*10	235	0		0
119	504	L	SAE	80*80*10	235	0		0
120	505	W	SAE	80*80*10	235	0		0
121	510	W	SAE	50*50*4	235	0		0
122	511	W	SAE	50*50*4	235	0		0
123	512	W	SAE	50*50*4	235	0		0
124	513	W	SAE	50*50*4	235	0		0
125	514	W	SAE	60*60*5	235	0		0
126	515	W	SAE	60*60*5	235	0		0
127	516	L	SAE	50*50*6	235	0		0
128	601	W	SAE	80*80*10	235	0		0
129	602	W	SAE	80*80*10	235	92.12	Comp	92.12
130	603	W	SAE	80*80*10	235	0		0
131	604	L	SAE	80*80*10	235	0		0
132	605	W	SAE	80*80*10	235	0		0
133	610	W	SAE	50*50*4	235	41.56	Comp	41.56
134	611	W	SAE	50*50*5	235	0		0
135	612	W	SAE	50*50*4	235	50.43	Comp	50.43
136	613	W	SAE	50*50*4	235	0		0
137	614	W	SAE	60*60*5	235	0		0
138	615	W	SAE	60*60*5	235	0		0

Table A.2 (Continued) *Structural Analysis Output of 154 kV PB Type Suspension Tower Under Extreme Wind and Ice Conditions*

Row #	Group Label	Group Description	Angle Type	Angle Size (mm)	Steel Strength (MPa)	Max Usage %	Usage Control	Max Usage In Comp. %
139	616	L	SAE	50*50*6	235	3.07	Comp	3.07
140	701	W	SAE	80*80*10	235	0		0
141	702	W	SAE	80*80*10	235	0		0
142	703	W	SAE	80*80*10	235	0		0
143	704	L	SAE	80*80*10	235	0		0
144	705	W	SAE	80*80*10	235	0		0
145	706	W	SAE	80*80*10	235	0		0
146	707	W	SAE	80*80*10	235	0		0
147	710	W	SAE	50*50*5	235	0		0
148	711	W	SAE	60*60*5	235	0		0
149	712	W	SAE	50*50*4	235	0		0
150	713	W	SAE	50*50*4	235	0		0
151	714	W	SAE	60*60*5	235	0		0
152	715	W	SAE	60*60*5	235	0		0
153	716	L	SAE	60*60*5	235	0		0
154	717	L	SAE	60*60*5	235	0		0
155	718	L	SAE	60*60*5	235	0		0

B.1. Trace Coordinates of the Fault Sources (Based on the data which is provided by Prof. Dr. Sinan Akkar and MTA) (Akkar, S. Personal Communication, 2018.)

Table B.1 *Trace Coordinates of the Faults*

Fault Code	Fault Name	Latitude (°N)	Longitude (°E)
1_21	Yeniçağa Segment	40.8101	32.0958
		40.7794	31.9752
		40.755	31.8393
		40.7315	31.7375
1_22	Bolu Segment	40.7243	31.7071
		40.6998	31.6082
		40.673	31.5075
		40.6513	31.4141
		40.6279	31.3364
1_23	Taşkesti Segment	40.627	31.3256
		40.6104	31.2322
		40.6044	31.1696
		40.5906	31.0758
1_24	Dokurcun Segment	40.5835	30.9906
		40.5786	30.9392
		40.5844	30.8994
		40.6039	30.809
		40.6177	30.7184
		40.6336	30.6368
		40.6534	30.5245
		40.6585	30.4452

Table B.1 (Continued) *Trace Coordinates of the Faults*

Fault Code	Fault Name	Latitude (°N)	Longitude (°E)
1_25	Düzce Segment	40.7779	31.0282
		40.7892	31.1015
		40.7774	31.1497
		40.7909	31.2367
		40.8012	31.3341
		40.8054	31.3837
		40.7925	31.4741
		40.7678	31.546
		40.7688	31.6124
1_26	Karadere Segment	40.6691	30.7121
		40.6946	30.7544
		40.7252	30.831
		40.7441	30.8878
		40.7682	30.9654
		40.8006	30.0384
		40.8367	31.0981
		40.8607	31.137
1_27	Arifiye Segment	40.7175	30.6442
		40.7143	30.5348
		40.7271	30.4487
		40.732	30.3984
1_28	Tepetarla Segment	40.7329	30.351
		40.7325	30.249
		40.7347	30.1729
		40.7377	30.0936
		40.7342	29.9809
1_29	Gölcük Segment	40.74	29.9231
		40.7434	29.8551
		40.7474	29.7933
		40.7519	29.7543

Table B.1 (Continued) *Trace Coordinates of the Faults*

Fault Code	Fault Name	Latitude (°N)	Longitude (°E)
1_30	Karamürsel Segment	40.7544	29.743
		40.7451	29.6913
		40.745	29.6407
		40.7402	29.5891
		40.7342	29.5652
1_31	Darıca Segment	40.7391	29.553
		40.7411	29.5118
		40.7423	29.483
		40.7455	29.4087
1_32	Adalar Segment	40.7376	29.4178
		40.7399	29.3588
		40.7473	29.2816
		40.7712	29.2028
		40.8033	29.1365
		40.8495	29.0329
		40.8923	28.953
1_33	Çınarcık Segment	40.76	28.8248
		40.7406	28.8885
		40.7266	28.9647
		40.7103	29.0292
		40.6955	29.0936
		40.6779	29.1572
		40.6977	29.2353
1_34	Avcılar Segment	40.8896	28.9442
		40.8981	28.8634
		40.898	28.7661
		40.893	28.6486
		40.8932	28.6072
		40.9059	28.5794
		40.878	28.4984

Table B.1 (Continued) *Trace Coordinates of the Faults*

Fault Code	Fault Name	Latitude (°N)	Longitude (°E)
1_35	Kumburgaz Segment	40.8882	28.4979
		40.8744	28.37
		40.8574	28.2577
		40.8339	28.1408
		40.8332	28.0675
		40.8458	28.013
1_36	Tekirdağ Segment	40.849	27.9931
		40.844	27.8587
		40.8445	27.7357
		40.8268	27.6294
		40.8303	27.5257
1_37	Ganos Segment	40.5704	26.5102
		40.5736	26.6339
		40.62	26.8027
		40.6806	27.0039
		40.753	27.2385
		40.7887	27.4065
		40.8304	27.5167
		40.8907	27.5958
		40.9322	27.6735
1_38	Saros Segment	40.4371	25.8637
		40.4719	25.9957
		40.4686	26.1267
		40.4878	26.2031
		40.5014	26.2787
		40.5168	26.3896
		40.5344	26.4686
156	Hendek Fault	40.7737	30.5745
		40.8085	30.691
		40.8319	30.7567
		40.8307	30.8371
		40.8548	30.9018
		40.9004	30.9561

Table B.1 (Continued) *Trace Coordinates of the Faults*

Fault Code	Fault Name	Latitude (°N)	Longitude (°E)
157	Çilimli Fault	40.9069	30.9654
		40.9228	31.0387
		40.9348	31.0909
		40.9453	31.1333
		40.9747	31.1759
		40.9869	31.2165
		41.0332	31.2612
158	Yığılca Fault	40.9439	31.2295
		40.948	31.2994
		40.9749	31.3317
		40.9754	31.3985
		40.9979	31.4494
		41.0084	31.5254
		41.0274	31.5826
		41.086	31.6793
159	Devrek Fault	41.0645	31.7197
		41.0974	31.7432
		41.1308	31.8025
		41.1694	31.8437
		41.2094	31.8791
		41.2706	31.9132
145	Barakfakı Fault	40.2674	29.2261
		40.2571	29.2778
		40.2507	29.3131
		40.2361	29.3461
146	Gençali Fault	40.3613	29.0393
		40.368	29.1273
		40.3868	29.1742
		40.3878	29.2079
		40.3978	29.2505
		40.4137	29.3096

Table B.1 (Continued) *Trace Coordinates of the Faults*

Fault Code	Fault Name	Latitude (°N)	Longitude (°E)
147	Gemlik Fault	40.427	29.2131
		40.4268	29.2819
		40.4176	29.3518
		40.4223	29.4039
		40.4089	29.5064
148	İznik-Mekece Fault	40.394	29.7289
		40.4162	29.8809
		40.4285	30.0088
		40.4627	30.1499
149	Geyve Fault	40.4404	30.1418
		40.4625	30.2194
		40.481	30.2868
		40.5009	30.422
		40.5295	30.5491
		40.5532	30.6586
		40.5773	30.792
		40.5817	30.8691
150	Armutlu Fault	40.5688	28.8776
		40.5777	28.9114
		40.588	28.9461
151	Esenköy Fault	40.6163	29.0131
		40.6041	29.0668
		40.5984	29.0892
		40.6024	29.1776
152	Orhangazi Fault	40.6954	29.3407
		40.5755	29.3992
		40.5344	29.4519
		40.5285	29.5075
		40.5087	29.5598
		40.4898	29.5926
		40.4846	29.5865

Table B.1 (Continued) *Trace Coordinates of the Faults*

Fault Code	Fault Name	Latitude (°N)	Longitude (°E)
153	Yalova Fault	40.6367	29.3297
		40.6183	29.3831
		40.6144	29.4358
		40.6061	29.4755
		40.6078	29.4972
		40.59	29.5512
154	Altınova Fault	40.6759	29.4907
		40.6833	29.5299
		40.7033	29.5641
		40.7068	29.598
155	Yalakdere Fault	40.5991	29.6073
		40.6175	29.677
		40.6211	29.7235
		40.6505	29.7855
		40.6724	29.8402
		40.6928	29.8798
136	Bursa Fault	40.2001	29.0885
		40.1664	29.1482
		40.1654	29.1798
		40.1675	29.2174
		40.1635	29.2743
		40.1405	29.3068
		40.1246	29.3168
		40.1239	29.3406
		40.1053	29.3616
		40.1111	29.3836
		40.0986	29.4245
		40.0926	29.4593
137	İnegol Fault Zone	40.0381	29.5824
		40.0199	29.6196
		40.0012	29.6599

Table B.1 (Continued) *Trace Coordinates of the Faults*

Fault Code	Fault Name	Latitude (°N)	Longitude (°E)
138	Oylat Fault	40.034	29.4657
		40.0093	29.5094
		39.9722	29.5534
		39.9514	29.5467
		39.9309	29.5937
		39.9141	29.6281
		39.9011	29.7255
139	Dodurga Fault	39.9128	29.7481
		39.9002	29.7731
		39.8862	29.8111
		39.8716	29.8506
		39.8482	29.9109
		39.8339	29.9476
		39.782	30.0015
		39.7565	30.0412
		39.7266	30.1077
		39.6828	30.1889
		39.6539	30.2313
		39.6381	30.2745
140	Eskişehir Fault	39.8356	29.973
		39.8	30.1475
		39.7998	30.299
		39.794	30.3775
		39.7363	30.5306
		39.7154	30.6263
		39.679	30.7267
141	Kaymaz Fault	39.5863	31.107
		39.5617	31.1976
		39.5286	31.2885
		39.4994	31.3926

Table B.1 (Continued) *Trace Coordinates of the Faults*

Fault Code	Fault Name	Latitude (°N)	Longitude (°E)
142	No-name Fault	39.584	30.1137
		39.5595	30.1608
		39.5383	30.2073
143	No-name Fault	39.5899	30.2894
		39.5612	30.3184
		39.5255	30.3757
144	Taycılar Fault	39.8947	30.8602
		39.9179	30.9035
		39.9502	30.9445
		39.9763	30.9997
		39.9821	31.0588
129	Tavşanlı Fault	39.4968	29.4305
		39.4808	29.4744
		39.4695	29.5308
		39.4686	29.5606
		39.4749	29.5989
130	Şahmelek Fault	39.4809	29.6449
		39.4862	29.6787
		39.4834	29.7046
		39.4983	29.7343
		39.4905	29.7795
		39.4712	29.8145
131	Kütahya Fault	39.4421	29.864
		39.4085	29.9981
		39.3651	30.1187
		39.3406	30.1977
		39.3129	30.3016
		39.2979	30.4007
132	Parmakören Fault	39.4509	29.9395
		39.4429	30.042
		39.4258	30.0589
		39.4269	30.1019

Table B.1 (Continued) *Trace Coordinates of the Faults*

Fault Code	Fault Name	Latitude (°N)	Longitude (°E)
133	Seyitomer Fault	39.5766	29.9235
		39.5375	29.9844
		39.5094	30.052
134	Orhaneli Fault	39.9802	28.9056
		39.8923	29.0788
		39.8503	29.1043
		39.8331	29.2027
135	Soğukpinar Fault	40.1044	29.1462
		40.0674	29.1758
		40.0308	29.305
		40.0148	29.3644
3	Kestanbol Fault	39.7791	26.2005
		39.7267	26.1929
		39.66	26.1636
		39.6356	26.1414
4	Evciler Fault	39.7355	26.6487
		39.7762	26.8009
		39.8303	26.9102
		39.8823	27.0244
		39.9414	27.1133
5	Edremit Fault Zone	39.5083	26.3332
		39.546	26.4744
		39.5787	26.6617
		39.6098	26.8141
		39.6606	26.9464
		39.7703	27.0456
6_1	Çan Segment	39.9896	26.9416
		40.0052	26.9949
		40.0216	27.0391
6_2	Yuvalar Segment	40.0315	27.0432
		40.0537	27.0956
		40.0741	27.1423

Table B.1 (Continued) *Trace Coordinates of the Faults*

Fault Code	Fault Name	Latitude (°N)	Longitude (°E)
6_3	Biga Segment	40.0491	27.0845
		40.1227	27.1638
		40.1679	27.2091
		40.2269	27.3182
7	Sarıkoy Fault	39.9788	27.0652
		40.0551	27.2533
		40.116	27.3504
		40.1835	27.4899
		40.2233	27.6366
		40.2359	27.7651
8	Sinekçi Fault	40.2746	27.4954
		40.2931	27.5252
		40.2897	27.6497
		40.3205	27.7061
		40.3355	27.7663
9	Edincik Fault	40.326	27.7966
		40.3949	27.9486
		40.4547	28.106
10	Bandırma Fault	40.3956	28.0881
		40.4183	28.2409
		40.4165	28.3554
		40.4191	28.4657
11	Zeytinbağı Fault	40.3699	28.4818
		40.3827	28.6242
		40.3716	28.7326
		40.3792	28.8484
		40.3922	28.9048
12	Ulubat Fault	40.0987	28.513
		40.097	28.599
		40.1099	28.6611
		40.1412	28.7584
		40.1771	28.8524
		40.1678	29.0029

Table B.1 (Continued) *Trace Coordinates of the Faults*

Fault Code	Fault Name	Latitude (°N)	Longitude (°E)
13	Mustafa Kemal Paşa Fault	40.0718	28.2736
		40.0118	28.5456
		40.0089	28.6591
		39.9608	28.7764
14	Gündoğan Fault	40.2007	27.5954
		40.1898	27.6895
		40.1883	27.7663
		40.1909	27.8493
15	Atıcıoba Fault	40.0487	27.4966
		40.0882	27.5501
		40.1036	27.6
		40.1559	27.6531
16	Yenice Gönen Fault	39.8682	27.0967
		39.9107	27.1456
		39.9349	27.3134
		39.9967	27.4773
		40.0478	27.5587
		40.0763	27.5932
		40.0987	277041
		40.1236	27.8168
		40.0746	27.9336
		40.0506	28.0195
17	Manyas Fault	40.1208	27.8654
		40.1172	27.955
		40.0933	28.0019
		40.087	28.0453
18	No-name Fault	40.1065	27.2028
		40.1354	27.218
		40.1695	27.2216
19	Bekten Fault	39.9336	27.1805
		39.9789	27.2487
		40.0091	27.3234
		40.0403	27.3451

Table B.1 (Continued) *Trace Coordinates of the Faults*

Fault Code	Fault Name	Latitude (°N)	Longitude (°E)
20	Pazarköy Fault	39.7685	27.1538
		39.7989	27.2661
		39.8248	27.3348
		39.8372	27.3864
		39.8991	27.5177
21	Şamli Fault	39.8667	27.7932
		39.8402	27.8405
		39.8122	27.8847
22	Susurluk Fault	39.8128	28.2315
		39.8806	28.2452
		39.9329	28.2461
23_1	Havran Segment	39.5208	27.0525
		39.5571	27.1391
		39.5568	27.2045
		39.5739	27.2576
23_2	Osmanlar Segment	39.5708	27.2843
		39.5945	27.3783
		39.6153	27.4561
		39.6484	27.5175
		39.6855	27.5808
23_3	Turplu Segment	39.6728	27.616
		39.7162	27.6864
		39.731	27.7437
		39.7334	27.7842
23_4	Ovacık Segment	39.7242	27.7934
		39.7461	27.8819
		39.7499	27.9398
		39.7271	28.0367
24_1	Gökçeyazı Segment	39.6028	27.5386
		39.6258	27.646
		39.6382	27.7961
		39.6631	27.9036
		39.6868	27.9871

Table B.1 (Continued) *Trace Coordinates of the Faults*

Fault Code	Fault Name	Latitude (°N)	Longitude (°E)
24_2	Kepsut Segment	39.6779	28.0093
		39.6653	28.1045
		39.6455	28.1728
		39.6316	28.2456
25	Zeytindağ Fault Zone	38.8844	27.0476
		38.9519	27.1032
		39.0351	27.1407
26	Bergama Fault	38.9226	27.0609
		39.0039	27.1026
		39.0568	27.1465
		39.0626	27.191
		39.0824	27.2556
27	Soma Kırkağaç Fault Zone	39.0924	27.446
		39.1356	27.5324
		39.1694	27.5936
		39.1598	27.6574
		39.1132	27.655
28_1	Doğu Segment	39.0342	27.9691
		39.1041	28.001
		39.1965	28.005
		39.2682	28.0338
28_2	Batı Segment	39.0393	27.8873
		39.1264	27.9438
		39.1802	27.9554
		39.257	28.0068
		39.3095	28.0501
29	Düvertepe Fault Zone	32.2674	28.3012
		39.2526	28.3598
		39.252	28.4114
30_1	Sındırgı Segment	39.2341	28.0852
		39.2026	28.1916
		39.2109	28.3054
		39.1947	28.3789
		39.1872	28.4718

Table B.1 (Continued) *Trace Coordinates of the Faults*

Fault Code	Fault Name	Latitude (°N)	Longitude (°E)
30_2	Çaysimav Segment	39.1755	28.4703
		39.1412	28.6218
		39.1069	28.7814
		39.0751	28.9418
		39.0328	29.0743
30_3	Şaphane Segment	39.0403	29.0815
		39.0077	29.1716
		38.9972	29.2347
120_1	Emet Segment	39.2921	29.3218
		39.1794	29.3704
		39.1229	29.4256
		39.1008	29.4462
128	Çavdarhisar Segment	39.2436	29.573
		39.1878	29.6267
		39.1485	29.6534
127	Naşa Fault Zone	39.1712	28.9323
		39.1405	29.0203
		39.0903	29.0577
		39.05	29.1146

C.1. Peak Ground Acceleration (g) and Wind Pressure (kg/m^2) Values for Each Transmission Tower of Path 1 Within 100 and 2500 Years Return Periods

Table C1 *Seismic load (g) and wind pressure (kg/m2) values and the corresponding standard deviations for each transmission tower of Path 1*

			Seismic Load (g)				Wind Pressure (kg/m2)			
			100 years		2500 years		100 years		2500 years	
(Path(i)-Tower(j))	Lat. (°N)	Lon. (°E)	μ_{PGA}	σ_{PGA}	μ_{PGA}	σ_{PGA}	Wind Pressure (kg/m^2)	σ_w (kg/m^2)	Wind Pressure (kg/m^2)	σ_w (kg/m^2)
P1-T1	39.618	29.444	0.190	0.067	0.929	0.325	2.802	1.037	4.469	1.654
P1-T2	39.618	29.443	0.190	0.067	0.929	0.325	2.802	1.037	4.469	1.654
P1-T3	39.618	29.439	0.190	0.067	0.929	0.325	2.802	1.037	4.469	1.654
P1-T4	39.619	29.435	0.190	0.067	0.929	0.325	2.802	1.037	4.469	1.654
P1-T5	39.619	29.43	0.190	0.067	0.929	0.325	2.802	1.037	4.469	1.654
P1-T6	39.62	29.425	0.190	0.067	0.929	0.325	2.802	1.037	4.469	1.654
P1-T7	39.62	29.421	0.190	0.067	0.929	0.325	2.802	1.037	4.469	1.654
P1-T8	39.621	29.416	0.190	0.067	0.929	0.325	2.802	1.037	4.469	1.654
P1-T9	39.621	29.412	0.190	0.067	0.929	0.325	2.802	1.037	4.469	1.654
P1-T10	39.622	29.407	0.190	0.067	0.929	0.325	2.802	1.037	4.469	1.654
P1-T11	39.623	29.405	0.190	0.067	0.929	0.325	2.802	1.037	4.469	1.654
P1-T12	39.625	29.401	0.190	0.067	0.929	0.325	2.802	1.037	4.469	1.654
P1-T13	39.627	29.397	0.191	0.067	0.929	0.325	2.802	1.037	4.469	1.654
P1-T14	39.629	29.393	0.191	0.067	0.929	0.325	2.802	1.037	4.469	1.654
P1-T15	39.631	29.389	0.191	0.067	0.929	0.325	2.802	1.037	4.469	1.654
P1-T16	39.633	29.386	0.191	0.067	0.929	0.325	2.802	1.037	4.469	1.654
P1-T17	39.636	29.382	0.191	0.067	0.929	0.325	2.802	1.037	4.469	1.654
P1-T18	39.638	29.378	0.191	0.067	0.929	0.325	2.802	1.037	4.469	1.654
P1-T19	39.64	29.374	0.191	0.067	0.929	0.325	2.802	1.037	4.469	1.654
P1-T20	39.642	29.37	0.191	0.067	0.929	0.325	2.802	1.037	4.469	1.654
P1-T21	39.644	29.367	0.191	0.067	0.929	0.325	2.802	1.037	4.469	1.654
P1-T22	39.646	29.363	0.191	0.067	0.929	0.325	2.802	1.037	4.469	1.654
P1-T23	39.648	29.359	0.191	0.067	0.929	0.325	2.802	1.037	4.469	1.654
P1-T24	39.65	29.355	0.191	0.067	0.929	0.325	2.802	1.037	4.469	1.654
P1-T25	39.652	29.351	0.191	0.067	0.929	0.325	2.802	1.037	4.469	1.654
P1-T26	39.654	29.348	0.191	0.067	0.929	0.325	2.802	1.037	4.469	1.654
P1-T27	39.656	29.344	0.191	0.067	0.930	0.325	2.802	1.037	4.469	1.654
P1-T28	39.658	29.34	0.191	0.067	0.930	0.325	2.802	1.037	4.469	1.654
P1-T29	39.66	29.336	0.191	0.067	0.930	0.325	2.802	1.037	4.469	1.654

Table C1 (continued) *Seismic load (g) and wind pressure (kg/m2) values and the corresponding standard deviations for each transmission tower of Path 1*

			Seismic Load (g)				Wind Pressure (kg/m2)			
			100 years		2500 years		100 years		2500 years	
(Path(i)-Tower(j))	Lat. (°N)	Lon. (°E)	μ_{PGA}	σ_{PGA}	μ_{PGA}	σ_{PGA}	Wind Pressure (kg/m^2)	σ_w (kg/m^2)	Wind Pressure (kg/m^2)	σ_w (kg/m^2)
P1-T30	39.663	29.332	0.191	0.067	0.930	0.325	2.802	1.037	4.469	1.654
P1-T31	39.665	29.328	0.191	0.067	0.930	0.325	2.802	1.037	4.469	1.654
P1-T32	39.667	29.325	0.191	0.067	0.930	0.325	2.802	1.037	4.469	1.654
P1-T33	39.669	29.321	0.191	0.067	0.930	0.325	2.802	1.037	4.469	1.654
P1-T34	39.671	29.317	0.191	0.067	0.930	0.325	2.802	1.037	4.469	1.654
P1-T35	39.673	29.313	0.191	0.067	0.930	0.325	2.802	1.037	4.469	1.654
P1-T36	39.675	29.309	0.191	0.067	0.930	0.325	2.802	1.037	4.469	1.654
P1-T37	39.677	29.305	0.191	0.067	0.930	0.325	2.802	1.037	4.469	1.654
P1-T38	39.679	29.302	0.191	0.067	0.930	0.325	2.802	1.037	4.469	1.654
P1-T39	39.681	29.298	0.191	0.067	0.930	0.325	2.802	1.037	4.469	1.654
P1-T40	39.683	29.294	0.191	0.067	0.930	0.325	2.802	1.037	4.469	1.654
P1-T41	39.685	29.29	0.191	0.067	0.930	0.325	2.802	1.037	4.469	1.654
P1-T42	39.687	29.286	0.191	0.067	0.930	0.325	2.802	1.037	4.469	1.654
P1-T43	39.689	29.282	0.191	0.067	0.930	0.325	2.802	1.037	4.469	1.654
P1-T44	39.691	29.279	0.191	0.067	0.930	0.325	2.802	1.037	4.469	1.654
P1-T45	39.693	29.275	0.191	0.067	0.930	0.325	2.802	1.037	4.469	1.654
P1-T46	39.695	29.271	0.191	0.067	0.930	0.325	2.802	1.037	4.469	1.654
P1-T47	39.697	29.267	0.191	0.067	0.930	0.325	2.802	1.037	4.469	1.654
P1-T48	39.699	29.263	0.191	0.067	0.930	0.325	2.802	1.037	4.469	1.654
P1-T49	39.701	29.259	0.191	0.067	0.930	0.325	2.802	1.037	4.469	1.654
P1-T50	39.703	29.255	0.191	0.067	0.930	0.325	2.802	1.037	4.469	1.654
P1-T51	39.705	29.251	0.191	0.067	0.930	0.325	2.802	1.037	4.469	1.654
P1-T52	39.707	29.247	0.191	0.067	0.930	0.325	2.802	1.037	4.469	1.654
P1-T53	39.709	29.243	0.191	0.067	0.930	0.325	2.802	1.037	4.469	1.654
P1-T54	39.711	29.239	0.191	0.067	0.930	0.325	2.802	1.037	4.469	1.654
P1-T55	39.713	29.235	0.191	0.067	0.930	0.325	2.802	1.037	4.469	1.654
P1-T56	39.715	29.232	0.191	0.067	0.930	0.325	2.802	1.037	4.469	1.654
P1-T57	39.717	29.228	0.191	0.067	0.930	0.325	2.802	1.037	4.469	1.654
P1-T58	39.719	29.224	0.191	0.067	0.930	0.325	2.802	1.037	4.469	1.654
P1-T59	39.721	29.22	0.191	0.067	0.930	0.325	2.802	1.037	4.469	1.654
P1-T60	39.723	29.216	0.191	0.067	0.930	0.325	2.802	1.037	4.469	1.654

Table C1 *(continued) Seismic load (g) and wind pressure (kg/m2) values and the corresponding standard deviations for each transmission tower of Path 1*

			Seismic Load (g)				Wind Pressure (kg/m2)			
			100 years		2500 years		100 years		2500 years	
(Path(i)-Tower(j))	Lat. (°N)	Lon. (°E)	μ_{PGA}	σ_{PGA}	μ_{PGA}	σ_{PGA}	Wind Pressure (kg/m^2)	σ_w (kg/m^2)	Wind Pressure (kg/m^2)	σ_w (kg/m^2)
P1-T61	39.725	29.212	0.191	0.067	0.930	0.325	2.802	1.037	4.469	1.654
P1-T62	39.727	29.208	0.191	0.067	0.930	0.325	2.802	1.037	4.469	1.654
P1-T63	39.729	29.204	0.191	0.067	0.930	0.325	2.802	1.037	4.469	1.654
P1-T64	39.731	29.2	0.191	0.067	0.930	0.325	2.802	1.037	4.469	1.654
P1-T65	39.733	29.196	0.191	0.067	0.930	0.325	2.802	1.037	4.469	1.654
P1-T66	39.735	29.192	0.191	0.067	0.930	0.325	2.802	1.037	4.469	1.654
P1-T67	39.736	29.188	0.191	0.067	0.930	0.325	2.802	1.037	4.469	1.654
P1-T68	39.739	29.185	0.191	0.067	0.930	0.325	2.802	1.037	4.469	1.654
P1-T69	39.74	29.181	0.191	0.067	0.930	0.325	2.802	1.037	4.469	1.654
P1-T70	39.742	29.177	0.191	0.067	0.930	0.325	2.802	1.037	4.469	1.654
P1-T71	39.744	29.173	0.191	0.067	0.930	0.325	2.802	1.037	4.469	1.654
P1-T72	39.746	29.169	0.191	0.067	0.930	0.325	2.802	1.037	4.469	1.654
P1-T73	39.748	29.165	0.191	0.067	0.930	0.325	2.802	1.037	4.469	1.654
P1-T74	39.75	26.161	0.151	0.053	0.828	0.290	2.802	1.037	4.469	1.654
P1-T75	39.752	29.157	0.192	0.067	0.930	0.325	2.802	1.037	4.469	1.654
P1-T76	39.755	29.154	0.192	0.067	0.930	0.325	2.802	1.037	4.469	1.654
P1-T77	39.758	29.151	0.192	0.067	0.930	0.325	2.802	1.037	4.469	1.654
P1-T78	39.76	29.148	0.192	0.067	0.930	0.325	2.802	1.037	4.469	1.654
P1-T79	39.763	29.144	0.192	0.067	0.930	0.325	2.802	1.037	4.469	1.654
P1-T80	39.765	29.141	0.192	0.067	0.930	0.325	2.802	1.037	4.469	1.654
P1-T81	39.768	29.138	0.192	0.067	0.930	0.325	2.802	1.037	4.469	1.654
P1-T82	39.771	29.135	0.192	0.067	0.930	0.325	2.802	1.037	4.469	1.654
P1-T83	39.773	29.131	0.192	0.067	0.930	0.325	2.802	1.037	4.469	1.654
P1-T84	39.776	29.128	0.192	0.067	0.930	0.325	2.802	1.037	4.469	1.654
P1-T85	39.779	29.125	0.192	0.067	0.930	0.325	2.802	1.037	4.469	1.654
P1-T86	39.781	29.122	0.192	0.067	0.930	0.325	4.165	1.602	6.643	2.556
P1-T87	39.784	29.119	0.192	0.067	0.930	0.325	4.165	1.602	6.643	2.556
P1-T88	39.786	29.116	0.192	0.067	0.930	0.325	4.165	1.602	6.643	2.556
P1-T89	39.789	29.112	0.192	0.067	0.930	0.325	4.165	1.602	6.643	2.556
P1-T90	39.792	29.109	0.192	0.067	0.930	0.325	4.165	1.602	6.643	2.556
P1-T91	39.794	29.106	0.192	0.067	0.930	0.325	4.165	1.602	6.643	2.556

Table C1 *(continued) Seismic load (g) and wind pressure (kg/m2) values and the corresponding standard deviations for each transmission tower of Path 1*

			Seismic Load (g)				Wind Pressure (kg/m2)			
			100 years		2500 years		100 years		2500 years	
(Path(i)-Tower(j))	Lat. (°N)	Lon. (°E)	μ_{PGA}	σ_{PGA}	μ_{PGA}	σ_{PGA}	Wind Pressure (kg/m^2)	σ_w (kg/m^2)	Wind Pressure (kg/m^2)	σ_w (kg/m^2)
P1-T92	39.797	29.103	0.192	0.067	0.930	0.325	4.165	1.602	6.643	2.556
P1-T93	39.8	29.099	0.192	0.067	0.930	0.325	4.165	1.602	6.643	2.556
P1-T94	39.802	29.096	0.192	0.067	0.930	0.325	4.165	1.602	6.643	2.556
P1-T95	39.805	29.093	0.192	0.067	0.930	0.325	4.165	1.602	6.643	2.556
P1-T96	39.808	29.09	0.192	0.067	0.930	0.325	4.165	1.602	6.643	2.556
P1-T97	39.81	29.087	0.192	0.067	0.930	0.325	4.165	1.602	6.643	2.556
P1-T98	39.813	29.084	0.192	0.067	0.930	0.325	4.165	1.602	6.643	2.556
P1-T99	39.814	29.082	0.192	0.067	0.930	0.325	4.165	1.602	6.643	2.556
P1-T100	39.817	29.08	0.192	0.067	0.930	0.325	4.165	1.602	6.643	2.556
P1-T101	39.82	29.077	0.192	0.067	0.930	0.325	4.165	1.602	6.643	2.556
P1-T102	39.823	29.074	0.192	0.067	0.930	0.325	4.165	1.602	6.643	2.556
P1-T103	39.826	29.072	0.192	0.067	0.930	0.325	4.165	1.602	6.643	2.556
P1-T104	39.829	29.069	0.192	0.067	0.930	0.325	4.165	1.602	6.643	2.556
P1-T105	39.832	29.066	0.192	0.067	0.930	0.325	4.165	1.602	6.643	2.556
P1-T106	39.835	29.064	0.192	0.067	0.930	0.325	4.165	1.602	6.643	2.556
P1-T107	39.838	29.061	0.192	0.067	0.930	0.325	4.165	1.602	6.643	2.556
P1-T108	39.841	29.058	0.192	0.067	0.930	0.325	4.165	1.602	6.643	2.556
P1-T109	39.844	29.056	0.192	0.067	0.930	0.325	4.165	1.602	6.643	2.556
P1-T110	39.847	29.053	0.192	0.067	0.930	0.325	4.165	1.602	6.643	2.556
P1-T111	39.85	29.05	0.192	0.067	0.930	0.325	4.165	1.602	6.643	2.556
P1-T112	39.853	29.048	0.192	0.067	0.930	0.325	4.165	1.602	6.643	2.556
P1-T113	39.856	29.045	0.192	0.067	0.930	0.325	4.165	1.602	6.643	2.556
P1-T114	39.859	29.043	0.192	0.067	0.930	0.325	4.165	1.602	6.643	2.556
P1-T115	39.862	29.04	0.192	0.067	0.930	0.325	4.165	1.602	6.643	2.556
P1-T116	39.865	29.038	0.192	0.067	0.930	0.325	4.165	1.602	6.643	2.556
P1-T117	39.868	29.035	0.192	0.067	0.930	0.325	4.165	1.602	6.643	2.556
P1-T118	39.871	29.033	0.192	0.067	0.930	0.325	4.165	1.602	6.643	2.556
P1-T119	39.876	29.029	0.192	0.067	0.930	0.325	4.165	1.602	6.643	2.556
P1-T120	39.878	29.027	0.192	0.067	0.930	0.325	4.165	1.602	6.643	2.556
P1-T121	39.881	29.025	0.192	0.067	0.930	0.325	4.165	1.602	6.643	2.556
P1-T122	39.886	29.022	0.192	0.067	0.930	0.325	4.165	1.602	6.643	2.556
P1-T123	39.888	29.02	0.192	0.067	0.930	0.325	4.165	1.602	6.643	2.556

Table C1 (continued) *Seismic load (g) and wind pressure (kg/m2) values and the corresponding standard deviations for each transmission tower of Path 1*

			Seismic Load (g)				Wind Pressure (kg/m2)			
			100 years		2500 years		100 years		2500 years	
(Path(i)-Tower(j))	Lat. (°N)	Lon. (°E)	μ_{PGA}	σ_{PGA}	μ_{PGA}	σ_{PGA}	Wind Pressure (kg/m^2)	σ_w (kg/m^2)	Wind Pressure (kg/m^2)	σ_w (kg/m^2)
P1-T124	39.891	29.017	0.192	0.067	0.930	0.325	4.165	1.602	6.643	2.556
P1-T125	39.895	29.014	0.192	0.067	0.930	0.325	4.165	1.602	6.643	2.556
P1-T126	39.897	29.012	0.192	0.067	0.930	0.325	4.165	1.602	6.643	2.556
P1-T127	39.9	29.01	0.192	0.067	0.930	0.325	4.165	1.602	6.643	2.556
P1-T128	39.904	29.007	0.192	0.067	0.930	0.325	4.165	1.602	6.643	2.556
P1-T129	39.908	29.003	0.192	0.067	0.930	0.325	4.165	1.602	6.643	2.556
P1-T130	39.913	29	0.192	0.067	0.930	0.325	4.165	1.602	6.643	2.556
P1-T131	39.916	28.997	0.192	0.067	0.930	0.325	4.165	1.602	6.643	2.556
P1-T132	39.919	28.995	0.192	0.067	0.930	0.325	4.165	1.602	6.643	2.556
P1-T133	39.921	28.993	0.192	0.067	0.930	0.326	4.165	1.602	6.643	2.556
P1-T134	39.923	28.992	0.192	0.067	0.930	0.326	4.165	1.602	6.643	2.556
P1-T135	39.926	28.989	0.192	0.067	0.930	0.326	4.165	1.602	6.643	2.556
P1-T136	39.931	28.985	0.192	0.067	0.930	0.326	4.165	1.602	6.643	2.556
P1-T137	39.935	28.984	0.193	0.067	0.930	0.326	4.165	1.602	6.643	2.556
P1-T138	39.941	28.982	0.193	0.067	0.930	0.326	4.165	1.602	6.643	2.556
P1-T139	39.945	28.981	0.193	0.067	0.930	0.326	4.165	1.602	6.643	2.556
P1-T140	39.948	28.981	0.193	0.067	0.930	0.326	4.165	1.602	6.643	2.556
P1-T141	39.954	28.979	0.193	0.067	0.930	0.326	4.165	1.602	6.643	2.556
P1-T142	39.958	28.978	0.193	0.067	0.930	0.326	4.165	1.602	6.643	2.556
P1-T143	39.962	28.977	0.193	0.067	0.930	0.326	4.165	1.602	6.643	2.556
P1-T144	39.967	28.976	0.193	0.067	0.930	0.326	4.165	1.602	6.643	2.556
P1-T145	39.968	28.975	0.193	0.067	0.930	0.326	4.165	1.602	6.643	2.556
P1-T146	39.97	28.975	0.193	0.067	0.930	0.326	4.165	1.602	6.643	2.556
P1-T147	39.974	28.974	0.193	0.067	0.930	0.326	4.165	1.602	6.643	2.556
P1-T148	39.979	28.973	0.193	0.067	0.930	0.326	4.165	1.602	6.643	2.556
P1-T149	39.982	28.972	0.193	0.067	0.930	0.326	4.165	1.602	6.643	2.556
P1-T150	39.983	28.971	0.193	0.067	0.930	0.326	4.165	1.602	6.643	2.556
P1-T151	39.987	28.97	0.193	0.067	0.930	0.326	4.165	1.602	6.643	2.556
P1-T152	39.99	28.97	0.193	0.067	0.930	0.326	4.165	1.602	6.643	2.556
P1-T153	39.993	28.969	0.193	0.067	0.930	0.326	4.165	1.602	6.643	2.556
P1-T154	39.994	28.968	0.193	0.067	0.930	0.326	4.165	1.602	6.643	2.556
P1-T155	39.997	28.968	0.193	0.067	0.930	0.326	4.165	1.602	6.643	2.556

Table C1 (continued) *Seismic load (g) and wind pressure (kg/m2) values and the corresponding standard deviations for each transmission tower of Path 1*

			Seismic Load (g)				Wind Pressure (kg/m2)			
			100 years		2500 years		100 years		2500 years	
(Path(i)-Tower(j))	Lat. (°N)	Lon. (°E)	μ_{PGA}	σ_{PGA}	μ_{PGA}	σ_{PGA}	Wind Pressure (kg/m^2)	σ_w (kg/m^2)	Wind Pressure (kg/m^2)	σ_w (kg/m^2)
P1-T156	40.001	28.967	0.193	0.067	0.930	0.326	4.165	1.602	6.643	2.556
P1-T157	40.004	28.966	0.193	0.068	0.930	0.326	4.165	1.602	6.643	2.556
P1-T158	40.006	28.965	0.193	0.068	0.930	0.326	4.165	1.602	6.643	2.556
P1-T159	40.011	28.964	0.193	0.068	0.930	0.326	4.165	1.602	6.643	2.556
P1-T160	40.014	28.963	0.193	0.068	0.930	0.326	4.165	1.602	6.643	2.556
P1-T161	40.017	28.963	0.193	0.068	0.930	0.326	4.165	1.602	6.643	2.556
P1-T162	40.02	28.962	0.193	0.068	0.930	0.326	4.165	1.602	6.643	2.556
P1-T163	40.022	28.961	0.193	0.068	0.930	0.326	4.165	1.602	6.643	2.556
P1-T164	40.023	28.961	0.193	0.068	0.930	0.326	4.165	1.602	6.643	2.556
P1-T165	40.027	28.961	0.193	0.068	0.930	0.326	4.165	1.602	6.643	2.556
P1-T166	40.029	28.96	0.193	0.068	0.930	0.326	4.165	1.602	6.643	2.556
P1-T167	40.03	28.96	0.193	0.068	0.930	0.326	4.165	1.602	6.643	2.556
P1-T168	40.033	28.959	0.193	0.068	0.930	0.326	4.165	1.602	6.643	2.556
P1-T169	40.035	28.959	0.193	0.068	0.930	0.326	4.165	1.602	6.643	2.556
P1-T170	40.04	28.959	0.193	0.068	0.930	0.326	4.165	1.602	6.643	2.556
P1-T171	40.045	28.958	0.193	0.068	0.930	0.326	4.165	1.602	6.643	2.556
P1-T172	40.047	28.958	0.193	0.068	0.930	0.326	4.165	1.602	6.643	2.556
P1-T173	40.052	28.957	0.193	0.068	0.930	0.326	4.165	1.602	6.643	2.556
P1-T174	40.055	28.956	0.193	0.068	0.930	0.326	4.165	1.602	6.643	2.556
P1-T175	40.057	28.956	0.193	0.068	0.930	0.326	4.165	1.602	6.643	2.556
P1-T176	40.062	28.955	0.193	0.068	0.930	0.326	4.165	1.602	6.643	2.556
P1-T177	40.064	28.955	0.193	0.068	0.930	0.326	4.165	1.602	6.643	2.556
P1-T178	40.066	28.954	0.193	0.068	0.930	0.326	4.165	1.602	6.643	2.556
P1-T179	40.068	28.954	0.193	0.068	0.930	0.326	4.165	1.602	6.643	2.556
P1-T180	40.07	28.954	0.193	0.068	0.930	0.326	4.165	1.602	6.643	2.556
P1-T181	40.073	28.953	0.193	0.068	0.930	0.326	4.165	1.602	6.643	2.556
P1-T182	40.077	28.953	0.193	0.068	0.930	0.326	4.165	1.602	6.643	2.556
P1-T183	40.08	28.952	0.193	0.068	0.930	0.326	4.165	1.602	6.643	2.556
P1-T184	40.081	28.952	0.193	0.068	0.930	0.326	4.165	1.602	6.643	2.556
P1-T185	40.085	28.952	0.193	0.068	0.930	0.326	4.165	1.602	6.643	2.556
P1-T186	40.088	28.953	0.193	0.068	0.930	0.326	4.165	1.602	6.643	2.556
P1-T187	40.091	28.953	0.193	0.068	0.930	0.326	4.165	1.602	6.643	2.556

Table C1 (continued) *Seismic load (g) and wind pressure (kg/m2) values and the corresponding standard deviations for each transmission tower of Path 1*

			Seismic Load (g)				Wind Pressure (kg/m2)			
			100 years		2500 years		100 years		2500 years	
(Path(i)-Tower(j))	Lat. (°N)	Lon. (°E)	μ_{PGA}	σ_{PGA}	μ_{PGA}	σ_{PGA}	Wind Pressure (kg/m^2)	σ_w (kg/m^2)	Wind Pressure (kg/m^2)	σ_w (kg/m^2)
P1-T188	40.093	28.953	0.193	0.068	0.930	0.326	4.165	1.602	6.643	2.556
P1-T189	40.096	28.953	0.193	0.068	0.930	0.326	4.165	1.602	6.643	2.556
P1-T190	40.101	28.953	0.194	0.068	0.930	0.326	4.165	1.602	6.643	2.556
P1-T191	40.11	28.954	0.194	0.068	0.930	0.326	4.165	1.602	6.643	2.556
P1-T192	40.112	28.954	0.194	0.068	0.930	0.326	4.165	1.602	6.643	2.556
P1-T193	40.114	28.954	0.194	0.068	0.930	0.326	4.165	1.602	6.643	2.556
P1-T194	40.118	28.954	0.194	0.068	0.930	0.326	4.165	1.602	6.643	2.556
P1-T195	40.123	28.954	0.194	0.068	0.930	0.326	4.165	1.602	6.643	2.556
P1-T196	40.128	28.954	0.194	0.068	0.930	0.326	4.165	1.602	6.643	2.556
P1-T197	40.131	28.954	0.194	0.068	0.930	0.326	4.165	1.602	6.643	2.556
P1-T198	40.134	28.954	0.194	0.068	0.930	0.326	4.165	1.602	6.643	2.556
P1-T199	40.142	28.955	0.194	0.068	0.930	0.326	4.165	1.602	6.643	2.556
P1-T200	40.146	28.955	0.194	0.068	0.930	0.326	4.165	1.602	6.643	2.556
P1-T201	40.149	28.955	0.194	0.068	0.930	0.326	4.165	1.602	6.643	2.556
P1-T202	40.155	28.955	0.194	0.068	0.930	0.326	4.165	1.602	6.643	2.556
P1-T203	40.16	28.955	0.194	0.068	0.930	0.326	4.165	1.602	6.643	2.556
P1-T204	40.164	28.955	0.194	0.068	0.930	0.326	4.165	1.602	6.643	2.556
P1-T205	40.166	28.956	0.194	0.068	0.930	0.326	4.165	1.602	6.643	2.556
P1-T206	40.17	28.956	0.194	0.068	0.930	0.326	4.165	1.602	6.643	2.556
P1-T207	40.176	28.956	0.194	0.068	0.930	0.326	4.165	1.602	6.643	2.556
P1-T208	40.18	28.956	0.194	0.068	0.931	0.326	4.165	1.602	6.643	2.556
P1-T209	40.183	28.956	0.194	0.068	0.931	0.326	4.165	1.602	6.643	2.556
P1-T210	40.186	28.956	0.194	0.068	0.931	0.326	4.165	1.602	6.643	2.556
P1-T211	40.195	28.956	0.195	0.068	0.931	0.326	4.165	1.602	6.643	2.556
P1-T212	40.2	28.956	0.195	0.068	0.931	0.326	4.165	1.602	6.643	2.556
P1-T213	40.202	28.956	0.195	0.068	0.931	0.326	4.165	1.602	6.643	2.556
P1-T214	40.204	28.956	0.195	0.068	0.931	0.326	4.165	1.602	6.643	2.556
P1-T215	40.209	28.957	0.195	0.068	0.931	0.326	4.165	1.602	6.643	2.556
P1-T216	40.211	28.957	0.195	0.068	0.931	0.326	4.165	1.602	6.643	2.556
P1-T217	40.215	28.957	0.195	0.068	0.931	0.326	4.165	1.602	6.643	2.556
P1-T218	40.218	28.958	0.195	0.068	0.931	0.326	4.165	1.602	6.643	2.556
P1-T219	40.222	28.96	0.195	0.068	0.931	0.326	4.165	1.602	6.643	2.556

Table C1 (continued) *Seismic load (g) and wind pressure (kg/m2) values and the corresponding standard deviations for each transmission tower of Path 1*

			Seismic Load (g)				Wind Pressure (kg/m2)			
			100 years		2500 years		100 years		2500 years	
(Path(i)-Tower(j))	Lat. (°N)	Lon. (°E)	μ_{PGA}	σ_{PGA}	μ_{PGA}	σ_{PGA}	Wind Pressure (kg/m^2)	σ_w (kg/m^2)	Wind Pressure (kg/m^2)	σ_w (kg/m^2)
P1-T220	40.226	28.962	0.195	0.068	0.931	0.326	4.165	1.602	6.643	2.556
P1-T221	40.229	28.964	0.195	0.068	0.931	0.326	4.165	1.602	6.643	2.556
P1-T222	40.231	28.965	0.195	0.068	0.931	0.326	4.165	1.602	6.643	2.556

C.2. Survival Probabilities and Reliability Indices in Each Failure Mode and the Component Survival Probability Bounds for the Transmission Towers of Path 1 for 1000 Years Return Period

Table C2 *Survival probabilities, reliability indices and reliability bounds of transmission towers*

Return Period	1000 Years									
Failure Modes		Seismic Load		Wind+Ice		Wind		Wearout	Component Survival Probability Bounds	
Tower	Return Period	β	P_S	β	P_S	β	P_S	P_S	Upper Bound	Lower Bound
P1-T1	1000	0.5873	0.7215	4.2033	1.0000	4.6792	1.0000	0.7800	0.7215	0.5628
P1-T2	1000	0.5873	0.7215	4.2033	1.0000	4.6792	1.0000	0.7800	0.7215	0.5628
P1-T3	1000	0.5873	0.7215	4.2033	1.0000	4.6792	1.0000	0.7800	0.7215	0.5628
P1-T4	1000	0.5873	0.7215	4.2033	1.0000	4.6792	1.0000	0.7800	0.7215	0.5628
P1-T5	1000	0.5873	0.7215	4.2033	1.0000	4.6792	1.0000	0.7800	0.7215	0.5628
P1-T6	1000	0.5873	0.7215	4.2033	1.0000	4.6792	1.0000	0.7800	0.7215	0.5628
P1-T7	1000	0.5873	0.7215	4.2033	1.0000	4.6792	1.0000	0.7800	0.7215	0.5628
P1-T8	1000	0.5873	0.7215	4.2033	1.0000	4.6792	1.0000	0.7800	0.7215	0.5628
P1-T9	1000	0.5873	0.7215	4.2033	1.0000	4.6792	1.0000	0.7800	0.7215	0.5628
P1-T10	1000	0.5873	0.7215	4.2033	1.0000	4.6792	1.0000	0.7800	0.7215	0.5628
P1-T11	1000	0.5873	0.7215	4.2033	1.0000	4.6792	1.0000	0.7800	0.7215	0.5628
P1-T12	1000	0.5873	0.7215	4.2033	1.0000	4.6792	1.0000	0.7800	0.7215	0.5628
P1-T13	1000	0.5873	0.7215	4.2033	1.0000	4.6792	1.0000	0.7800	0.7215	0.5628
P1-T14	1000	0.5873	0.7215	4.2033	1.0000	4.6792	1.0000	0.7800	0.7215	0.5628
P1-T15	1000	0.5873	0.7215	4.2033	1.0000	4.6792	1.0000	0.7800	0.7215	0.5628
P1-T16	1000	0.5873	0.7215	4.2033	1.0000	4.6792	1.0000	0.7800	0.7215	0.5628
P1-T17	1000	0.5873	0.7215	4.2033	1.0000	4.6792	1.0000	0.7800	0.7215	0.5628
P1-T18	1000	0.5873	0.7215	4.2033	1.0000	4.6792	1.0000	0.7800	0.7215	0.5628
P1-T19	1000	0.5873	0.7215	4.2033	1.0000	4.6792	1.0000	0.7800	0.7215	0.5628
P1-T20	1000	0.5873	0.7215	4.2033	1.0000	4.6792	1.0000	0.7800	0.7215	0.5628
P1-T21	1000	0.5873	0.7215	4.2033	1.0000	4.6792	1.0000	0.7800	0.7215	0.5628
P1-T22	1000	0.5873	0.7215	4.2033	1.0000	4.6792	1.0000	0.7800	0.7215	0.5628
P1-T23	1000	0.5873	0.7215	4.2033	1.0000	4.6792	1.0000	0.7800	0.7215	0.5628
P1-T24	1000	0.5873	0.7215	4.2033	1.0000	4.6792	1.0000	0.7800	0.7215	0.5628
P1-T25	1000	0.5873	0.7215	4.2033	1.0000	4.6792	1.0000	0.7800	0.7215	0.5628
P1-T26	1000	0.5873	0.7215	4.2033	1.0000	4.6792	1.0000	0.7800	0.7215	0.5628
P1-T27	1000	0.5873	0.7215	4.2033	1.0000	4.6792	1.0000	0.7800	0.7215	0.5628
P1-T28	1000	0.5873	0.7215	4.2033	1.0000	4.6792	1.0000	0.7800	0.7215	0.5628
P1-T29	1000	0.5873	0.7215	4.2033	1.0000	4.6792	1.0000	0.7800	0.7215	0.5628
P1-T30	1000	0.5873	0.7215	4.2033	1.0000	4.6792	1.0000	0.7800	0.7215	0.5628
P1-T31	1000	0.5873	0.7215	4.2033	1.0000	4.6792	1.0000	0.7800	0.7215	0.5628
P1-T32	1000	0.5873	0.7215	4.2033	1.0000	4.6792	1.0000	0.7800	0.7215	0.5628
P1-T33	1000	0.5873	0.7215	4.2033	1.0000	4.6792	1.0000	0.7800	0.7215	0.5628
P1-T34	1000	0.5873	0.7215	4.2033	1.0000	4.6792	1.0000	0.7800	0.7215	0.5628
P1-T35	1000	0.5873	0.7215	4.2033	1.0000	4.6792	1.0000	0.7800	0.7215	0.5628
P1-T36	1000	0.5873	0.7215	4.2033	1.0000	4.6792	1.0000	0.7800	0.7215	0.5628

Table C2 *Survival probabilities, reliability indices and reliability bounds of transmission towers*

Return Period	1000 Years									
Failure Modes		Seismic Load		Wind+Ice		Wind		Wearout	Component Survival Probability Bounds	
Tower	Return Period	β	P_S	β	P_S	β	P_S	P_S	Upper Bound	Lower Bound
P1-T37	1000	0.5873	0.7215	4.2033	1.0000	4.6792	1.0000	0.7800	0.7215	0.5628
P1-T38	1000	0.5873	0.7215	4.2033	1.0000	4.6792	1.0000	0.7800	0.7215	0.5628
P1-T39	1000	0.5873	0.7215	4.2033	1.0000	4.6792	1.0000	0.7800	0.7215	0.5628
P1-T40	1000	0.5873	0.7215	4.2033	1.0000	4.6792	1.0000	0.7800	0.7215	0.5628
P1-T41	1000	0.5873	0.7215	4.2033	1.0000	4.6792	1.0000	0.7800	0.7215	0.5628
P1-T42	1000	0.5873	0.7215	4.2033	1.0000	4.6792	1.0000	0.7800	0.7215	0.5628
P1-T43	1000	0.5873	0.7215	4.2033	1.0000	4.6792	1.0000	0.7800	0.7215	0.5628
P1-T44	1000	0.5873	0.7215	4.2033	1.0000	4.6792	1.0000	0.7800	0.7215	0.5628
P1-T45	1000	0.5873	0.7215	4.2033	1.0000	4.6792	1.0000	0.7800	0.7215	0.5628
P1-T46	1000	0.5873	0.7215	4.2033	1.0000	4.6792	1.0000	0.7800	0.7215	0.5628
P1-T47	1000	0.5873	0.7215	4.2033	1.0000	4.6792	1.0000	0.7800	0.7215	0.5628
P1-T48	1000	0.5873	0.7215	4.2033	1.0000	4.6792	1.0000	0.7800	0.7215	0.5628
P1-T49	1000	0.5873	0.7215	4.2033	1.0000	4.6792	1.0000	0.7800	0.7215	0.5628
P1-T50	1000	0.5873	0.7215	4.2033	1.0000	4.6792	1.0000	0.7800	0.7215	0.5628
P1-T51	1000	0.5873	0.7215	4.2033	1.0000	4.6792	1.0000	0.7800	0.7215	0.5628
P1-T52	1000	0.5873	0.7215	4.2033	1.0000	4.6792	1.0000	0.7800	0.7215	0.5628
P1-T53	1000	0.5873	0.7215	4.2033	1.0000	4.6792	1.0000	0.7800	0.7215	0.5628
P1-T54	1000	0.5873	0.7215	4.2033	1.0000	4.6792	1.0000	0.7800	0.7215	0.5628
P1-T55	1000	0.5873	0.7215	4.2033	1.0000	4.6792	1.0000	0.7800	0.7215	0.5628
P1-T56	1000	0.5873	0.7215	4.2033	1.0000	4.6792	1.0000	0.7800	0.7215	0.5628
P1-T57	1000	0.5873	0.7215	4.2033	1.0000	4.6792	1.0000	0.7800	0.7215	0.5628
P1-T58	1000	0.5873	0.7215	4.2033	1.0000	4.6792	1.0000	0.7800	0.7215	0.5628
P1-T59	1000	0.5873	0.7215	4.2033	1.0000	4.6792	1.0000	0.7800	0.7215	0.5628
P1-T60	1000	0.5873	0.7215	4.2033	1.0000	4.6792	1.0000	0.7800	0.7215	0.5628
P1-T61	1000	0.5873	0.7215	4.2033	1.0000	4.6792	1.0000	0.7800	0.7215	0.5628
P1-T62	1000	0.5873	0.7215	4.2033	1.0000	4.6792	1.0000	0.7800	0.7215	0.5628
P1-T63	1000	0.5873	0.7215	4.2033	1.0000	4.6792	1.0000	0.7800	0.7215	0.5628
P1-T64	1000	0.5873	0.7215	4.2033	1.0000	4.6792	1.0000	0.7800	0.7215	0.5628
P1-T65	1000	0.5873	0.7215	4.2033	1.0000	4.6792	1.0000	0.7800	0.7215	0.5628
P1-T66	1000	0.5873	0.7215	4.2033	1.0000	4.6792	1.0000	0.7800	0.7215	0.5628
P1-T67	1000	0.5873	0.7215	4.2033	1.0000	4.6792	1.0000	0.7800	0.7215	0.5628
P1-T68	1000	0.5873	0.7215	4.2033	1.0000	4.6792	1.0000	0.7800	0.7215	0.5628
P1-T69	1000	0.5873	0.7215	4.2033	1.0000	4.6792	1.0000	0.7800	0.7215	0.5628
P1-T70	1000	0.5873	0.7215	4.2033	1.0000	4.6792	1.0000	0.7800	0.7215	0.5628
P1-T71	1000	0.5873	0.7215	4.2033	1.0000	4.6792	1.0000	0.7800	0.7215	0.5628
P1-T72	1000	0.5873	0.7215	4.2033	1.0000	4.6792	1.0000	0.7800	0.7215	0.5628
P1-T73	1000	0.5873	0.7215	4.2033	1.0000	4.6792	1.0000	0.7800	0.7215	0.5628
P1-T74	1000	0.5873	0.7215	4.2033	1.0000	4.6792	1.0000	0.7800	0.7215	0.5628
P1-T75	1000	0.5873	0.7215	4.2033	1.0000	4.6792	1.0000	0.7800	0.7215	0.5628
P1-T76	1000	0.5873	0.7215	4.2033	1.0000	4.6792	1.0000	0.7800	0.7215	0.5628
P1-T77	1000	0.5873	0.7215	4.2033	1.0000	4.6792	1.0000	0.7800	0.7215	0.5628
P1-T78	1000	0.5873	0.7215	4.2033	1.0000	4.6792	1.0000	0.7800	0.7215	0.5628

Table C2 *Survival probabilities, reliability indices and reliability bounds of transmission towers*

Return Period	1000 Years									
Failure Modes		Seismic Load		Wind+Ice		Wind		Wearout	Component Survival Probability Bounds	
Tower	Return Period	β	P_S	β	P_S	β	P_S	P_S	Upper Bound	Lower Bound
P1-T79	1000	0.5873	0.7215	4.2033	1.0000	4.6792	1.0000	0.7800	0.7215	0.5628
P1-T80	1000	0.5873	0.7215	4.2033	1.0000	4.6792	1.0000	0.7800	0.7215	0.5628
P1-T81	1000	0.5873	0.7215	4.2033	1.0000	4.6792	1.0000	0.7800	0.7215	0.5628
P1-T82	1000	0.5873	0.7215	4.2033	1.0000	4.6792	1.0000	0.7800	0.7215	0.5628
P1-T83	1000	0.5873	0.7215	4.2033	1.0000	4.6792	1.0000	0.7800	0.7215	0.5628
P1-T84	1000	0.5873	0.7215	4.2033	1.0000	4.6792	1.0000	0.7800	0.7215	0.5628
P1-T85	1000	0.5873	0.7215	4.2033	1.0000	4.6792	1.0000	0.7800	0.7215	0.5628
P1-T86	1000	0.5873	0.7215	3.8405	0.9999	4.5204	1.0000	0.7800	0.7215	0.5628
P1-T87	1000	0.5873	0.7215	3.8405	0.9999	4.5204	1.0000	0.7800	0.7215	0.5628
P1-T88	1000	0.5873	0.7215	3.8405	0.9999	4.5204	1.0000	0.7800	0.7215	0.5628
P1-T89	1000	0.5873	0.7215	3.8405	0.9999	4.5204	1.0000	0.7800	0.7215	0.5628
P1-T90	1000	0.5873	0.7215	3.8405	0.9999	4.5204	1.0000	0.7800	0.7215	0.5628
P1-T91	1000	0.5873	0.7215	3.8405	0.9999	4.5204	1.0000	0.7800	0.7215	0.5628
P1-T92	1000	0.5873	0.7215	3.8405	0.9999	4.5204	1.0000	0.7800	0.7215	0.5628
P1-T93	1000	0.5873	0.7215	3.8405	0.9999	4.5204	1.0000	0.7800	0.7215	0.5628
P1-T94	1000	0.5873	0.7215	3.8405	0.9999	4.5204	1.0000	0.7800	0.7215	0.5628
P1-T95	1000	0.5873	0.7215	3.8405	0.9999	4.5204	1.0000	0.7800	0.7215	0.5628
P1-T96	1000	0.5873	0.7215	3.8405	0.9999	4.5204	1.0000	0.7800	0.7215	0.5628
P1-T97	1000	0.5873	0.7215	3.8405	0.9999	4.5204	1.0000	0.7800	0.7215	0.5628
P1-T98	1000	0.5873	0.7215	3.8405	0.9999	4.5204	1.0000	0.7800	0.7215	0.5628
P1-T99	1000	0.5873	0.7215	3.8405	0.9999	4.5204	1.0000	0.7800	0.7215	0.5628
P1-T100	1000	0.5873	0.7215	3.8405	0.9999	4.5204	1.0000	0.7800	0.7215	0.5628
P1-T101	1000	0.5873	0.7215	3.8405	0.9999	4.5204	1.0000	0.7800	0.7215	0.5628
P1-T102	1000	0.5873	0.7215	3.8405	0.9999	4.5204	1.0000	0.7800	0.7215	0.5628
P1-T103	1000	0.5873	0.7215	3.8405	0.9999	4.5204	1.0000	0.7800	0.7215	0.5628
P1-T104	1000	0.5873	0.7215	3.8405	0.9999	4.5204	1.0000	0.7800	0.7215	0.5628
P1-T105	1000	0.5873	0.7215	3.8405	0.9999	4.5204	1.0000	0.7800	0.7215	0.5628
P1-T106	1000	0.5873	0.7215	3.8405	0.9999	4.5204	1.0000	0.7800	0.7215	0.5628
P1-T107	1000	0.5873	0.7215	3.8405	0.9999	4.5204	1.0000	0.7800	0.7215	0.5628
P1-T108	1000	0.5873	0.7215	3.8405	0.9999	4.5204	1.0000	0.7800	0.7215	0.5628
P1-T109	1000	0.5873	0.7215	3.8405	0.9999	4.5204	1.0000	0.7800	0.7215	0.5628
P1-T110	1000	0.5873	0.7215	3.8405	0.9999	4.5204	1.0000	0.7800	0.7215	0.5628
P1-T111	1000	0.5873	0.7215	3.8405	0.9999	4.5204	1.0000	0.7800	0.7215	0.5628
P1-T112	1000	0.5873	0.7215	3.8405	0.9999	4.5204	1.0000	0.7800	0.7215	0.5628
P1-T113	1000	0.5873	0.7215	3.8405	0.9999	4.5204	1.0000	0.7800	0.7215	0.5628
P1-T114	1000	0.5873	0.7215	3.8405	0.9999	4.5204	1.0000	0.7800	0.7215	0.5628
P1-T115	1000	0.5873	0.7215	3.8405	0.9999	4.5204	1.0000	0.7800	0.7215	0.5628
P1-T116	1000	0.5873	0.7215	3.8405	0.9999	4.5204	1.0000	0.7800	0.7215	0.5628
P1-T117	1000	0.5873	0.7215	3.8405	0.9999	4.5204	1.0000	0.7800	0.7215	0.5628
P1-T118	1000	0.5873	0.7215	3.8405	0.9999	4.5204	1.0000	0.7800	0.7215	0.5628
P1-T119	1000	0.5873	0.7215	3.8405	0.9999	4.5204	1.0000	0.7800	0.7215	0.5628
P1-T120	1000	0.5873	0.7215	3.8405	0.9999	4.5204	1.0000	0.7800	0.7215	0.5628

Table C2 *Survival probabilities, reliability indices and reliability bounds of transmission towers*

Return Period	1000 Years									
Failure Modes		Seismic Load		Wind+Ice		Wind		Wearout	Component Survival Probability Bounds	
Tower	Return Period	β	P_S	β	P_S	β	P_S	P_S	Upper Bound	Lower Bound
P1-T121	1000	0.5873	0.7215	3.8405	0.9999	4.5204	1.0000	0.7800	0.7215	0.5628
P1-T122	1000	0.5873	0.7215	3.8405	0.9999	4.5204	1.0000	0.7800	0.7215	0.5628
P1-T123	1000	0.5873	0.7215	3.8405	0.9999	4.5204	1.0000	0.7800	0.7215	0.5628
P1-T124	1000	0.5873	0.7215	3.8405	0.9999	4.5204	1.0000	0.7800	0.7215	0.5628
P1-T125	1000	0.5873	0.7215	3.8405	0.9999	4.5204	1.0000	0.7800	0.7215	0.5628
P1-T126	1000	0.5873	0.7215	3.8405	0.9999	4.5204	1.0000	0.7800	0.7215	0.5628
P1-T127	1000	0.5873	0.7215	3.8405	0.9999	4.5204	1.0000	0.7800	0.7215	0.5628
P1-T128	1000	0.5873	0.7215	3.8405	0.9999	4.5204	1.0000	0.7800	0.7215	0.5628
P1-T129	1000	0.5873	0.7215	3.8405	0.9999	4.5204	1.0000	0.7800	0.7215	0.5628
P1-T130	1000	0.5873	0.7215	3.8405	0.9999	4.5204	1.0000	0.7800	0.7215	0.5628
P1-T131	1000	0.5873	0.7215	3.8405	0.9999	4.5204	1.0000	0.7800	0.7215	0.5628
P1-T132	1000	0.5873	0.7215	3.8405	0.9999	4.5204	1.0000	0.7800	0.7215	0.5628
P1-T133	1000	0.5873	0.7215	3.8405	0.9999	4.5204	1.0000	0.7800	0.7215	0.5628
P1-T134	1000	0.5873	0.7215	3.8405	0.9999	4.5204	1.0000	0.7800	0.7215	0.5628
P1-T135	1000	0.5873	0.7215	3.8405	0.9999	4.5204	1.0000	0.7800	0.7215	0.5628
P1-T136	1000	0.5873	0.7215	3.8405	0.9999	4.5204	1.0000	0.7800	0.7215	0.5628
P1-T137	1000	0.5873	0.7215	3.8405	0.9999	4.5204	1.0000	0.7800	0.7215	0.5628
P1-T138	1000	0.5873	0.7215	3.8405	0.9999	4.5204	1.0000	0.7800	0.7215	0.5628
P1-T139	1000	0.5873	0.7215	3.8405	0.9999	4.5204	1.0000	0.7800	0.7215	0.5628
P1-T140	1000	0.5873	0.7215	3.8405	0.9999	4.5204	1.0000	0.7800	0.7215	0.5628
P1-T141	1000	0.5873	0.7215	3.8405	0.9999	4.5204	1.0000	0.7800	0.7215	0.5628
P1-T142	1000	0.5873	0.7215	3.8405	0.9999	4.5204	1.0000	0.7800	0.7215	0.5628
P1-T143	1000	0.5873	0.7215	3.8405	0.9999	4.5204	1.0000	0.7800	0.7215	0.5628
P1-T144	1000	0.5873	0.7215	3.8405	0.9999	4.5204	1.0000	0.7800	0.7215	0.5628
P1-T145	1000	0.5873	0.7215	3.8405	0.9999	4.5204	1.0000	0.7800	0.7215	0.5628
P1-T146	1000	0.5873	0.7215	3.8405	0.9999	4.5204	1.0000	0.7800	0.7215	0.5628
P1-T147	1000	0.5873	0.7215	3.8405	0.9999	4.5204	1.0000	0.7800	0.7215	0.5628
P1-T148	1000	0.5873	0.7215	3.8405	0.9999	4.5204	1.0000	0.7800	0.7215	0.5628
P1-T149	1000	0.5873	0.7215	3.8405	0.9999	4.5204	1.0000	0.7800	0.7215	0.5628
P1-T150	1000	0.5873	0.7215	3.8405	0.9999	4.5204	1.0000	0.7800	0.7215	0.5628
P1-T151	1000	0.5873	0.7215	3.8405	0.9999	4.5204	1.0000	0.7800	0.7215	0.5628
P1-T152	1000	0.5873	0.7215	3.8405	0.9999	4.5204	1.0000	0.7800	0.7215	0.5628
P1-T153	1000	0.5873	0.7215	3.8405	0.9999	4.5204	1.0000	0.7800	0.7215	0.5628
P1-T154	1000	0.5873	0.7215	3.8405	0.9999	4.5204	1.0000	0.7800	0.7215	0.5628
P1-T155	1000	0.5873	0.7215	3.8405	0.9999	4.5204	1.0000	0.7800	0.7215	0.5628
P1-T156	1000	0.5873	0.7215	3.8405	0.9999	4.5204	1.0000	0.7800	0.7215	0.5628
P1-T157	1000	0.5873	0.7215	3.8405	0.9999	4.5204	1.0000	0.7800	0.7215	0.5628
P1-T158	1000	0.5873	0.7215	3.8405	0.9999	4.5204	1.0000	0.7800	0.7215	0.5628
P1-T159	1000	0.5873	0.7215	3.8405	0.9999	4.5204	1.0000	0.7800	0.7215	0.5628
P1-T160	1000	0.5873	0.7215	3.8405	0.9999	4.5204	1.0000	0.7800	0.7215	0.5628
P1-T161	1000	0.5873	0.7215	3.8405	0.9999	4.5204	1.0000	0.7800	0.7215	0.5628
P1-T162	1000	0.5873	0.7215	3.8405	0.9999	4.5204	1.0000	0.7800	0.7215	0.5628

Table C2 *Survival probabilities, reliability indices and reliability bounds of transmission towers*

Return Period	1000 Years									
Failure Modes		Seismic Load		Wind+Ice		Wind		Wearout	Component Survival Probability Bounds	
Tower	Return Period	β	P_S	β	P_S	β	P_S	P_S	Upper Bound	Lower Bound
P1-T163	1000	0.5873	0.7215	3.8405	0.9999	4.5204	1.0000	0.7800	0.7215	0.5628
P1-T164	1000	0.5873	0.7215	3.8405	0.9999	4.5204	1.0000	0.7800	0.7215	0.5628
P1-T165	1000	0.5873	0.7215	3.8405	0.9999	4.5204	1.0000	0.7800	0.7215	0.5628
P1-T166	1000	0.5873	0.7215	3.8405	0.9999	4.5204	1.0000	0.7800	0.7215	0.5628
P1-T167	1000	0.5873	0.7215	3.8405	0.9999	4.5204	1.0000	0.7800	0.7215	0.5628
P1-T168	1000	0.5873	0.7215	3.8405	0.9999	4.5204	1.0000	0.7800	0.7215	0.5628
P1-T169	1000	0.5873	0.7215	3.8405	0.9999	4.5204	1.0000	0.7800	0.7215	0.5628
P1-T170	1000	0.5873	0.7215	3.8405	0.9999	4.5204	1.0000	0.7800	0.7215	0.5628
P1-T171	1000	0.5873	0.7215	3.8405	0.9999	4.5204	1.0000	0.7800	0.7215	0.5628
P1-T172	1000	0.5873	0.7215	3.8405	0.9999	4.5204	1.0000	0.7800	0.7215	0.5628
P1-T173	1000	0.5873	0.7215	3.8405	0.9999	4.5204	1.0000	0.7800	0.7215	0.5628
P1-T174	1000	0.5873	0.7215	3.8405	0.9999	4.5204	1.0000	0.7800	0.7215	0.5628
P1-T175	1000	0.5873	0.7215	3.8405	0.9999	4.5204	1.0000	0.7800	0.7215	0.5628
P1-T176	1000	0.5873	0.7215	3.8405	0.9999	4.5204	1.0000	0.7800	0.7215	0.5628
P1-T177	1000	0.5873	0.7215	3.8405	0.9999	4.5204	1.0000	0.7800	0.7215	0.5628
P1-T178	1000	0.5873	0.7215	3.8405	0.9999	4.5204	1.0000	0.7800	0.7215	0.5628
P1-T179	1000	0.5873	0.7215	3.8405	0.9999	4.5204	1.0000	0.7800	0.7215	0.5628
P1-T180	1000	0.5873	0.7215	3.8405	0.9999	4.5204	1.0000	0.7800	0.7215	0.5628
P1-T181	1000	0.5873	0.7215	3.8405	0.9999	4.5204	1.0000	0.7800	0.7215	0.5628
P1-T182	1000	0.5873	0.7215	3.8405	0.9999	4.5204	1.0000	0.7800	0.7215	0.5628
P1-T183	1000	0.5873	0.7215	3.8405	0.9999	4.5204	1.0000	0.7800	0.7215	0.5628
P1-T184	1000	0.5873	0.7215	3.8405	0.9999	4.5204	1.0000	0.7800	0.7215	0.5628
P1-T185	1000	0.5873	0.7215	3.8405	0.9999	4.5204	1.0000	0.7800	0.7215	0.5628
P1-T186	1000	0.5873	0.7215	3.8405	0.9999	4.5204	1.0000	0.7800	0.7215	0.5628
P1-T187	1000	0.5873	0.7215	3.8405	0.9999	4.5204	1.0000	0.7800	0.7215	0.5628
P1-T188	1000	0.5873	0.7215	3.8405	0.9999	4.5204	1.0000	0.7800	0.7215	0.5628
P1-T189	1000	0.5873	0.7215	3.8405	0.9999	4.5204	1.0000	0.7800	0.7215	0.5628
P1-T190	1000	0.5873	0.7215	3.8405	0.9999	4.5204	1.0000	0.7800	0.7215	0.5628
P1-T191	1000	0.5873	0.7215	3.8405	0.9999	4.5204	1.0000	0.7800	0.7215	0.5628
P1-T192	1000	0.5873	0.7215	3.8405	0.9999	4.5204	1.0000	0.7800	0.7215	0.5628
P1-T193	1000	0.5873	0.7215	3.8405	0.9999	4.5204	1.0000	0.7800	0.7215	0.5628
P1-T194	1000	0.5873	0.7215	3.8405	0.9999	4.5204	1.0000	0.7800	0.7215	0.5628
P1-T195	1000	0.5873	0.7215	3.8405	0.9999	4.5204	1.0000	0.7800	0.7215	0.5628
P1-T196	1000	0.5873	0.7215	3.8405	0.9999	4.5204	1.0000	0.7800	0.7215	0.5628
P1-T197	1000	0.5873	0.7215	3.8405	0.9999	4.5204	1.0000	0.7800	0.7215	0.5628
P1-T198	1000	0.5873	0.7215	3.8405	0.9999	4.5204	1.0000	0.7800	0.7215	0.5628
P1-T199	1000	0.5873	0.7215	3.8405	0.9999	4.5204	1.0000	0.7800	0.7215	0.5628
P1-T200	1000	0.5873	0.7215	3.8405	0.9999	4.5204	1.0000	0.7800	0.7215	0.5628
P1-T201	1000	0.5873	0.7215	3.8405	0.9999	4.5204	1.0000	0.7800	0.7215	0.5628
P1-T202	1000	0.5873	0.7215	3.8405	0.9999	4.5204	1.0000	0.7800	0.7215	0.5628
P1-T203	1000	0.5873	0.7215	3.8405	0.9999	4.5204	1.0000	0.7800	0.7215	0.5628
P1-T204	1000	0.5873	0.7215	3.8405	0.9999	4.5204	1.0000	0.7800	0.7215	0.5628

Table C2 *Survival probabilities, reliability indices and reliability bounds of transmission towers*

Return Period	1000 Years									
Failure Modes		Seismic Load		Wind+Ice		Wind		Wearout	Component Survival Probability Bounds	
Tower	Return Period	β	P_S	β	P_S	β	P_S	P_S	Upper Bound	Lower Bound
P1-T205	1000	0.5873	0.7215	3.8405	0.9999	4.5204	1.0000	0.7800	0.7215	0.5628
P1-T206	1000	0.5873	0.7215	3.8405	0.9999	4.5204	1.0000	0.7800	0.7215	0.5628
P1-T207	1000	0.5873	0.7215	3.8405	0.9999	4.5204	1.0000	0.7800	0.7215	0.5628
P1-T208	1000	0.5873	0.7215	3.8405	0.9999	4.5204	1.0000	0.7800	0.7215	0.5628
P1-T209	1000	0.5873	0.7215	3.8405	0.9999	4.5204	1.0000	0.7800	0.7215	0.5628
P1-T210	1000	0.5873	0.7215	3.8405	0.9999	4.5204	1.0000	0.7800	0.7215	0.5628
P1-T211	1000	0.5873	0.7215	3.8405	0.9999	4.5204	1.0000	0.7800	0.7215	0.5628
P1-T212	1000	0.5873	0.7215	3.8405	0.9999	4.5204	1.0000	0.7800	0.7215	0.5628
P1-T213	1000	0.5873	0.7215	3.8405	0.9999	4.5204	1.0000	0.7800	0.7215	0.5628
P1-T214	1000	0.5873	0.7215	3.8405	0.9999	4.5204	1.0000	0.7800	0.7215	0.5628
P1-T215	1000	0.5873	0.7215	3.8405	0.9999	4.5204	1.0000	0.7800	0.7215	0.5628
P1-T216	1000	0.5873	0.7215	3.8405	0.9999	4.5204	1.0000	0.7800	0.7215	0.5628
P1-T217	1000	0.5873	0.7215	3.8405	0.9999	4.5204	1.0000	0.7800	0.7215	0.5628
P1-T218	1000	0.5873	0.7215	3.8405	0.9999	4.5204	1.0000	0.7800	0.7215	0.5628
P1-T219	1000	0.5873	0.7215	3.8405	0.9999	4.5204	1.0000	0.7800	0.7215	0.5628
P1-T220	1000	0.5873	0.7215	3.8405	0.9999	4.5204	1.0000	0.7800	0.7215	0.5628
P1-T221	1000	0.5873	0.7215	3.8405	0.9999	4.5204	1.0000	0.7800	0.7215	0.5628
P1-T222	1000	0.5873	0.7215	3.8405	0.9999	4.5204	1.0000	0.7800	0.7215	0.5628